Preparation of Stable Gold Colloids for Sensitivity Enhancement of Progesterone Immunoassay using Surface Plasmon Resonance

A thesis
Submitted in partial fulfilment
of the requirements for the degree
of
Master of Science in Chemistry
at the
University of Waikato
by

Kevin Su-Wei Wu

February 2007

Abstract

The purpose of this study was to prepare concentrated and stable gold colloids for the enhancement of the signal response of the SPR technique for detecting small molecules such as progesterone. The gold colloids developed in this study were prepared by hydrazine hydrate, sodium borohydride, and tri-potassium citrate reduction routes. The study revealed that the sodium borohydride reduced gold colloids were extremely stable and it was able to be utilised in the progesterone immunoassay developed previously by Mitchell et al. The experiment was carried out on BIAcore 3000 using two different sensor surfaces (CM5 and SAM). The results showed that the enhancement species prepared from the borohydride-reduced gold colloids were able to improve the SPR signal response by 13 times higher than SPR signal produced without the enhancement species on the CM5 surface. The signal enhancement on the SAM surface using the same enhancement species was even greater at 29 times higher. The sensitivity of the assay was, however, unable to be determined due to time constraint. The limit of detection (LOD) of the progesterone assay using the CM5 chip was estimated to be *ca.* 5-20 pg/mL. Whilst for the SAM chip, the LOD of the progesterone assay was estimated to be *ca.* 5-20 fg/mL. Further work is required to confirm these estimated LOD values.

Acknowledgements

This study have not been possible without the continued guidance and support of my supervisors **Dr. Michael Mucalo** (University of Waikato) and **Dr. Yinqiu Wu** (HortResearch, Ruakura). I am also very grateful for the advice and recommendations given by **Jing Yuan** (HortResearch, Ruakura) during the course of this project.

I would also like to show my appreciation to the people at University of Waikato who assisted me during this study and supported me until the end of the project.

Prof. Brian Nicholson for the encouragement given during the first year of this study. **Wendy Jackson**, **Pat Gread**, **Jannine Rhodes**, **Annie Barker**, and **Amu Upreti** for their assistance with various laboratory related issues during the two years.

The continued support of my family and friends has been unprecedented during the study.

Last but not least, the financial assistance from HortResearch at Ruakura, Hamilton was greatly appreciated.

Table of Contents

List of Figures

List of Tables

List of Terms and Abbreviations

c.c.c.	critical coagulation concentration
TEM	transmission electron microscope
Ppb	parts per billion
SERS	surface enhanced Raman scattering
SPR	surface plasmon resonance
SAM	self-assembled monolayer
ELISA	enzyme-linked immunosorbent assay
kDa	kilo Dalton
mAb	monoclonal antibody
SAb (IgG)	secondary antibody (immunoglobulin)
SAb-Au	secondary antibody (immunoglobulin)-gold colloids conjugate
pg	picogram ($1x10^{-12}$ gram)
fg	femtogram ($1x10^{-15}$ gram)
PCS	photon correlation spectroscopy
DLS	dynamic light scattering
QELS	quasi-elastic light scattering
Z_{ave}	mean particle size measured using the Zetasizer
GE	General Electric
HEPES	4-(2-hydroxyethyl)-1-piperazineethanesulfonic acid
HBS-EP (HBS)	HEPES buffered silane with EDTA and P-20 surfactant
LC	liquid chromatography
IFC	integrated micro-fluidic cartridge
EDTA	ethylenediaminetetraacetic acid
RU	response unit
EDC	*N*-ethyl-*N*-(3-dimethylaminopropyl)-carbodiimide
NHS	*N*-hydroxysuccinimide
EAH	ethanolamine hydrochloride
ADME	absorption, distribution, metabolism, and excretion
AG	arabinogalactan
LMCT	ligand to metal charge transfer
A_{350}	absorbance at wavelength of 350 nm
kCps	kilo counts per second
LOD	limit of detection

OVA	ovalbumin
PEG	polyethylene glycol
P4-PEG-OVA	progesterone-polyethylene glycol-ovalbumin conjugate
Reg	regeneration
DMF	N, N-dimethylformamide
UF	ultra-fine

1. Introduction

1.1 Definitions of Colloids, Sols, & Nanoparticles

Colloids and sols are terms that define particles falling within a size range of 1 nm to 1 μm [1]. Nanoparticles are meant to refer to particles in the nanometre size range. Although the three terms are used interchangeably in many scientific studies of this area, the terms do have strict definitions. Colloids are submicroscopic particles that are uniformly dispersed in a dispersion medium. The dispersed particles take the form of a liquid, gas or solid. Dispersions of liquids in another liquid are called an "emulsions" while dispersions of gases in liquid are called, "foams". For the case of dispersions of solid in liquids, if the solid is polymeric in nature, the dispersion is termed a "latex". However, if the solid is non-polymeric such as metal, the dispersion is usually referred to as a "sol" [2]. As a further distinction, sols can be differentiated according to the dispersion medium. If the dispersion medium is aqueous, the term "hydrosols" is used; whereas dispersions in organic liquids are referred to as "organosols" [2]. With the recent advances in nanotechnology, "nanoparticle" is becoming the more popular term that describes particles of nanometre dimensions.

Fogs, smokes, milk, paints, mud, jellies, and ruby stained glass are just some simple colloidal systems that are encountered in everyday life. Many biological structures are also colloidal in nature. For example, blood is a dispersion of corpuscles in serum, and bone is fundamentally a solid state dispersion of hydroxyapatite in collagen[3].

1.2 Preparation of Colloidal Dispersions

The preparation of colloidal dispersions is divided into two categories namely dispersion and condensation [4], of which the latter is for more fine (with smaller particle size) material and more of significance in this study. In the dispersion method, a sample of bulk material is broken down to colloidal dimensions by a mechanical process. The most direct method is by grinding in a colloid mill. This device involves forcing coarse suspension of particles through a narrow gap between two rapidly rotating surfaces. Particles are torn apart by the shearing process, and the colloidal dispersion is formed, provided that the dispersion medium keeps small particles from aggregating (see Section 1.4.5 in Chapter 1). Ultrasonication is a method that uses high frequency sound waves to produce emulsions from a mixture solution with two phases [4]. Condensation methods involve reprecipitation, condensation from vapour, or chemical reaction. An example of reprecipitation method is the formation of zinc oxide colloids. This can be prepared by dissolving zinc (II) salt in an aqueous solution. The resulting solution is then added to a solution of urea to form solid zinc complex, which is decomposed to zinc oxide upon heating to > 300°C [5]. The formation of fog or mist from supersaturated vapour exemplifies the second category of condensation methods described above.

When using chemical methods of synthesis, colloidal particles are formed by "growing" nuclei until a particle in the typical colloid size range is reached. Nucleation or formation of dispersed species with a size in an intermediate range of 1 to 10 nm occurs initially before these species come together to form colloidal particles. This process can be illustrated by Figure 1.2-1, which is a plot of the concentration of the dispersed species (nuclei concentration) versus the extent of reaction. The model

explains that in order for nucleation of the nuclei to occur, the concentration of these dissolved species must firstly be above the saturation concentration of the system, that is the system must be supersaturated with the dispersed species. Only at a certain value of the supersaturation concentration, will nucleation occur. Once nuclei are formed, subsequent depositions of the newly formed nuclei will occur on the already formed nuclei. By controlling the temperature and concentration during the reaction, the growth-rate of dispersed nuclei can be varied. As a result, colloidal particles with different sizes can be produced. Preparation of monodisperse colloids have become quite important, as these systems allow a more precise study and understanding of the properties that colloids possess. To prepare monodisperse colloids, it is necessary for large amount of nuclei to be formed in a short period of time at the beginning of the chemical reaction. The nuclei formed will grow rapidly at first and this causes the concentration of the dispersed species to drop below the nucleation concentration. As a result, no new nuclei are formed and simultaneous growth of existing nuclei thus takes place.

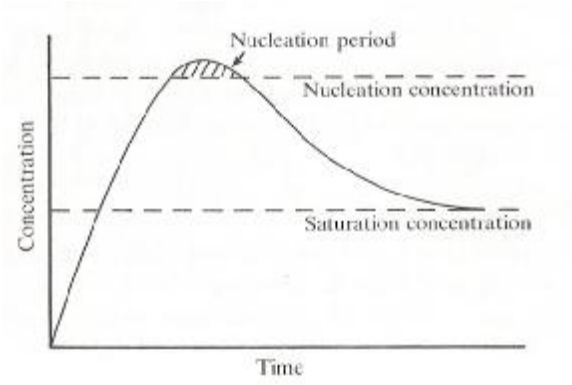

Figure 1.2-1 a plot of the nuclei concentration versus the extent of reaction [4]

Chemical methods include oxidation or reduction of anions or cations. Various oxidation or reducing agents can be used in the preparation. For instance, sulphur

colloids can be prepared by oxidising hydrogen sulphide or thiosulphate [4]. Silver colloids may be conventionally prepared by reducing silver nitrate with reducing agents like tri-sodium citrate, sodium borohydride, or carbon monoxide. Reduction of metal salts using UV or gamma irradiation has also been reported [6, 7]. Hydrolysis of metal salts is another important technique for preparing highly monodisperse sols of the transition metal oxides and hydroxides [8, 9].

1.3 Important Properties of Colloids

1.3.1 Brownian motion

Particles in colloidal suspension exhibit rapid and erratic motion called, "Brownian motion". This phenomenon was first observed in 1827 by Robert Brown who carried out microscope examination of pollen particles floating on top of pond water at the time. An explanation was provided based on the kinetic-molecular theory of matter, which postulated that the erratic motion observed was caused by the fluctuating forces that surrounding molecules of the dispersion medium were applying to the particle surface through random bombardment. Under such circumstances, a net force with varying magnitude and direction will be exerted on a particle at any given moment from the surrounding molecules, leading to a random motion of the particle.

1.3.2 Electrophoresis and electro-osmosis

Electrically charged particles tend to move under the influence of an electric field. The motion of a charged particle relative to the surrounding liquid is termed, "electrophoresis". A similar phenomenon can occur for the oppositely charged

solution ions or counter-ions surrounding a charged particle (see Section 1.4.1). The movement of the counter-ions relative to the charged particle is called, “electro-osmosis”. This phenomenon occurs when the solid is in the form of a capillary or a porous plug which is filled with the liquid. When an electric field is applied to the charged wall of the capillary the solution can be moved in response to the field [10].

1.3.3 Scattering of light

The optical properties of a colloidal suspension were first observed by Faraday in his work on gold colloids in the 19th century. Further study by Tyndall led to the discovery of the Tyndall effect, which describes the scattering of light by submicroscopic particles when a light beam is passed through a colloidal system. In the study, Tyndall suggested that the intensity of the scattered light is proportional to the volume of the colloidal particles [11].

The basic theory underlying the interactions between light and matter is based on Rayleigh’s theory on light scattering by particles with dimensions that are much smaller than the wavelength of light. When a small particle is subjected to an electric field from light the whole particle is subjected to the same field, and a dipole moment is induced. As the light passes over the particle, the electric field and the induced dipole fluctuate in magnitude. The oscillating dipole is induced from the movement of electrons in the particle. The electron movement constitutes in effect an oscillating current which produces its own electromagnetic field and radiates light of the same frequency as the incident light [3]. The theory also suggested that since the particles are much smaller than the wavelength of the passing light, every part of each particle

should experience the same magnitude of electromagnetic radiation as the light passes over the particle. Hence, light that are scattered at different angles by the same particle should have equal intensity.

Rayleigh's theory, however, only applies to spherical particles with small particle size. The particle size limit is determined by the size parameter, a. Rayleigh's theory only applies to particles with $a << 1$ [11]. a is described by the equation, $a = 2pa/l$, where a is the radius of the particle and λ is the wavelength of the incident light.

The Rayleigh-Debye-Gans theory and Mie theory were later developed and overcame the limitations faced by Rayleigh's theory. Debye and Gans put forward ideas based on Rayleigh's theory that when light interacts with a larger particle all parts of the particle are not subjected to the same electric field. Therefore, the intensity of the scattered light varies at different scattering angles. As a result, the theory becomes very complex as particles become much larger. Mie Theory takes into account the absorption of light from a large particle and also illustrated that the intensity of scattered light is angle-dependent.

All of the above mentioned light scattering theories are limited to dilute dispersions of particles. In more concentrated colloidal dispersions light scattered by the colloidal particles can be further scattered by other particles within the dispersion before leaving the dispersed system (i.e. there is multiple scattering). This becomes a problem when carrying out size measurements using light scattering techniques such as dynamic light scattering as the intensity of the scattered light becomes independent of the particle size (see Section 2.2.2 in Chapter 2).

1.4 Colloidal Stability

1.4.1 Electrical double layer

Colloidally suspended particles possess negative or positive charges at their surfaces. In accordance with Coulomb's law on electrostatic theory, like-charges repel while opposites attract. Hence, for a negatively charged electrolyte an excess of positively charged ions will surround a given negatively charged ion and vice versa. This model; for describing the distribution of charged ions in solution is called the ionic atmosphere model [3]. For colloidal systems, the ionic atmosphere around a charged colloidal particle is an important factor in determining the stability of the dispersion.

For a charged particle, the charge separation between the surface of the particle and the bulk electrolyte is called the electrical double layer. The concept of this electrical double layer was first introduced by Helmholtz who suggested that the double layer consists of two fixed layers of opposite charge like a parallel plate capacitor. The model was then improved independently by Gouy and Chapman to compensate for the thermal diffusion gradients, which can disrupt the fixed ionic layer proposed in Helmholtz's theory. The Gouy-Chapman's diffusion model also suggested the potential at the surface decreases exponentially with distance due to the diffuse layer of counter-ions from the solution [10], in contrast to the linear decrease in potential through a Helmholtz double layer.

The Gouy-Chapman-Stern theory is based on both Helmholtz theory and Gouy-Chapman theory [3]. This theory basically served as a compromise of the two models so that both the charge ordering (predicted by Helmholtz) plus random

ordering effect of ions (predicted by Guoy-Chapman) around a charged particle or interface could be accounted for. Hence it proposed that an electrical double layer consisted of an inner layer or the Stern layer which contains a monolayer of ions that are tightly bound to the charged particle/interface (Helmholtz theory) with an outer more loosely bound layer (the "diffuse layer") consisting of randomly ordered ions (Gouy-Chapman theory). In this compromise model, the potential varied linearly with distance through the Helmholtz layer and then exponentially with distance through the diffuse layer of the model.

Within the diffused layer there is a theoretical boundary within which the ions and the particle centre act as one entity. When the particle moves the associated ions move with it. Any ion beyond this boundary does not move with the particle. This boundary is called the slipping plane or shear plane (see Figure 1.4-1). The potential at this plane is termed the ***zeta potential*** [10]. The stability of a colloidal dispersion can be determined from the magnitude of the zeta potential. Colloidal dispersions with zeta potential of greater than ±30 eV are considered to be stable against aggregation.

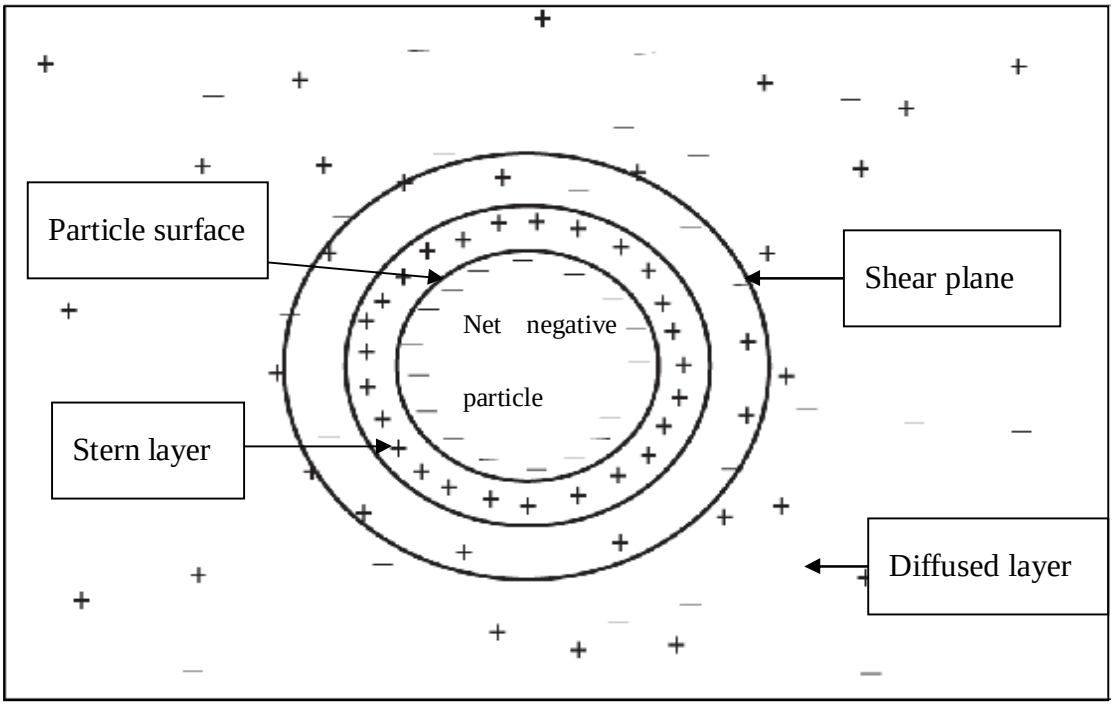

Figure 1.4-1 The double layer region surrounding a negatively charged particle

1.4.2 Inter-particle attractive forces

The origin of attraction between colloidal particles does not lie in strong intermolecular interaction, but in the weak interactions known as van der Waals forces [1]. This weak interaction may be created from three possible sources: Keesom interactions, Debye interactions, and London (dispersion) interactions.

Keesom interactions describe the attraction between two permanent dipole centres. Debye interactions involve permanent dipole and induced dipole attraction. The London interactions, which arise between two temporary dipoles, is the most important of the three because the interaction is long-range and much stronger than the Keesom and Debye contributions in most colloidal dispersions [1]. In general, a temporary dipole is induced by the movement of electron cloud around a nucleus. As two nuclei come in contact with each other the temporary dipoles become aligned and

interaction occurs.

Other forces of attraction may include hydrophobic forces and polymeric bridging forces [11]. Hydrophobic interactions may occur naturally or be induced by the adsorbed hydrophobic species on the particle surface. If one considers hydrophobic particles in a polar solvent, contact between the particle surface and polar solvent molecule is avoided. Therefore these particle surfaces have a preference to associate with each other to minimise the surface-solvent interaction. An example of this is the aggregation of coal or graphite, which possesses natural hydrophobicity, in polar solvents. Adsorption of hydrophobic surfactants on particle surfaces may also induce hydrophobicity on particles in polar solvents.

Polymers adsorbed on the surface of a particle may also induce repulsion (see Section 1.4.3) as well as attraction. The nature of the interaction depends on the interactions between the adsorbed polymers and the dispersion medium. If the adsorbed polymers are compatible with the solvent molecules, the suspension will remain stable. On the other hand, if the polymers are not compatible with the dispersion medium, the thickness of the adsorbed layer of polymer will decrease and there will be a tendency for the adsorbed polymers on a particle to interpenetrate into an adsorbed layer of polymers on another particle [11]. Hence, aggregation may occur depending on the density of the adsorbed polymers on the surfaces (see Section 1.4.4).

Polymers can be attached to two or more particles if polymers have several active sites and providing the particles are not fully covered by the polymers. If particles are fully covered with polymers, bridging between particles can happen only when a portion of the adsorbed polymer becomes detached, and provides sites for adsorption

on other particles or bonding with other polymers.

1.4.3 Inter-particle repulsive forces

The two major repulsive forces between colloidal particles are the electrostatic repulsion induced by the electrical double layer model and steric repulsion induced by adsorbed polymers on interacting particle surfaces.

As mentioned in Section 1.4.1, a charged colloidal particle and a portion of the ionic atmosphere around it act as a single entity. When a charged colloidal particle moves its associated counter-ions move with it. These counter-ions act as a protecting shield, which prevents the charged colloidal particles from interacting with each other by the van der Waals force (see Section 1.4.2). The thickness of the electrical double layer, which depends on the ionic strength of the dispersion, can affect the magnitude of the electrostatic repulsion. As ionic strength in the dispersion is increased through addition of a salt, the thickness of the electrical double layer decreases [2]. Hence the strength of the electrostatic repulsion can be overpowered by the van der Waals force and aggregation may occur.

Adsorption of polymers on particle surfaces can also induce repulsive forces between interacting particles. Following on from Section 1.4.2, polymers adsorbed on any given colloidal particle can interpenetrate into the molecular domain of another adsorbed polymer on another colloidal particle upon collision. However, this process has two consequences. Firstly, the local density of polymers increases, which causes the dispersion medium to diffuse into the region between the surfaces, which acts to reduce the polymer concentration so pushing the two surfaces apart (osmotic effect).

Secondly, since the polymers are tangled together, the number of configurations that these polymers can adopt decreases. This means a reduction in the entropy of the system has occurred and an increase in the free energy of the system [3]. This is unfavourable thermodynamically so favouring the separation of the two particles (entropic effect). These mechanisms serve to explain how certain polymers when added to colloidal dispersions can impart greater colloidal stability on a system. Polymers or other molecules fulfilling such a role in a colloidal system are called "protecting agents" and the colloids that are stabilised by them are termed "protected colloids".

1.4.4 DLVO theory for explaining the interactions between colloidal particles

In the 1940s, Derjaguin and Landau, and independently by Verwey and Overbeek developed this theory that describes the interaction between colloidal particles. It states that the stability of a colloidal system is determined by the total potential energy between the van der Waals force and the electrical double-layer repulsive force. However, further study has found that not all colloidal systems can be explained in terms of the DLVO theory [4]. The steric repulsive force was found to be the missing factor in the total potential energy. The revised theory is illustrated in Figure 1.4-2.

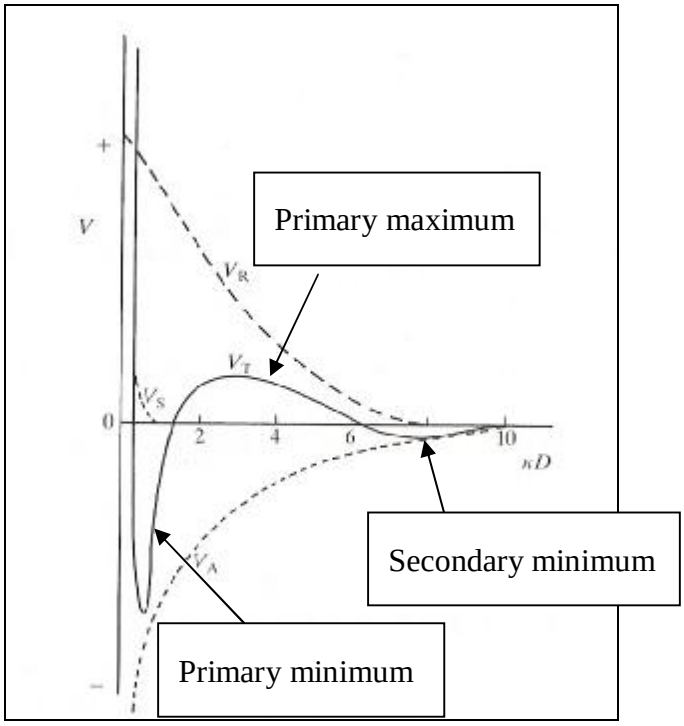

Figure 1.4-2 DLVO theory describing the total potential energy of inter-particle interaction versus inter-particle distances. V_T is the total potential energy of interaction between two approaching particles; V_R is the potential energy of the repulsive force; V_A is the potential energy of the attractive force; and V_S is the potential energy arises from solvent layer adjacent to the particle surfaces [4].

The diagram shows the total potential energy as a function of inter-particle distances. The minimum that occurs at longer inter-particle distance is termed the ***secondary minimum***. At this region, the van der Waals force is strong enough to induce loose aggregation (known as flocculation) which can usually be redispersed. With repulsive forces such as electrostatic and steric repulsions, the secondary minimum can be overcome. The primary maximum is shown by the increase in potential energy between two colloidal particles at close proximity. This energy barrier indicates the potential energy required to be overcome by the collision between two particles, in order for aggregation to occur. If the maximum is sufficiently large, it ensures that the rate of coagulation is slow so that the suspension has a long-term stability. If the

energy barrier is absent, collision between two particles will rapidly bring the potential energy to the region on the graph where a large drop in potential energy is observed. This region is called the *primary minimum*, and at this area rapid coagulation between particles results.

1.4.5 Aggregation of colloidal particles

The term aggregation generally describes the process by which colloidal particles become irreversibly attached to one another through interaction. Coagulation and flocculation are two terms that clearly define the morphology of the aggregated particles. Coagulation is derived from the Latin verb "coagulare", which means "to cause to curdle". Flocculation, on the other hand, is derived from "floccus", which means a flock of wool [2]. These two terms are often used interchangeably. However, differentiation should be made between the two terms.

Flocculation involves the loose aggregation of particles without the destruction of each particle's individuality [3]. In contrast, coagulation involves the process of particle growth upon aggregation. Flocculation can be induced when the total free energy of a system decreases (the DVLO theory) and a flocculated colloid can be redipersed via disruption of the flocs through some externally applied disintegration process such as ultrasonication.

Coagulation of sols by addition of electrolytes was observed by Faraday in 1856. The independent studies of Schulze and Hardy led to the conclusion that flocculation was controlled mainly by the nature of the added counter-ions and under certain conditions the effectiveness of the counter-ion was strongly dependent on its valency. The

minimum concentration of electrolyte required to induce flocculation or coagulation is termed the critical coagulation concentration (c.c.c.). As the valency on the ion increases, the value of the c.c.c decreases which demonstrates the valence dependency.

As mentioned in Section 1.4.4, the kinetics of coagulation depends on the magnitude of the energy barrier (primary maximum). In the absence of this barrier, coagulation occurs rapidly as a result of inter-particle collisions.

1.5 Application of Colloids

The properties of colloidal systems were observed and utilised by man since the earliest days of civilisation, even though the true nature of colloids had not been fully understood [3]. Preparation of butter, cheese, yoghurt, and the making of bread, bricks and ink pigment are just some examples of simple colloidal systems applied in the early days of civilisation. With the modern advances made in colloid science, the chemical and physical properties of colloids are better understood and able to be manipulated.

The technical applications of colloidal systems are becoming more sophisticated in various areas. In biological applications, biomolecules have been encapsulated in mesoporous silica nanoparticles for controlled release applications by destabilisation of aqueous silica precursors in the water droplets of a water-in-oil emulsion. [12]. Metal colloids have also been used for virus capture [13], biomolecule labelling for TEM imagery, and also in developing ultra-sensitive immunoassays [14] (the subject of this thesis).

Nanocomposite coatings made from 3-glycidoxypropyltrimethoxysilane (GPTMS) and various metal oxide nanoparticles have unique properties such as absorbing harmful UV radiation. Since different metal nanoparticles may have different properties, resulting materials may serve in applications such as optical, protective, catalytic, guest-host, and multifunctional coatings [15].

Metal nanoparticles (Pt, Au, or Cu) together with multi-walled and single-walled carbon nanotubes solubilised in Nafion have been used to form nanocomposites for electrochemical detection of trinitrotoluene (TNT) and several other nitroaromatics. Using these nanocomposites, adsorptive stripping voltammetry for TNT resulted in a detection limit of 1 ppb [16].

1.6 Gold Colloids

1.6.1 Introduction

In mediaeval times, colloidal gold was once prepared by alchemists mainly in two forms, viz., "aureum potable" or drinkable gold (regarded as the Elixir of Life) and purple of Cassius, which was used to make ruby glass. In 1774, Macquer had speculated that these systems had gold present in a finely divided form. However, it was not until 1856 that Michael Faraday had confirmed Macquer's speculation, and made the first comprehensive scientific study of gold colloids at that time. This study put forward ideas that can still be seen in modern theories concerning the factors responsible for the stability of colloidal dispersions. In a series of experiments with gold sols, Faraday demonstrated many important properties of colloidal dispersions: light scattering, sedimentation, coagulation by salts, and "protection" from

coagulating effects of salt which was bestowed by use of gelatine [3].

A number of simple preparative methods of charge-stabilised gold colloids by reduction of gold salt were developed in the early twentieth century. The most popular method is the citrate reduction route, which leads to size-tuned and monodisperse gold colloids [17]. More recently, protected metal colloids are being utilised in more and more scientific studies. Due to stability issue, the gold colloids prepared in this study by various (citrate, hydrazine, and borohydride) reduction routes were also protected by a purified oligosaccharide (protecting agent) called, "arabinogalactan" (see Section 3.1 in Chapter 3).

1.6.2 Some properties and applications of colloidal gold

One of the characteristic features of gold colloids is the various colours that the colloidal dispersions may exhibit. The different colours of gold colloids arise from the interaction between visible light and the gold particles in the dispersion. Depending on the size of the gold colloidal particles, the colour of stable gold colloids can vary from brown (particle diameter < 5 nm) [18] through to red (15 nm – 90 nm), and blue (*ca.* > 100 nm) [19]. Aggregated gold colloids, in contrast, are grey/black in colour.

Gold colloids have most notably been used in the Raman-based spectroscopic technique of Surface Enhanced Raman Scattering (SERS). This effect arises through a surface plasmon resonance (SPR) phenomenon, which will be described in more detail in Section 2.1.2 in Chapter 2. Basically, this phenomenon arises when a band of electrons on the metal surface resonates with the incident monochromatic radiation (provided by a laser) creating an induced evanescent wave at the surface of the

particles. The enhancement of Raman scattering occurs when both the induced evanescent wave and the incident radiation interacts with the Raman active vibrations of molecules adsorbed at the gold colloid surface. The induced dipole moment in the molecule is then greatly increased, and the resulting Raman signal is enhanced by a significant degree over what is expected for its concentration in solution [20]. This can be useful if wishing to acquire spectra of molecules which are present in solutions at low concentrations.

The resistance of gold metal against oxidation and other forms of reaction is another characteristic and advantage that gold has over other SPR inducible metals such as silver, copper and aluminium [21]. However, despite the well known lack of reactivity of metallic gold, immobilisations of thiol-molecules are readily performed, as sulfur has a good affinity for gold, as predicted from the hard-soft acid base theory. [22] [23]. Immobilisation can be achieved by immersing naked gold metal in a solution of thiol-containing molecules [24]. The immobilising process is a widely utilised technique in self-assembled monolayer (SAM) science which is used when different reactive sites are grafted onto a gold surface.

The utilisation of gold colloids in biological studies is rapidly increasing. One of the growing areas of interest is signal enhancement of biomolecular interaction analysis systems such as SPR based instruments, BIAcore (see Section 2.4 in Chapter 2). This will form the basis for the research reported in this thesis.

1.6.3 The use of gold colloids in biomolecular interaction analysis systems

Protein-protein interactions are commonly analysed by using the Enzyme-Linked ImmunoSorbent Assay, or ELISA. Its high sensitivity in antigen/antibody concentration analysis is the reason for this technique being preferred over other techniques such as SPR based instruments.

However, ELISA is a labour-intensive technique, which often requires from hours to days to obtain results from an analysis. One of the limitations of this technique is the non-specificity or cross reactivity that an ELISA assay can have with similar proteins. The sensitivity and specificity of ELISA may also vary between different laboratories. Thus, variations of analyses/results of the same specimen often occur when the specimen is analysed by different laboratories.

In the past decade, intensive effort has been put into developing techniques that are able to overcome the limitations of ELISA, and at the same time achieve a comparable sensitivity of ELISA. SPR based instruments (or biosensors) have been widely studied using different antigen-antibody interactions [25] with a view to providing this practical alternative. Biosensors were found to have the potential to replace ELISA due to their rapid and on-line (real-time) analysis (ie sample analysis can be performed outside a laboratory). A drawback, however, is the comparatively low sensitivity (compared to ELISA) of these techniques which means that biosensors are not yet in a position to totally replace ELISA as the technique of choice for analysing protein-protein interactions.

Recent studies have applied *enhancement species*, such as metal colloids, to improve the electronic signals given by biosensors (see Chapter 2 for the theory of SPR based instrument and Chapter 4 on details of signal enhancement of the instrument). Significant improvements (signal enhancement of 25 times the original signal response) through mass increase using gold colloids have been reported by Lyon et al [24], and this type of mass increase-based signal enhancement method is now being widely used in the SPR studies especially for small molecules (molecular weight of < 2 kDa).

The detection of small molecules, such as progesterone, using SPR technology is quite challenging, as small molecules by virtue of their small mass produce little change in refractive index on the surface of the sensor chip (See Section 2.4 in Chapter 2 for more details on the theory behind SPR technique). Previous studies by Karlsson et al have utilised SPR technology to detect small molecules such as biotin, theophylline, and peptide (< 1200 Da) with immobilised antibodies [26, 27]. However, the information obtained from the studies was more qualitative than quantitative due to SPR's low sensitivity towards analytes with small molecular weight.

In the study by Mitchell et al, progesterone was the small molecule of interest because of its unprecedented importance in the New Zealand agricultural industry. Progesterone is a non-aromatic female sex steroid hormone that sustains and controls pregnancy of mammals. Progesterone plays a major role in the oestrous cycle at which pregnancy may occur with timed insemination. The detection of progesterone, therefore, is the key in determining the timing of artificial insemination of livestock. Undetected or falsely detected oestrous can cause significant losses of income for the dairy and meat industries due to unexploited potential of milk and calf production.

Reports suggested that a 100% detection rate without false oestrous alert may be impossible [28]. However, with better developed sensors and techniques, significant improvement on oestrous detection can be achieved.

Mitchell et al have developed a sensitive progesterone immunoassay by using an indirect measurement protocol for the progesterone concentration in a sample. This was achieved by using an SPR based BIAcore instrument (see Section 2.4 in Chapter 2 for the underyling theory of this technique) to monitor the interactions between immobilised progesterone molecules and the anti-progesterone monoclonal antibody (mAb). The sensitivity of the BIAcore response was greatly improved by binding an enhancement species, viz., a secondary antibody immunoglobulin or SAb (IgG) conjugated to Au colloidal particles, or "SAb-Au" (see Chapter 4 for more details) on top of the mAb. The detection limit of progesterone using this "response-enhanced" assay was reported to be at 8.60 pg/mL compared to 3.56 ng/mL from a previous study (which did not use any enhancement species) by Gillis et al [29]. The enhancement species developed by Mitchell et al, however, was not at its at its most optimised. There was still room for improvement in the response that could be achieved by this enhancement method. This goal provided the impetus for this thesis.

1.7 Aim of the study

The purpose of this study was thus to improve upon the sensitive BIAcore SPR-based progesterone immunoassay that was developed by Mitchell et al. Mitchell et al.'s progesterone immunoassay used an indirect measurement in order to determine the concentration of progesterone (this involved using immobilised progesterone on the sensor surface to detect monoclonal anti-progesterone antibodies (mAb) that are not

complexed with the free progesterone molecules in a sample). The BIAcore signal enhancement in this technique was achieved using secondary antibody (IgG) conjugate with gold colloid. The resultant large mass increase (on the sensor surface) that is created by the conjugation with gold colloids was found to induce a greater response through refractive index change at the interface of the sensor from the SPR instrument (see later for theory relating to this technique). This novel enhancement system, however, suffered a drawback. The citrate-generated gold colloids prepared by Mitchell et al were susceptible to aggregation when concentrations greater than 0.1 g/L of gold salt were used. As a compromise to avoid the aggregation problems, diluted (*ca.* 0.1 g/L gold salt) gold colloids were used (to minimise or eliminate the aggregation of the colloids). As a result, the level of enhancement observed was not perceived to be at an optimum level (i.e. there was room for improvement in the enhancement). Moreover, the unstable nature of the citrate-reduced gold colloids meant preparation of fresh colloids was required frequently. Hence the "shelf-life" for any potential commercial application of this technology was severely limited. This was a potentially serious issue identified by Mitchell et al [30] in the work done.

Two main objectives were set out for this project. The first objective was to identify a suitable gold colloid preparation which could be prepared with different particle sizes and at higher concentrations than those used in studies by Mitchell et al [30]. The second objective was to use the stabilised gold colloids to prepare stable secondary antibody (IgG) – gold conjugates for BIAcore (SPR) signal enhancement.

2. Theory of Instrumental Techniques

This chapter provides a brief theoretical background to the techniques used in this study.

2.1 UV-Vis

UV-Visible spectrophotometry is a common analytical technique that is widely used in many areas of science. It can be used for colorimetric analysis, concentration measurements as well as kinetic studies.

The optical diagram of a standard dual beam UV-Vis spectrophotometer is shown in Figure 2.1-1.

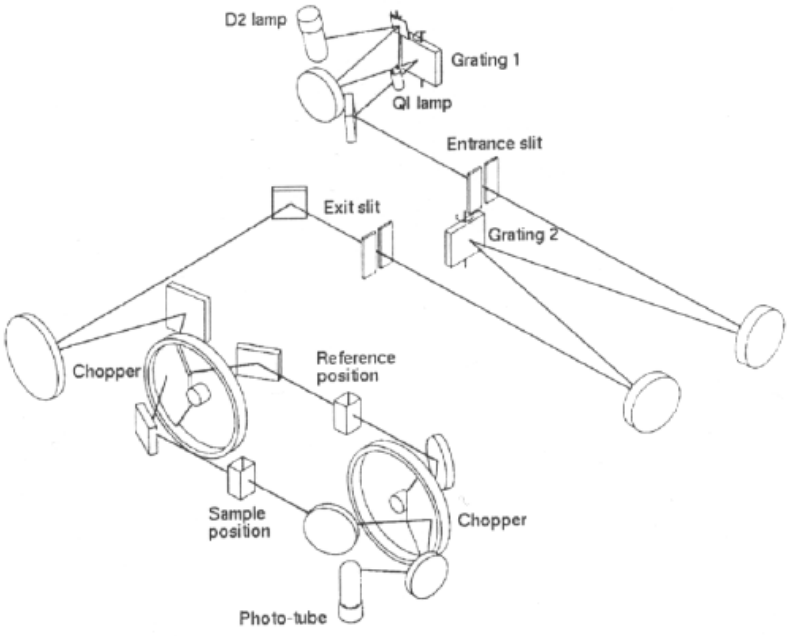

Figure 2.1-1 Optical diagram of Cary 100 UV-Visible spectrometer [58]

UV-Vis spectrometry involves absorption of electromagnetic radiation in the ultraviolet and visible region (10-800 nm) which leads to transitions between electronic energy levels in molecules. The electronic transitions (change in energy of the molecule from ground state to higher energy levels) involved are dependent and characteristic of the molecules that are being analysed.

The Beer-Lambert Law is the fundamental law underlying UV-Vis spectroscopy that relates the concentration of the sample with the absorbance of the sample. The Beer-Lambert equation is shown below. The law states that for monochromatic radiation, absorbance (*A*) is directly proportional to the pathlength (*b*) through the medium and concentration (*c*) of the absorbing species.

$$A = ebc$$

Where e = the molar absorptivity and has units of L cm^{-1} mol^{-1}.

Table 2.1-1 illustrates the relationship between absorbed colour (its wavelength) and the observed colour that is transmitted by the solution. The table is of interest in this study as gold colloids can vary in colour depending on their particle size which depends directly on their UV/Vis absorption behaviour (see Section 3.4.3 in Chapter 3).

Table 2.1-1 Colour absorbed by a sample in relation to sample colour observed

Colour Absorbed	Colour Observed	Absorbed Radiation (nm)
Violet	Yellow-green	400-435
Blue	Yellow	435-480
Green-blue	Orange	480-490
Blue-green	Red	490-500
Green	Purple	500-560
Yellow-green	Violet	560-580
Yellow	Blue	580-595
Orange	Green-blue	595-605
Red	Blue-green	605-750

2.2 TEM

Transmission electron microscopy (TEM) is a well-known imaging technique that is widely used in all branches of science but most notably in the Materials and Biological Sciences fields.

A TEM operates similarly to light microscopy. However, instead of a light beam, it uses a beam of electrons. The resolution of a TEM microscope is described by Abbe's equation, which was developed by Ernst Abbe in the 1870s.

$$Resolution\ power\ (RP) = 0.61\,l\,N.A.$$

Where l is the wavelength of the light source. $N.A.$ is the numerical aperture of the lens, which defines the maximum cone of light that a lens can take up from a point on the specimen [31]. The term $N.A.$ can be expressed as $nsina$, where n is the refractive index of the medium (approximately 1 for the vacuum in TEM), and a is the angle within the lens in which the most divergent rays can pass and form an image

(approximately 0.3° for a TEM) [31]. For an optical-light microscope, the resolution is limited by the wavelength of visible light, as the wavelength is restricted to 400-700 nm. The wavelength of electrons, however, can be adjusted to a much lower wavelength depending on the voltage at which the electrons are generated. At 50 kV, the wavelength of the electron beam is 0.005 nm which according to Abbe's equation can give a 100,000 fold increase in resolution. This is not realised in practice due to lens aberrations. The scale of improvement is in fact about 1000 times better which is enough for most purposes.

The general configuration of a TEM microscope can be illustrated by Figure 2.2-1 shown below.

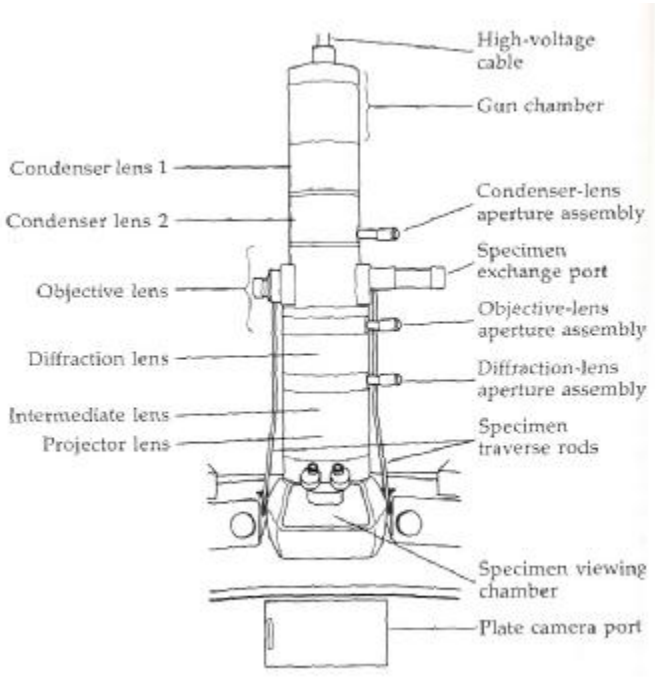

Figure 2.2-1 drawing which shows the different parts of the TEM column [32].

A beam of electron is generated in the electron gun which is found at the top of the chamber. A tungsten filament is commonly used as the source of electrons though LaB_6 filaments are also used and have a longer lifetime. Under the vacuum that exists

in the instrument, emitted electrons are accelerated by an electric field, instead of glass lenses that focus the light in a light microscope. Focus to a very thin beam of elecetrons can be achieved in TEM. The electron beam then travels through the sample, which is carefully deposited onto a collodion coated copper grid. The sample grid is inserted into the system using a specimen rod similar to the one shown in Figure 2.2-2.

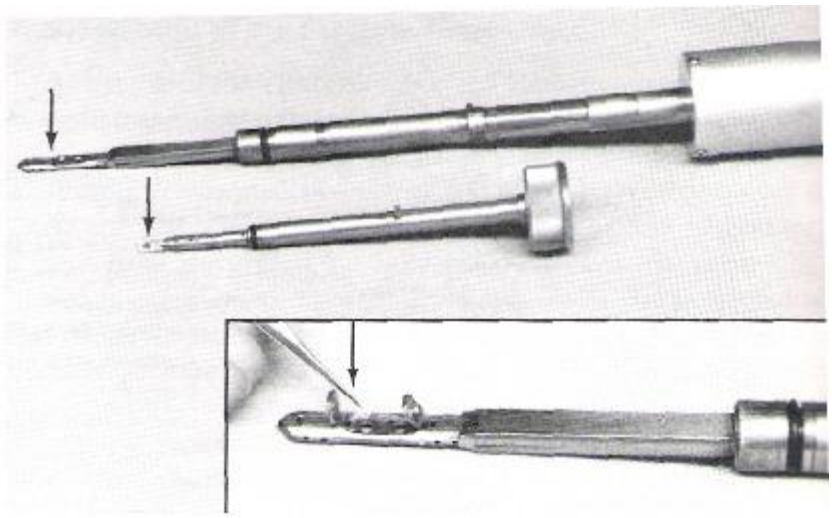

Figure 2.2-2 TEM specimen rod. The sample (deposited on the copper grid) is inserted at the place on the rod indicated by the arrow and the sample grid is held in place by a spring clip [32].

As the beam strikes the specimen on the collodion coated grid, the electrons can exhibit three different interactions. Electrons may be absorbed into a thick portion of the specimen or by atoms with high atomic numbers. Absorption processes may cause a build-up of heat in the area and result in distortion or destruction of the sample. In TEM, absorption of electrons does not contribute significantly to image contrast. Another interaction involves the elastic scattering of electrons. This occurs when electrons from the beam interact with the *nuclei* in specimen atoms. The electrons undergo by virtue of the interaction a large deviation in their path without loss of

energy. Elastically scattered electrons contribute to both amplitude and diffraction contrast in a TEM image. The third interaction is inelastic scattering, which is produced when electrons from the beam interact with *electrons* in specimen atoms. This interaction is particularly important for imaging samples of low atomic number. Inelastically scattered electrons contribute to chromatic aberration and phase contrast [31]. The image formation is based on the amount of electrons that are being scattered which is essentially dependent on the thickness or density of the sample. The image can be captured with a digital camera which is fitted into most conventional instruments and studied (e.g. for particle size measurements) using image processing software.

2.3 Zetasizer

2.3.1 Introduction

Colloids prepared need to be characterised in terms of their particles size distributions and their zeta potential. Traditionally colloidal systems have had their particle size distributions measured by TEM where the colloidal particles are removed from solution by evaporation onto a collodion coated copper grid [32, 33, 34]. Images from the TEM are then analysed using pixel measurements available on an image processing program. Thus TEM is an *ex* situ method for measuring particle size. Where *in* situ particle size measurements are needed, a light scattering photon correlation spectroscopy (PCS)-based technique must be used. The Zetasizer is an instrument which incorporates a PCS technique (see later) to measure the size and zeta-potential of colloidal particles.

The electronic setup of a typical Zetasizer 3000HS by Malven is illustrated in Figure 2.3-1.

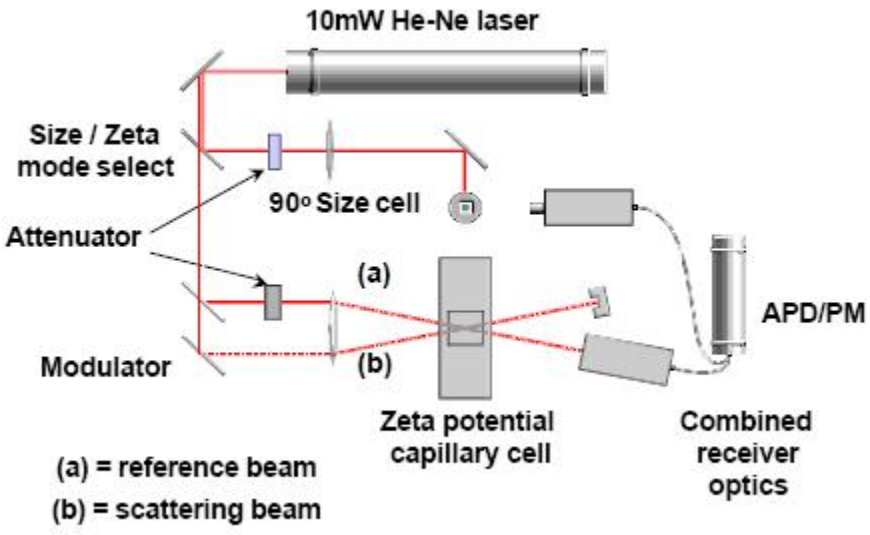

Figure 2.3-1 Optical diagram of Zetasizer 3000HS [38]

With conventional dynamic light scattering (DLS) instrument such as Zetasizer 3000HS, the particle size is an important factor in determining the maximum concentration at which the sample can be measured. Each sample has its own optimal measuring condition. If the concentration is too low or the particle size is too small, the amount of light scattered is not sufficient to make a measurement. If the sample is too concentrated, multiple scattering can occur. This involves scattered light interacting with other particles before reaching the detector. Consequently, the apparent measured particle size is reduced [35].

2.3.2 How size is measured on Zetasizer instrument

Dynamic light scattering (DLS), also known as quasi-elastic light scattering (QELS)

or photon correlation spectroscopy (PCS) is a technique that can quickly determine the particle size with minimal sample preparation.

When the laser light from the Zetasizer hits small particles the light scatters in all directions with equal intensity (Rayleigh scattering). With large particles, the intensity is angle dependent (Mie scattering). In both cases, a time-dependent fluctuation in the scattering intensity is observed. These fluctuations are due to the Brownian motion that the colloidal particles are undergoing in the dispersion medium. The scattered light by a particle can either form constructive or destructive interference with light scattered by the neighbouring particles within the illuminated zone. These interferences give rise to the intensity fluctuation at the detector plane. The moving speckle pattern can be detected by a photon correlator, which works by counting the number of speckles/photons in a different time span rather than measuring the intensities of the scattered light [36]. A correlator has over a hundred channels to carry out the measurement, and each channel measures the fluctuation at a particular time span or time delay. With a short time delay, τ, the particles have not moved a great distance between the initial measurement at time (t) and the measurement at time (t + τ). Hence, the correlation between them is high. However, with larger values of τ, the particles have moved some way from their initial positions due to Brownian motion, and the measurement made at time (t + τ) is therefore much less correlated to the initial measurement. An autocorrelation function can be derived from the number of photons counted at each time delay. As time delay increases, the autocorrelation function decreases exponentially.

Now, with large particles, the Brownian motion is relatively slow compared to small particles which move more quickly. Therefore, the autocorrelation function of large

particles decays at a slower rate. This rate of decay is essentially related to the translational diffusion coefficient (D) of the colloidal particle. This can then be related mathematically to a hydrodynamic radius using the well known Stokes-Einstein equation.

$$D = \frac{kT}{6phR}$$

Where D is the diffusion coefficient; R is the hydrodynamic radius; k is Boltzmann's constant; T is the temperature in Kelvin, and h is the viscosity of the suspension.

Particle size distributions are obtained by numerically processing the autocorrelation function with algorithms based on assumed distributions. A monodisperse sample would give rise to a single exponential decay, and the distribution calculation can be easily performed. For polydisperse samples, a series of exponential decays are involved and several complex algorithms have to be applied for calculating the distribution. In the Malven Zetasizer, there are five modes of analysis to choose from, namely Monomodal, Multimodal, Contin, Non-negatively Constrained Least Squares (NNLS), and Auto.

For Malvern Zetasizer, the conversion of scattered light intensity to particle size is based on Rayleigh's theory, which implies that the light scattering intensity, I, is dependent on the radius of the colloidal particle, R, to the sixth power (ie. $I \propto R^6$). This relationship is critical to the PCS technique as it essentially means that the scattering intensity of larger particles (large R value) will dominate over the scattering intensity of smaller particles. Hence, if two particle size distributions on either sides

of the size scale are present in a colloidal sample, the size distribution at a lower size range may be overlooked as the scattered light produced by larger particles is much intense than the scattered light produced by smaller particles. More importantly if aggregated or large macroparticles of dust are present these will also contribute to the signal and may distort the particle size result. Therefore, when interpreting the Zetasizer size results it is important to look at all four mean particle size values, namely intensity based mean particle size, volume based mean particle size, number based mean particle size, and Z-average (Z_{ave}) value (see Section 3.4.5 in Chapter 3 for more details on the four particle size measurements and the relative accuracy of each).

2.3.3 Making a measurement

Sample preparation for zetasizer measuremens is minimal before analysis as colloids can be sampled directly as received in most case. Sample concentration, however, is an important issue for size measurement. In order to satisfy Rayleigh and Mie theory, dilution of colloidal dispersion is required for particle size analysis to avoid multiple light-scattering by particles. Dilution of sample for size measurement should be done with the dispersion medium in which the colloidal particles are suspended in [37]. Particle count-rate which is measurable on the instrument using a screen counter in the software is a good indication for the scale of dilution required before analysis. Count-rate of around 100 to 250 KCps (thousand counts per second) are considered ideal for size measurements.

Cleanness of the sample cell is also crucial prior to analysis. Contaminants and air bubbles can skew the size measurements as mentioned earlier. Since materials such as

dusts particles are much larger than colloidal particles, the intensity of light scattered by them will dominate over the light scattered the sample. Even random measurements of passing dust paticles within the measurement zone of the sample can affect the results though there is a facility within the software which can reject any skewed results caused by random dust particle scattering in the sample during measurement.

The Zetasizer size result has four major parameters for determining the quality of the results produced by the instrument. These four categories are listed and explained in Table 2.3-1. The particle size result is treated as a "fail" if any of the criteria shown in Table 2.3-2 are met.

Table 2.3-1 Four parameters given by the Zetasizer to indicate the quality of the particle size result [37]

Polydispersity	The width of the distribution
Quality	This is an indication of the success of the measurement. Only two values are displayed, pass or fail
Merit %	Signal to background ratio for the experiment. Sample dependent, may vary between 5% to 90%
In range %	Guide to the success of an experiment. Over 98% is excellent. Over 95% is good and can be used for a distribution analysis. Over 85%, is satisfactory, but the data are only good enough for a cumulants analysis and not a distribution analysis
Fit	Indication of the success of the measurement and analysis. Any value greater than 0.01 is a poor fit

Table 2.3-2 Some of the common failing criteria when measuring the particle size using the Zetasizer [37]

Parameter	**Fail criteria**
Count rate	< 10Kcps, or > 500Kcps
Merit	<10%, > 99%
Polydispersity	> 0.7
Fit Error	> 0.005
In Range	< 80%

2.4 BIAcore

2.4.1 Introduction

BIAcore is currently an emerging analytical technique that monitors the interactions between biomolecules in ***real-time***. It is capable of performing quantitative analyses as well as carrying out kinetic studies. The name, BIA, is short for Biomolecular Interaction Analysis. The company that developed the series of BIAcore instruments is based in Uppsala, Sweden, and it is now part of GE Healthcare.

BIAcore 3000 was the model used in this study (see later). The BIAcore consists of a running mobile phase, which is continuously pumping HEPES (4-(2-hydroxyethyl)-1-piperazineethanesulfonic acid) buffered Silane (HBS) running buffer through a microfluidic flow-cell (see later) and sensor chip compartment (see Figure 2.4-1).

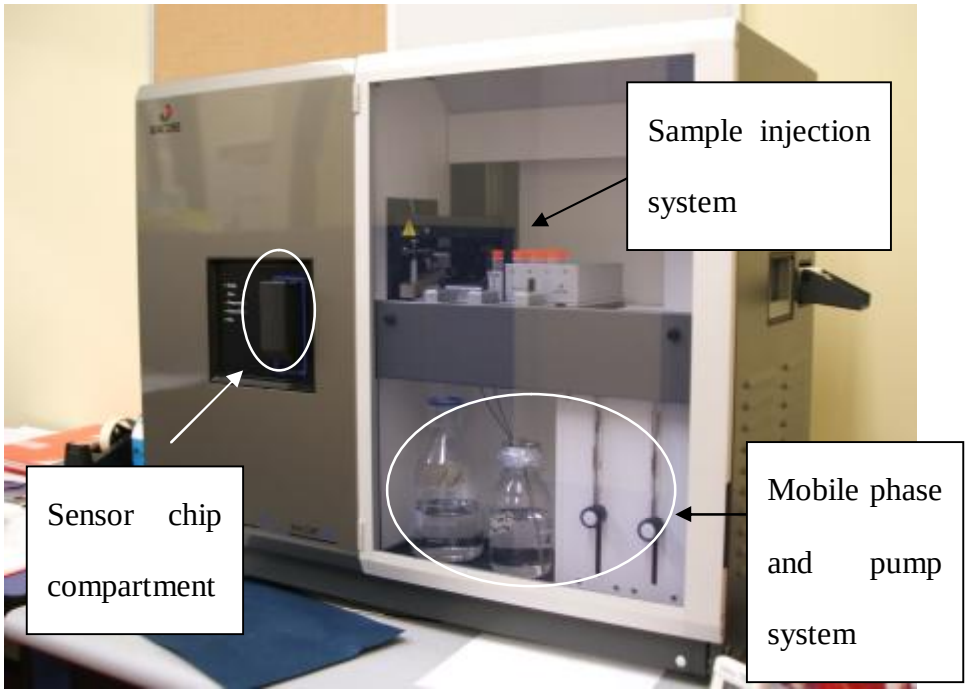

Figure 2.4-1 A BIAcore instrument

The preparation of the HBS-EP running buffer is made up of 0.01 mol/L HEPES [pH 7.4], 0.15 mol/L sodium chloride, 0.003 mol/L EDTA, 0.005% v/v P-20 surfactant (Biacore AB, Uppsala, Sweden). The sensor chip, which can contain self-assembled monolayers of reactive sites, such as carboxyl, amino, epoxy, and biotinyl groups [38], acts like a column in an LC system; interactions between analytes and immobilised ligands occur on the surface of the sensor chip. Samples are fed into the microfluidic flow system by an auto sampler, which can take volumes of sample ranging from 5 µL up to 325 µL. The method of injection can be chosen from a list of options. "Quickinjection" is often used when conservation of sample is required. "Injection", which requires slightly higher injection volume, is used for immobilisation of ligands. When target analytes are flowed over the sensor chip surface the interactions with the immobilised ligands are monitored using surface plasmon resonance (SPR) technology (see later for theory). The BIAcore instrument thus monitors the analyte-ligand interactions in ***real-time*** through changes in refractive index on the

surface of the sensor chip. These changes in refractive index are induced by the accumulation of mass at the chip/solution interface which occurs due to the analyte-ligand interactions. The refractive index changes wrought by the surface interactions are reported in graphs called, "sensorgrams", which will be described in more detail later in this chapter.

2.4.2 Microfluidic Flow-cell system

The microfluidic flow-cell is an important component of the BIAcore system. It allows precise deliveries of analyte to the sensor chip surface. An integrated micro-fluidic cartridge (IFC) has four independent flow-cells in standard BIAcore 3000. These four cells can be used to analyse interactions between different analytes and different binding partners in series, like a separating column. The cells can also be used independently or in combination, in which the latter method involves reference subtraction to eliminate non-specific binding or solvent effects and obtain sensorgrams that reflect true surface interactions.

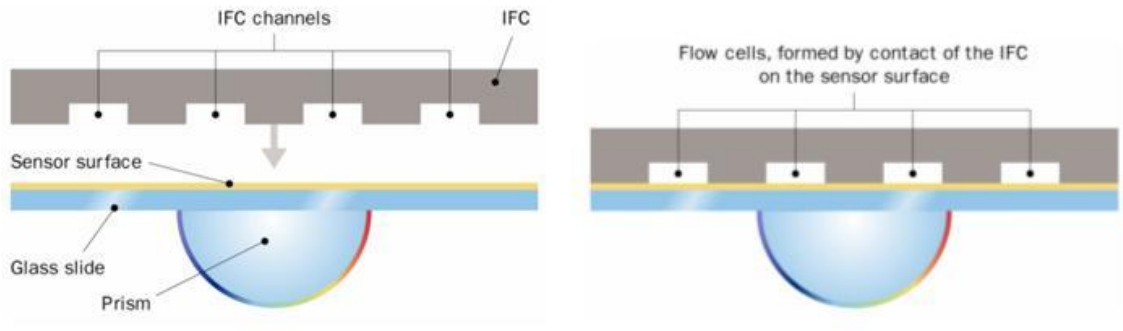

Figure 2.4-2 Formation of microfluidic flow-cells on the surface of a sensor chip (www.biacore.com)

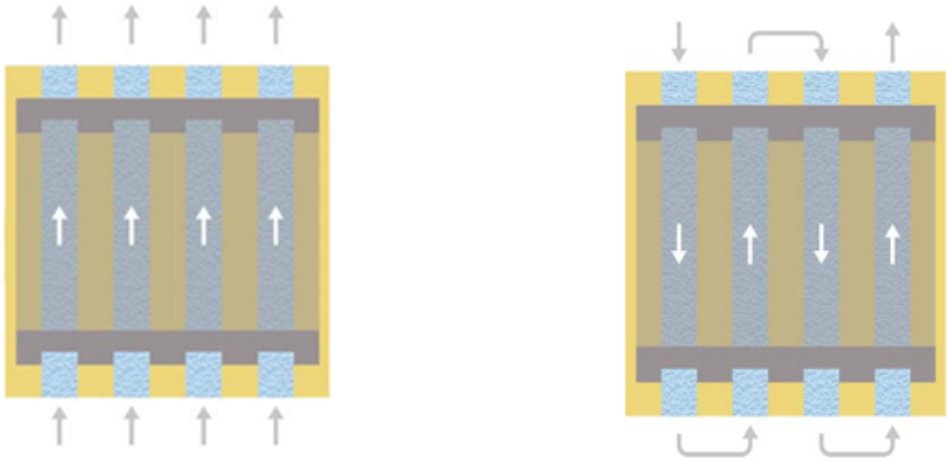

Figure 2.4-3 The four flow-cells can be used independently (left) or in series (right) (www.biacore.com)

2.4.3 Surface plasmon resonance (SPR)

SPR is the underlying technique used in BIAcore instruments. SPR is an optical-electrical phenomenon induced by the interaction of light with a metal surface. In the case of a BIAcore, a thin gold film deposited on the sensor chip is involved with generating the SPR effect. The interaction involves an energy transfer from photons of light to clusters of free electrons on the gold surface at a specific resonance wavelength. This is a special phenomenon which is restricted to substrates like silver, gold, and copper and is responsible for such phenomena which underlie techniques like SERS (Surface Enhanced Raman Scattering). It is also responsible for the surface plamson resonance peaks that are detected in the UV-Visible spectra of gold, silver, and copper colloids and which give rise to the characteristic colours of these colloidal dispersions.

The sensor chip of BIAcore is made up of a glass plate coated with a 50 nm thick film of gold (see Figure 2.4-4). On top of the gold film, a coupling layer may be grafted (or

which is available commercially with the layer already applied to the gold chip surface) that contains numerous active sites such as carboxyl or amine groups (the coupling layers used in this study will be discussed in Section 4.3 in Chapter 4). Ligand molecules can be immobilised at these active sites after surface activation (see later).

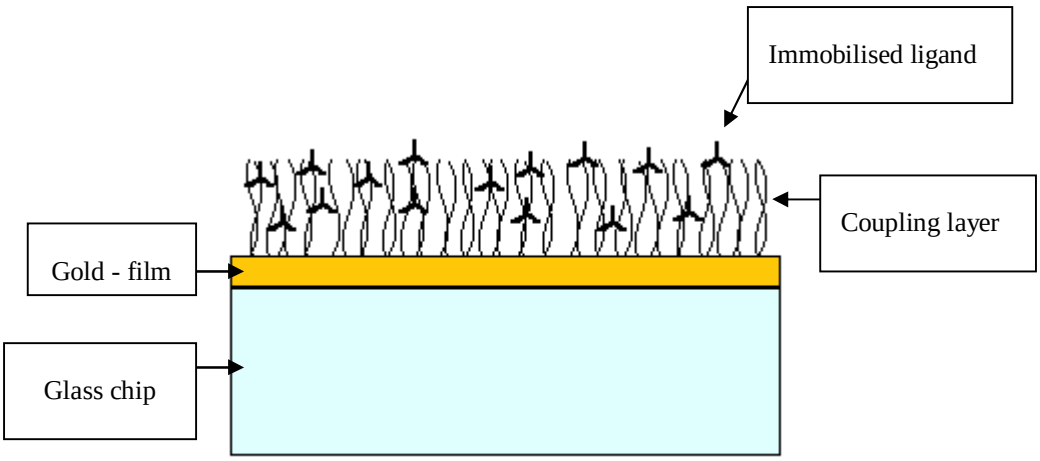

Figure 2.4-4 Illustration of the modified sensor surface

Each sensor chip is encased in a plastic cover for storage. In order for SPR to occur, a prism is mounted on the glass-side of the sensor chip, and the incident light is passed through this prism and on to the gold surface. The use of prism allows parts of the incident light to couple with the metal surface and other parts to be reflected off to the detector. As light travels from a medium with higher refractive index to a medium with lower refractive index above a certain angle, total internal reflection of light occurs. When a thin gold film is inserted in between the two media most wavelengths will be reflected off the metal surface. However, at a specific wavelength or the resonance wavelength which satisfies the resonance conditions, the light is almost completely absorbed by the gold surface (see Figure 2.4-5). This creates a drop in intensity of the reflected light, which can be identified by a spectrophotometer. The angle at which this sharp decrease in intensity of reflected light occurs is termed the

SPR angle.

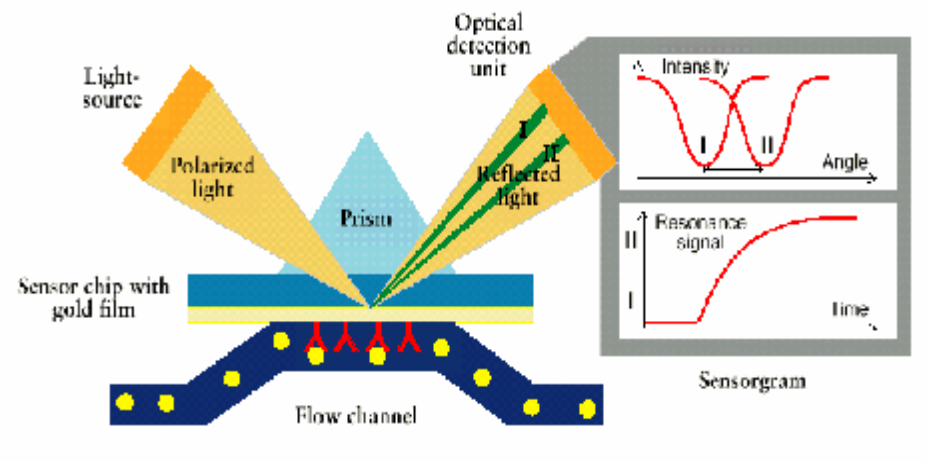

Figure 2.4-5 A diagram which shows how the instrument detects the change in SPR angle and produces a response signal [39]

Plasmons, a group of excited electrons which behave like a single electrical entity, are created when light is coupled to the metal surface, and this coupling is responsible for the drop in intensity of the reflected light. The plasmon, in turn, generates an *evanescent* electrical field which extends about 300 nanometres above and below the metal surface. Any change in chemical composition or refractive index at the metal surface results in a change in the wavelength at which the light resonates with the surface electrons. SPR is also able to monitor the accumulation of mass at the metal surface (see Section 4.1 in Chapter 4). This is essentially the principle behind signal enhancement of SPR technique. When the mass/refractive index on the metal surface changes a change in the SPR angle is observed. The detector is thus able monitor the movement of the SPR angle in real-time, and the data are presented in graphs called sensorgrams.

A sensorgram (see Figure 2.4-6) is a simple graphical representation of the interaction

between the surface of the sensor chip and the analytes with respect to time.

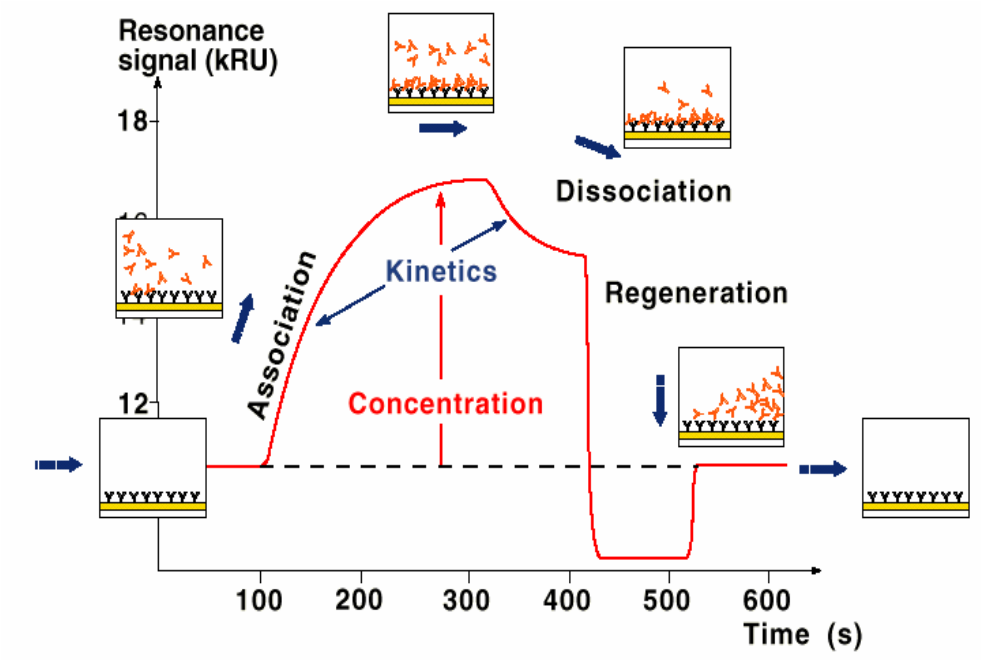

Figure 2.4-6 Illustration of the characteristic response signal of different types of interaction [39]

The response in response unit (RU) is on the y-axis of the sensorgram. It fluctuates according to changes in refractive index on the sensor chip surface. If interaction occurs between the analytes and the surface, the response would gradually increase over a period of time until no more analytes are flowed pass the surface. With strong analyte-surface interaction, the response would stay above the baseline, and regeneration buffer is required to remove the analyte from the surface, and bring the response back down to the baseline (see Figure 2.4-6). In the case of weak interaction, analytes would gradually dissociate from the surface with running buffer; therefore, surface regeneration is not required. The dissociation is illustrated by a gradual decrease of response to the baseline (see Figure 2.4-7).

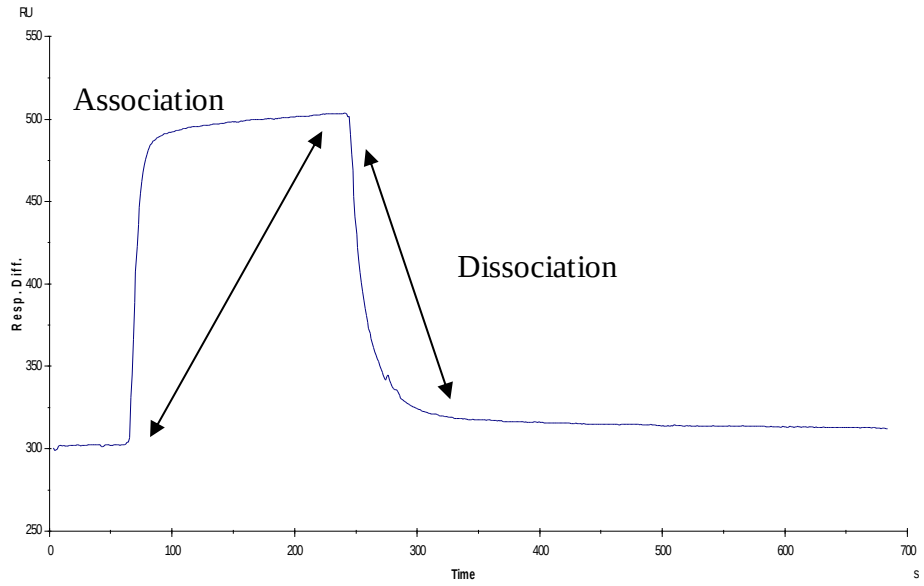

Figure 2.4-7 Sensorgram of a system involving a weak binding interaction, which does not require regeneration

2.4.4 Immobilisation of macromolecules

Various types of macromolecules/ligands can be immobilised onto the sensor chip surface after it is activated with a mixture of *N*-ethyl-*N*-(3-dimethylaminopropyl)-carbodiimide (EDC) and *N*-hydroxysuccinimide (NHS). This process converts the carboxylic acid groups on the surface to active esters. Under the appropriate pH, macromolecules can then be immobilised on the surface by forming amide linkages with the amino groups of these molecules[40]. Other linkages such as biotinyl, carboxyl, and epoxy are also possible [38].

The optimum pH for immobilisation should give the highest response when passing macromolecules over the surface. This can be determined by "pH scouting", which involves a "trial and error" approach to monitor the responses of the inactivated sensor surface towards the molecule at different values of the pH. Once the

macromolecules are immobilised on the surface, the un-reacted carboxylic acid groups are deactivated by reaction with ethanolamine to ensure minimal non-specific binding and no further immobilisation.

After immobilisation, the surface is purged with weak HCl, NaOH, glycine, or organic solvent such as acetonitrile [41] to ensure any unbound macromolecules are removed from the sensor surface. Any unbound or weakly bound macromolecules in the system would give inconsistent responses from the instrument. The choice of regeneration buffer is very important, as it should wash away any weakly associated analytes on the surface without stripping off the immobilised macromolecules.

2.4.5 Applications

Since the introduction of BIAcore in 1990, the system has been widely used for thermodynamics, kinetics, affinity, and concentration analyse in various areas namely, protein interaction study in basic researches, drug discovery and development [42], herbicide detection [43], as well as quality control in industries such as the dairy industry [44].

In drug discovery, preliminary steps such as target identification, screening and optimisation of lead candidates are very important. SPR based instruments provide the essential technology for rapid and informative study of the interactions between drug compound and drug target. BIAcore has been used in many studies involving drug screening. Some of them are listed in Table 2.4-1.

In addition to these screening applications, absorption, distribution, metabolism, and

excretion (ADME) predictive assays have also been developed using BIAcore. One of these assays is based on interactions between small molecules and liposome surfaces for prediction of absorption properties [45]. Another assay involves the determination of the complex affinity between drug and albumin interactions, which essentially provide information on drug compatibility and appropriate dosing levels [46].

Table 2.4-1 Some of the drug targets and binding partners that were being studied by using BIAcore [47]

Drug Target	**Interaction Partner**
DNA	Indolcarbazole analogues
DNA	R 132 compound
DNA	Furonapthalimides
DNA	Chromomycin, mithramycin, distamycin
DNA	Furmidine analogues
Elastase, hyaluraonidase, and lysozyme	Sulfated polysaccharides
Estrogen receptor	Agonists and antagonists
HIV-1 protease	Transition state analogue inhibitors
Quadruplex DNA	Ditercalinium
Thrombin	Thrombin inhibitors

Concentration analysis of residue chemical, drugs, toxins, or nutrients in food industry is one of the most important applications of the SPR technology. The presence of herbicides or pesticides in vegetables, crops, and fruits as well as veterinary drugs in meats, milk, and fish are serious issues for farmers, food industry, and consumers. The appropriate level of nutrients that are being added to food products is also an interest for the industry and the consumers. Direct detection of bacterial species such as Salmonella using immobilised antibodies in BIAcore has been reported [48]. A rapid sandwich immunoassay was also developed to determine the level of protein toxin, staphylococcal enterotoxin B in milk and meat [49]. The development of inhibition assays based on competition between antibodies binding to immobilised antigens and

free antigens in the sample have also been widely reported [47]; for example, measurement of progesterone in milk [29]. Inhibition assays involving progesterone-antibody interactions are of relevance to this study.

3. Preparation & Characterisation of Gold Nanoparticles

3.1 Introduction

This chapter is devoted to research done on finding a suitable gold colloid preparation to be used as an enhancement species for the BIAcore SPR work. The preparation of gold (Au) colloids is well established in the chemical literature. There are various methods available for preparing colloidal gold. The preparations in this study involved the chemical reduction of Au (III) salts to Au metal. Three reducing agents were used in this study; hydrazine hydrate, sodium borohydride, and tri-potassium citrate.

Au colloids, especially when concentrated, are generally unstable as these unprotected particles are susceptible to aggregation and sedimentation over time. Hence, the use of a protecting agent to induce steric stabilisation is crucial for keeping Au colloidal particles suspended in solution. Arabinogalactan (AG), a polysaccharide extracted from trees of genus Larix (known as "Western Larch"), has been demonstrated to be effective in maintaining colloidal particles in a stable suspension [50]. AG consists of a backbone of D-galactopyranose residues with individual D-galactopyranose linked together by β-(1→3) configuration. The majority of these residues bear branches consisting of either one or two D-galactopyranosyl residues linked β-(1→6) [50]. The study by Ponder et al. suggests that single AG molecules undergo transition to form trimers with spherical shape [51].

Arabinogalactan was the protecting agent of choice because it is highly soluble in water. Moreover, the viscosity of arabinogalactan solution does not increase dramatically when high concentrations of the polysaccharide are dissolved in water [52].

In finding a recipe which produces stable colloidal Au suitable as an enhancement species in BIAcore-based SPR measurements, various concentrations of Au salt, reducing agent, and arabinogalactan were employed. After each preparation, the Au colloids were subjected to a series of characterisation analyses including pH measurements, UV-Vis spectrophotometry, Zetasizer size analysis, and TEM size measurements.

3.2 Materials

The gold salt used in this study was potassium tetrabromoaurate (III) ($KAuBr_4$) salt (assayed as 98% pure) provided by Monash University, Melbourne Australia. 99-100% hydrazine hydrate (BDH Chemical Ltd, Poole England), 98% sodium borohydride powder (Aldrich, Milwaukee, WI, USA), and tri-potassium citrate (BDH, Poole, England) were the reducing agents used. The protecting agent, arabinogalactan (UF powder) was provided by Larex Inc. (now trading as Lonza Group Ltd. as of 2006). 70% nitric acid (Ajax Finechem, Australia) and 36% hydrochloric acid (Ajax Finechem, Australia) were used for cleaning glassware.

3.3 Gold Nanoparticle Preparation

In the previous study by J. Mitchell, citrate reduction of tetrachloroauric acid ($HAuCl_4$) was the preferred method for the preparation of colloidal gold. The reason for this was because it was a preparation for which particle size of the resultant colloids was well controlled/predicted and it gave monodisperse colloids However, the citrate reduced colloids prepared in that study had short-term stability which necessitated the use of low concentrations of starting gold(III) salts (0.01 % w/v or 2.9×10^{-4} mol/L) salts when preparing the colloids.

In this study, the use of the reducing agents stated above together with the arabinogalactan were tested as alternative synthetic methods for preparing colloidal gold with the aim of producing higher stability and more concentrated gold colloids that could be used in the BIACore measurements as enhancement species.

Prior to each preparation, all glassware was cleaned with aqua regia, which was prepared by adding 75 mL of concentrated hydrochloric acid (HCl) to 25 mL of concentrated nitric acid (HNO_3). After washing, the glassware was rinsed with 18 M Ω Milli Q water.

Numerous preparations which used varying starting concentrations of potassium tetrabromoaurate, $KAuBr_4$, the reducing agents and the arabinogalactan were tested before identifying the optimum synthetic procedure that was then used consistently in this study (see Section 3.3.1 to 3.3.3). Table A-1 and A-2 in Appendix A contains all the gold colloid recipes tested in this study. The reactions used concentrations of 3 to 50 g/L for arabinogalactan dissolved in 0.0014 to 0.007 mol/L of $KAuBr_4$ solution.

The concentrations of hydrazine hydrate used ranged from 0.0002 to 0.002 mol/L, and sodium borohydride concentration used ranged from 0.008 to 0.08 mol/L. No extensive study was carried out with potassium citrate (i.e. at different concentrations) in this project, since this method of reduction is well established. All colloidal samples were prepared by adding 5 mL of reducing agent dropwise to an identical volume of $KAuBr_4$ solution in a stirred beaker at room temperature. This led to the immediate formation of ruby red, purple or blue gold colloids. The gold colloids were then characterised by performing pH, UV-Vis and size analyses, and stored at room temperature away from sunlight at room temperature. Colloid samples were regarded as stable, if no visual evidence of sedimentation was detected two weeks after preparation. The following sections give details of the optimum gold colloid preparations decided upon after the development work described above.

3.3.1 Gold colloids prepared by hydrazine reduction

0.0014 mol/L of $KAuBr_4$ solution was prepared in 18 MΩ deionised water. The $KAuBr_4$ solution was normally prepared in batches of 20, 25, or 50 mL. 0.05 g of arabinogalactan was dissolved in each of three 5 mL aliquots of the 0.0014 mol/L $KAuBr_4$ solution to obtain an initial AG concentration of 10 g/L. 8.7 µL, 17.5 µL, and 35 µL of neat hydrazine hydrate were diluted with 18 MΩ deionised water to make 25 mL of 0.007 mol/L, 0.014 mol/L, and 0.029 mol/L of hydrazine hydrate respectively. Each 5 mL aliquot of $KAuBr_4$ with 10 g/L arabinogalactan was agitated with the magnetic stirrer on a medium speed setting. 5 mL of each concentration of hydrazine hydrate was then added drop-wise to the three respective 5 mL aliquots of $KAuBr_4$ solutions with stirring. The orange colour of the $KAuBr_4$ solution changed to ruby red or purple (depending on the concentration of the hydrazine hydrate added)

after the addition of the hydrazine hydrate solution. The stirring was continued for a further 30 seconds after the addition of hydrazine hydrate. The magnetic stirrers were removed from the samples, and each sample was stored in a closed vial at room temperature.

3.3.2 Gold colloids prepared by sodium borohydride reduction

0.0014 mol/L of $KAuBr_4$ solution was used in the reactions involving sodium borohydride reduction of Au(III) to colloidal Au. 0.05 g of arabinogalactan was dissolved in each of three 5 mL aliquots of the $KAuBr_4$ solution to produce 10 g/L arabinogalactan in $KAuBr_4$ solution. 0.007 mol/L, 0.014 mol/L, and 0.029 mol/L sodium borohydride, $NaBH_4$ samples, were prepared by dissolving 0.0066, 0.0137, and 0.0273 g of sodium borohydride respectively in three separate flasks containing 25 mL of 18 MΩ deionised water. The three 5 mL aliquots of 0.0014 mol/L $KAuBr_4$ solution and the three different concentrations of sodium borohydride solutions were cooled to ~4 °C on ice. Stirring of the cooled $KAuBr_4$ solutions was then commenced and to each solution, 5 mL of each concentration of sodium borohydride was then added drop-wise. The orange $KAuBr_4$ solution turned to an orange/brown colour upon the addition of each concentration of sodium borohydride. The stirring continued for a further 30 seconds after the addition of sodium borohydride. The colloid samples were stored without further in a sealed vial at room temperature.

The same procedure was carried out with a $KAuBr_4$ solution at the higher concentration of 0.0072 mol/L, so that more concentrated colloids could be obtained.

The concentrations of sodium borohydride solution were also were also scaled up to 0.036, 0.072, and 0.144 mol/L. The resulting colloidal samples were stored at room temperature.

3.3.3 Gold colloids prepared by tri-potassium citrate reduction

0.007 mol/L, 0.014 mol/L, and 0.029 mol/L tri-potassium citrate solutions were prepared in 18 MΩ deionised water. 5 mL of 0.04% w/v or 0.0014 mol/L $KAuBr_4$ solution was added to each of three 20 mL round bottom flasks. The $KAuBr_4$ solutions were then brought to the boil. Immediately after the boiling point was reached, 5 mL of each concentration of tri-potassium citrate was added drop-wise to the respective flasks. The orange $KAuBr_4$ solution underwent a series of colour changes while the citrate solution was being added (see Section 3.4.1 for details on the colour changes). The final colour of the gold colloids was ruby red for the two samples with 0.007 and 0.014 mol/L of tri-potassium citrate. The colloids made from the 0.029 mol/L tri-potassium citrate turned purple. They were then gently boiled for 10 minutes before being cooled to room temperature. These three samples of Au colloids were transferred into three separate capped sample vials and stored at room temperature.

Two further samples of Au colloids were prepared again with 0.007 and 0.014 mol/L tri-potassium citrate by following the procedure described above. Each sample was subsequently divided into two parts and labelled “with arabinogalactan” and “without arabinogalactan”. 5 mL of each of these separate colloidal sample parts was added to

three separate sample vials into which. 0.025 g of arabinogalactan was dissolved and thoroughly mixed. These constituted the “with arabinogalactan” samples. Any remaining colloids of each sample were transferred to three other sample vials. These constituted the “without arabinogalanctan” samples. All four vials were capped, and samples stored at room temperature until further analysis.

All samples of gold colloids prepared from the three different routes of reduction are summarised in Table 3.3-1. The sample numbering protocol comprises the date of preparation (first 6 digits of the sample number) and the concentration of the reducing agent used (last digit, where 1 = least concentrated and 3 = most concentrated). In the case of citrate reduction, the letters A and B were also used to distinguish between samples with and without added arabinogalactan (A = without and B = with).

Table 3.3-1 Summary of the gold colloids prepared

Reducing Agent	**Sample**	**Concentration of $KAuBr_4$ (mol/L)**	**Concentration of Reducing Agent (mol/L)**	**Mole Ratio ($KAuBr_4$: Reducing Agent)**
Hydrazine Hydrate	010806-1	0.00144	0.007	1 : 5
	010806-2	0.00144	0.014	1 : 10
	010806-3	0.00144	0.029	1 : 20
Sodium Borohydride	040806-1	0.00144	0.007	1 : 5
	040806-2	0.00144	0.014	1 : 10
	040806-3	0.00144	0.029	1 : 20
	130806-1	0.00721	0.036	1 : 5
	130806-2	0.00721	0.072	1 : 10
	130806-3	0.00721	0.144	1 : 20
Tri-potassium Citrate	070806-1	0.00144	0.007	1 : 5
	070806-2	0.00144	0.014	1 : 10
	070806-3	0.00144	0.029	1 : 20
	160806-1A	0.00144	0.07	1 : 5
	160806-1B	0.00144	0.07	1 : 5
	160806-2A	0.00144	0.014	1 : 10
	160806-2B	0.00144	0.014	1 : 10

3.4 Observations, characterisation, and general discussion on gold colloids prepared for this study

3.4.1 Observations

Gold colloids are intensely coloured. From the orange solution of $KAuBr_4$, it can be converted into colloidal gold with colours ranging from brown, red, purple, blue, and yellow depending on the size of the colloidal particles. The colour transformation can be easily picked up by the naked eye, and this is a simple method for checking whether the reduction reaction of Au (III) ions to Au metal has taken place; though a more rigorous confirmation of reaction completion was achieved through the use of UV-Vis spectrophotometric measurements on the colloids (see later).

Colloids prepared via citrate reduction underwent a series of colour transformation during the preparation. When the orange $KAuBr_4$ solution started to boil the addition of a few drops of tri-potassium citrate caused the colour of the solution to fade to yellow. With addition of a little more citrate, the solution became clear. Before all of the 5 mL of tri-potassium citrate was added to the $KAuBr_4$ solution, the colour of the solution changed to indigo before finally turning purple. This was the final colour of the colloids prepared with 0.029 mol/L tri-potassium citrate. This sample of gold colloids later aggregated, as it cooled to room temperature. In contrast, the two other samples prepared with lower concentrations (0.007 and 0.014 mol/L) of citrate underwent colour changes from purple to ruby red as a final colour, which suggested

that these two samples had smaller particle sizes and that aggregation had not occurred to any great extent during the preparation.

Less variable colour change was observed in the preparation of the hydrazine and borohydride reduced gold colloids. In these preparations, the $KAuBr_4$ solution turned ruby red with the first few drops of reducing agent added. The final colour was red for most of the samples after the reactions were completed. However, gold colloids prepared by reducing 0.0072 mol/L $KAuBr_4$ solution with 0.144 mol/L sodium borohydride turned red with a tint of purple. As expected, the subtle purple colour was caused by some large particles in the sample of colloids, an observation that Faraday explained in his famous 1856 [3] paper.

For gold colloids prepared by reducing 0.0014 mol/L $KAuBr_4$ solution with 0.007 mol/L and 0.014 mol/L sodium borohydride, the colloid colours were brown/red. The brown colour might be an indication that very small colloidal particles were present in the dispersion [53]. The colour of the colloids was suspiciously similar to the colour of the $KAuBr_4$ solution; however, the UV-Vis spectra of these samples later confirmed that most, if not all, of the Au (III) were reduced to Au metal (see later).

Colloidal samples prepared by hydrazine reduction were particularly unstable because they usually aggregated within two weeks of preparation. Indeed, colloids prepared from 0.0014 mol/L $KAuBr_4$ solution with 0.029 mol/L hydrazine hydrate aggregated and dropped out of solution one day after the preparation while the other two colloidal samples prepared from 0.007 and 0.014 mol/L hydrazine hydrate had changed from red to purple within a week, with sedimentation occurring after one week. These observations indicated that larger particles sizes had been generated in these

preparations.

Borohydride reduced gold colloids were in contrast very stable. No aggregation was observed in most samples after many weeks of storage at room temperature. One of the more concentrated gold colloids prepared from 0.0072 mol/L $KAuBr_4$ solution and 0.144 mol/L sodium borohydride did, however, aggregate immediately after the preparation.

Gold colloids prepared from 0.0014 mol/L $KAuBr_4$ solution with 0.029 mol/L tri-potassium citrate was aggregated immediately after preparation. The 0.007 and 0.014 mol/L tri-potassium citrate reduced gold colloids were unstable without arabinogalactan as the colour of the unprotected colloids changed from red to purple over the period of a day. After approximately one week, sedimentation occurred for these colloids. The samples with added arabinogalactan on the other hand were fully stable as the colour stayed red for more than a week, and no sedimentation was observed during that period of time.

3.4.2 pH measurement

The temperatures of the colloidal samples were measured using a mercury thermometer. The pH meter used was a WTW Microprocessor pH 539 pH meter with a Sensorex epoxy body combination pH electrode. It was calibrated with pH 7 and pH 9.28 buffers. The pH 7 buffer was prepared by dissolving a pH 7 buffer tablet (BDH Laboratory Supplies, Poole, England) in 100 mL of 18 MΩ deionised water. The pH 9.28 buffer was prepared by adding 1.905 g sodium borate (Aldrich, Milwaukee, WI, USA) to 100 mL of 18 MΩ deionised water. The pH measurements of the gold

colloids are shown in Table 3.4-1. The pH of 0.00144 mol/L $KAuBr_4$ solution was 3.60 at 19°C.

Table 3.4-1 pH measurements of the gold colloids prepared

Reducing Agent	**$KAuBr_4$ Concentration (mol/L)**	**Added Arabinogalactan (Yes/No)**	**Concentration (mol/L)**	**pH**	**Temperature (°C)**
Tri-potassium Citrate	0.00144	N	0.007	6.42	20
	0.00144	N	0.007	6.23	16
	0.00144	Y	0.007	6.59	16
	0.00144	N	0.014	6.87	16
	0.00144	Y	0.014	6.92	16
	0.00144	N	0.014	6.8	20
	0.00144	N	0.029	6.58	20
Sodium Borohydride	0.00144	Y	0.007	8.9	21
	0.00144	Y	0.014	9.64	21
	0.00144	Y	0.029	10.04	21
	0.00721	Y	0.036	9.22	18
	0.00721	Y	0.072	9.89	18
	0.00721	Y	0.144	10.33	18
Hydrazine Hydrate	0.00144	Y	0.007	4.07	19
	0.00144	Y	0.014	8.66	19
	0.00144	Y	0.029	11.37	19

The results showed that the pH of gold colloids prepared from hydrazine reduction was dependent on the concentration of hydrazine hydrate used. The colloids were alkaline if a large excess of hydrazine hydrate was used. The alkalinity was caused by hydrazine hydrate reacting with water, which in term produced hydroxyl ions (similarly to ammonia in water). This finding was confirmed by the preliminary samples of hydrazine reduced Au colloids (see Table A-1 in Appendix A), which had a large excess of hydrazine hydrate reducing agent added. The pH values of the

preliminary gold colloid samples prepared were consistently around pH 11-13. Sodium borohydride reduced gold colloids were also moderately alkaline. The measured pH values of the gold colloids were in the range 8.7 - 10.0 for the various concentrations of sodium borohydride reducing agent. The unprotected gold colloids prepared from the citrate reduction reaction were by contrast effectively pH neutral. The latter addition of arabinogalactan to these unprotected colloids had a negligible effect on the pH of the colloidal dispersions.

3.4.3 Characterisation of gold colloids by UV-Vis spectrophotometry

Samples for UV/Vis analysis were normally diluted before measurements with deionised water. The dilution consisted of adding 1 mL of colloidal dispersion or gold salt to 1 mL of deionised water. The Cary 100 model UV/Vis spectrophotometer from Varian was used in this study. It is a double beam, dual chopper, recording spectrophotometer controlled by a computer operating under Windows 2000, and running WinUV software. The instrument has a 0.28 M Czerny-Turner monochromator with a [1200 lines/mm] grating. The light sources are tungsten halogen for visible light and a deuterium arc for ultra-violet light. This creates a working wavelength ranging from 190 to 900 nm. It also has a working range up to 3.5 absorbance units. Samples are analysed in quartz cuvette 1 cm pathlength cells.

In this study, UV-Vis spectroscopy was used mainly for qualitative analysis. By comparing the spectrum of the gold salt with that of the gold colloids, albeit could be used to determine the stability of the colloidal dispersions and whether the reduction

of the starting Au (III) salt to gold metal was completed (see later). A comparative scale of the concentrations of colloidal gold in samples from preparation to preparation was also achieved by using UV-Vis spectroscopy. A relative density value can be calculated by multiplying the dilution factor by the measured absorbance of the diluted sample at an arbitrary wavelength. In this study the absorbance values were taken at 350 nm, a region free of any spectral interferences from other absorption maxima.

The UV-Vis spectrum of 0.00072 mol/L $KAuBr_4$ solution is shown in Figure 4.3-1. The spectrum features an intense band at *ca*. 249 nm and a band (containing a shoulder at longer wavelengths) at *ca*. 382 nm. The band at 249 and 382 nm are known to be caused by ligand to metal charge transfer (LMCT) electronic transitions between bromine ligands and the Au (III) ion [54]. This charge transfer occurs when considerable electron density is transferred from the bromine ligand atoms to the Au (III) centre[55].

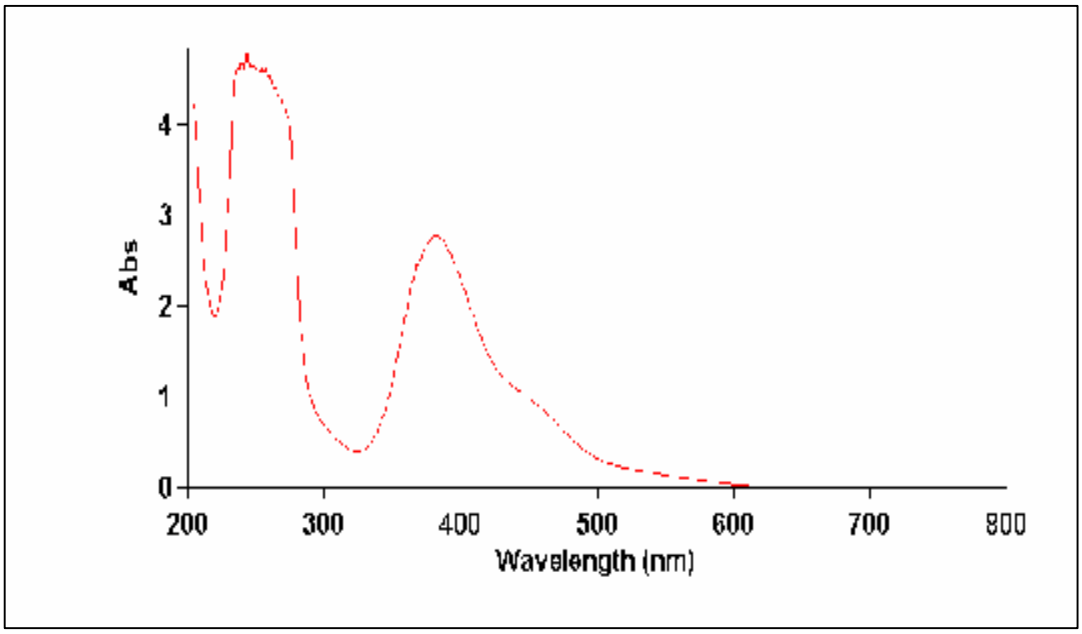

Figure 3.4-1 UV-Visible spectrum of 0.00072 mol/L $KAuBr_4$ solution

Figure 3.4-2 to 3.4-6 are the UV-Vis spectra of gold colloids generated by hydrazine, borohydride, and citrate reduction. The absorbance spectrum of colloidal gold always feature a single peak at around 500-530 nm. This is known to be due to the localised plasmon resonance absorbance of the colloidal gold particles. Previous work has shown that the absorbance wavelength and the width of the plasmon resonance peak are dependent on the size and stability of the colloidal gold under study. Plasmon resonances observed at higher wavelengths in spectra of the colloids indicate that the colloidal particles in this dispersions are larger in size whilst smaller-sized colloidal particle dispersions generally give rise to plasmon resonance peak at shorter wavelengths [54]. The breadth of the peak and appearance at longer wavelengths suggest large particles/aggregates are present in the system [53, 54]. Broadening of the plasmon resonance peaks may also be caused by dampened plasmon resonance effects induced by small colloidal particles [51], however, if small colloidal particles are present, the wavelength at which these plasmon resonance peaks occur would be shorter compare to colloidal dispersions with large particles.

Figure 3.4-2 shows the UV-Vis spectra of colloidal gold prepared by hydrazine reduction. The plasmon resonance peaks of the three colloidal samples generated by 0.007, 0.014, and 0.029 mol/L hydrazine hydrate are listed in Table 3.4-2.

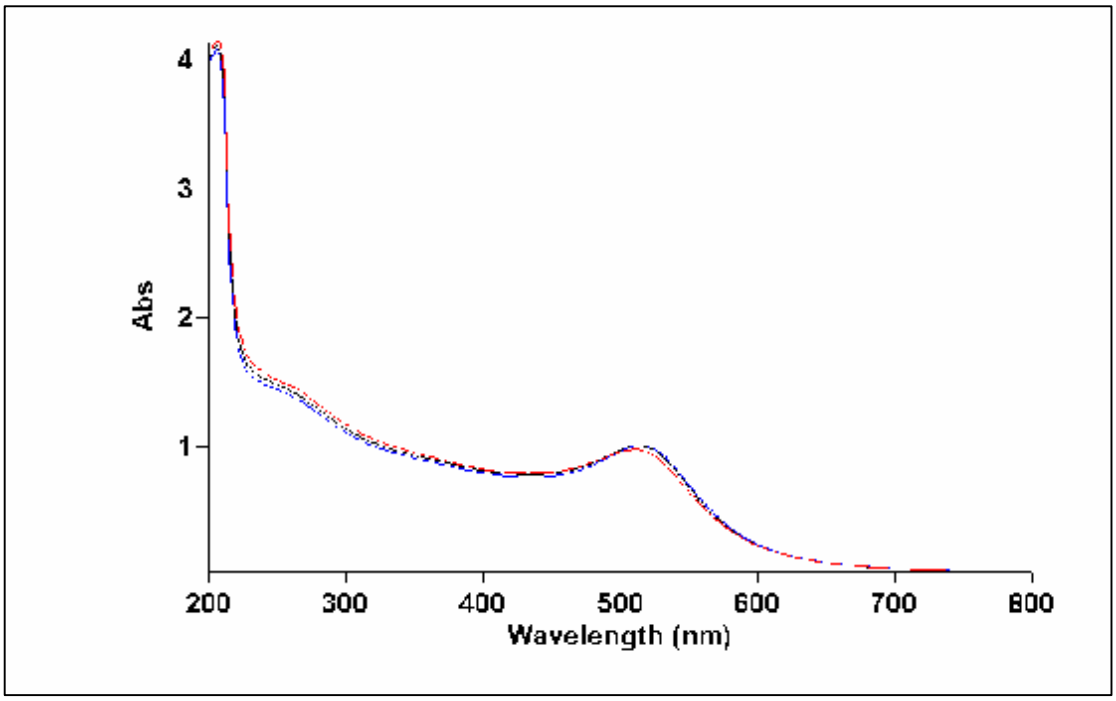

Figure 3.4-2 UV-Visible spectra of the three hydrazine hydrate reduced gold colloids

Table 3.4-2 Comparison of the observed colour of colloidal gold prepared using hydrazine reduction with the UV-Vis plasmon resonance peaks of the same samples

Sample	**Concentration of $KAuBr_4$ (mol/L)**	**Concentration of Reducing Agent (mol/L)**	**Peak (nm)**	**Initial colour of the colloids**
010806-1	0.00144	0.007	515	Red
010806-2	0.00144	0.014	513	Red
010806-3	0.00144	0.029	510	Red

The plasmon resonance peaks and the colours of the colloids suggested that 010806-1 and 010806-2 were similar in size, and 010806-3 might be of smaller size (due to the shorted wavelength at which the plasmon resonance peak was observed for 010806-3) during the course of the analysis. The shape of the plasmon resonance peaks suggested that the colloidal dispersions were very stable. However, as mentioned earlier in Section 3.4.1 in Chapter 3, all three samples prepared by hydrazine

reduction had aggregated, and that 010806-3 was the least stable sample of the three gold colloids generated by hydrazine reduction. A discussion on this observation will be made later on in this chapter.

Figure 3.4-3 shows the UV-Vis spectra of gold colloids prepared by using 0.007, 0.014, and 0.029 mol/L sodium borohydride reducing agent. The plasmon resonance peaks of these colloidal samples are listed in Table 3.4-3.

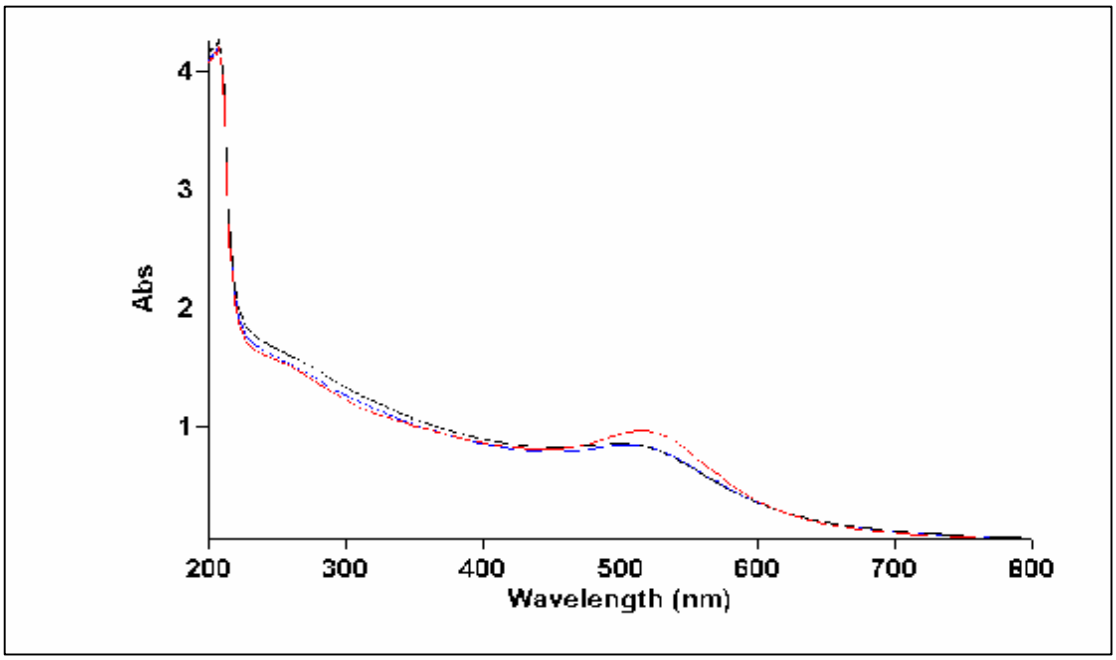

Figure 3.4-3 UV-Visible spectra of the three sodium borohydride reduced gold colloids with 0.00144 mol/L $KAuBr_4$ solution

Table 3.4-3 Comparison of the observed colour of colloidal gold prepared using borohydride reduction with the UV-Vis plasmon resonance peaks of the same samples

Sample	**Concentration of $KAuBr_4$ (mol/L)**	**Concentration of Reducing Agent (mol/L)**	**Peak (nm)**	**Initial colour of the colloids**
040806-1	0.00144	0.007	506	Red
040806-2	0.00144	0.014	500	Red
040806-3	0.00144	0.029	514	Red

The plasmon resonance peaks indicated that the gold colloids prepared from sodium borohydride were overall smaller in size compared to the gold colloids prepared from the hydrazine reduction method. The breadth of the plasmon resonance peaks of gold colloids generated from borohydride reduction also indicated that the size of the borohydride reduced colloidal gold particles was very small.

The sharper plasmon resonance peak of 040806-3 at 514 nm shown in Figure 3.4-3 suggested that the colloidal particles in the dispersion were larger compared to the other two colloidal samples prepared from 0.007 and 0.014 mol/L sodium borohydride. This can be explained by the particle growth model mentioned in Section 1.2 in Chapter 1, which illustrated that larger colloidal particles are formed when the supersaturation concentration of the metal nuclei is reached rapidly during the synthesis reaction. This rapid rate of nuclei formation can be achieved by increasing the concentration of the metal salt or the reducing agent.

As expected, when the concentration of $KAuBr_4$ solution was increased from 0.00144 mol/L to 0.00721 molL and the concentrations of sodium borohydride were changed from 0.007 and 0.014 mol/L to 0.036 and 0.072 respectively, colloidal dispersions

with larger particles were obtained. This was illustrated by Figure 3.4-4, which shows that the plasmon resonance peaks were shifted to a higher wavelength (see Table 3.4-4) and that the shape of the peaks was more distinctive compared to the peaks in Figure 3.4-3.

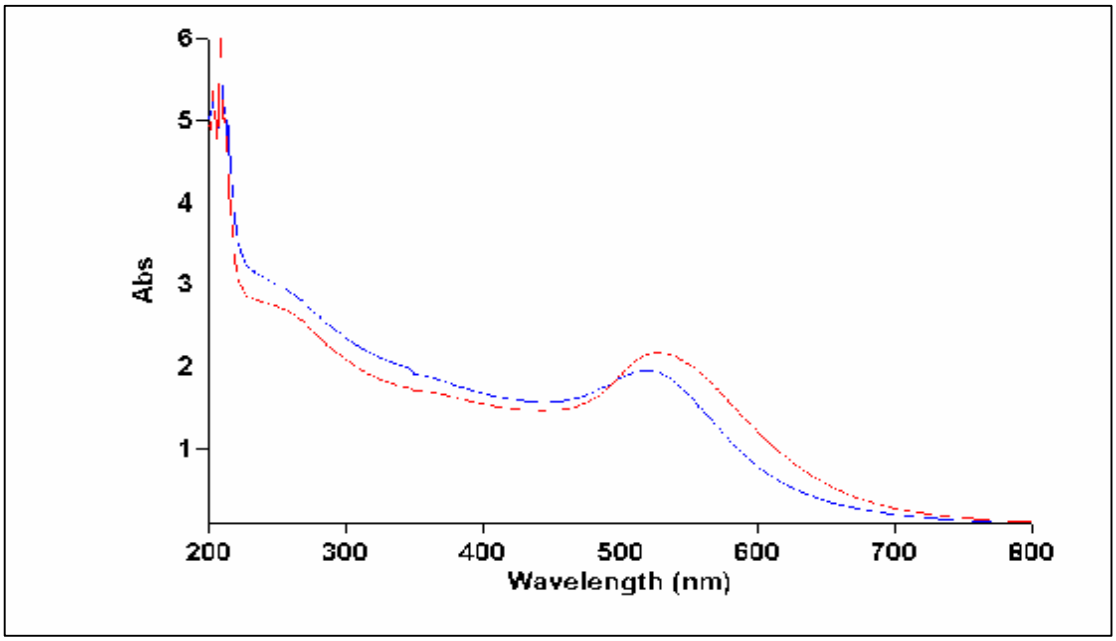

Figure 3.4-4 UV-Visible spectra of 0.036 and 0.072 mol/L sodium borohydride reduced gold colloids with 0.00721 mol/L $KAuBr_4$ solution

Table 3.4-4 Comparison of the observed colour of colloidal gold prepared using higher concentrations of $KAuBr_4$ solution and borohydride with the UV-Vis plasmon resonance peaks observed for the same samples

Sample	**Concentration of $KAuBr_4$ (mol/L)**	**Concentration of Reducing Agent (mol/L)**	**Peak (nm)**	**Initial colour of the colloids**
130806-1	0.00721	0.036	519	Red
130806-2	0.00721	0.072	528	Red/Purple

The plasmon resonance peaks of unprotected citrate reduced gold colloids are shown in Figure 3.4-5. The wavelength at which these peaks occur suggested that the gold colloids generated by citrate reduction had yielded colloidal particles that were significantly larger than the gold colloids prepared by borohydride reduction. By comparing the UV-Vis spectrum of gold colloids prepared by 0.029 mol/L hydrazine reduction (Figure 3.4-2) with the UV-Vis spectrum of 0.029 mol/L citrate reduced gold colloids (see Figure 3.4-5), it suggested that the rate of aggregation of hydrazine reduced gold colloids was hindered by the addition of arabinogalactan. Unprotected 0.029 mol/L citrate reduced gold colloids showed sign of aggregation (broad peak at a longer wavelength shown in Table 3.4-5) in Figure 3.4-5. However, the UV-Vis spectrum of gold colloids reduced with 0.029 mol/L hydrazine did not show any spectroscopic signs of aggregation.

Weak peaks at around 250 nm suggest that some unreduced $AuBr_4^-$ ions were still present in the colloidal dispersions.

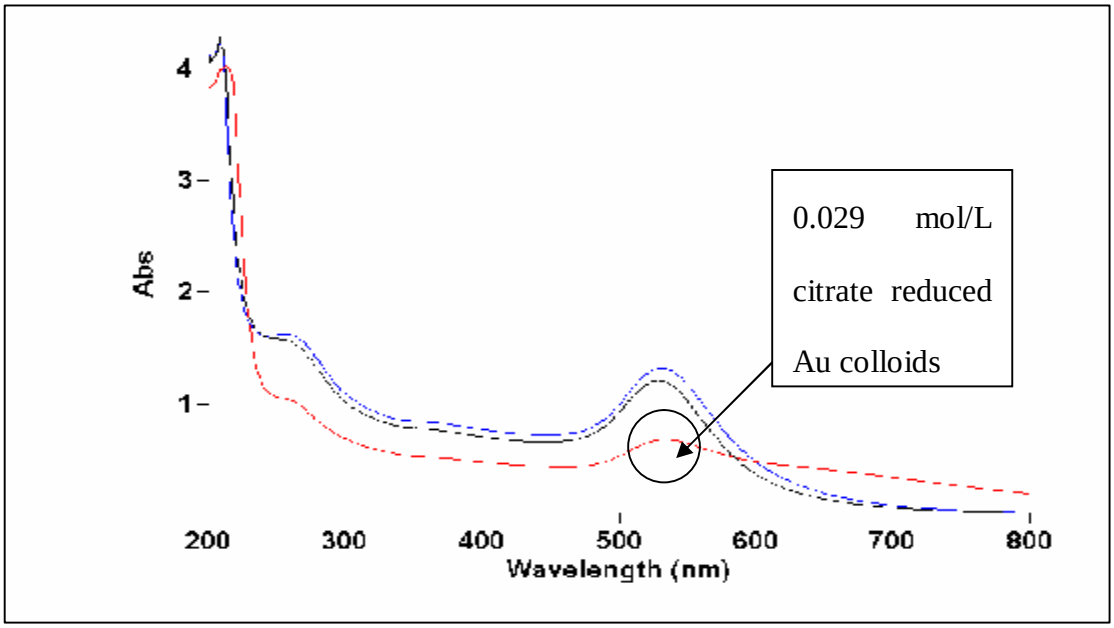

Figure 3.4-5 UV-Visible spectra of 0.007, 0.014, 0.029 mol/L tri-potassium citrate reduced gold colloids

Table 3.4-5 Comparison of the observed colour of colloidal gold prepared using citrate reduction with the UV-Vis plasmon resonance peaks of the same samples

Sample	**Concentration of $KAuBr_4$ (mol/L)**	**Concentration of Reducing Agent (mol/L)**	**Peak (nm)**	**Initial colour of the colloids**
070806-1	0.00144	0.007	531	Red
070806-2	0.00144	0.014	528	Red
070806-3	0.00144	0.029	533	Purple

The stability of unprotected versus arabinogalactan-protected citrate-reduced gold colloids is clearly illustrated in Figure 3.4-6. The unprotected colloidal samples gave rise to the two broad plasmon resonance peaks. The breadth of the peaks suggested that aggregation had occurred in the two colloidal samples (160806-1A and 160806-2A) which did not have arabinogalactan added. In contrast, U.V./Vis spectra of the two arabinogalactan-protected colloids featured two relatively sharper peaks at

ca. 530 nm (see Table 3.4-6).

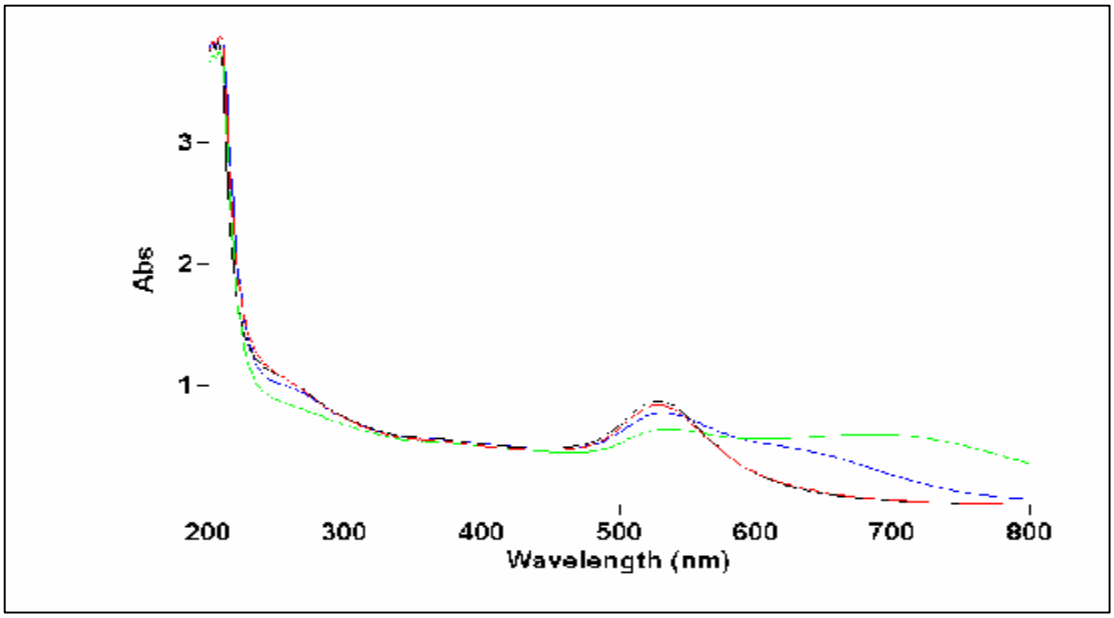

Figure 3.4-6 UV-Visible spectra of AG protected and unprotected gold colloids

Table 3.4-6 Comparison of the observed colour of protected and unprotected colloidal gold prepared using citrate reduction with the observed UV-Vis plasmon resonance peaks of the same samples

Sample	**Added Arabinogalactan**	**Concentration of $KAuBr_4$ (mol/L)**	**Concentration of Reducing Agent (mol/L)**	**Peak (nm)**	**Initial colour of the colloids**
160806-1A	No	0.00144	0.07	532	Purple
160806-1B	Yes	0.00144	0.07	528	Red
160806-2A	No	0.00144	0.014	535	Purple
160806-2B	Yes	0.00144	0.014	529	Red

The relative concentrations of the gold colloids prepared by hydrazine, borohydride, and citrate reduction reactions (as reflected by the magnitude of the A_{350} values) were obviously dependent on the concentration of the starting $KAuBr_4$ solution used. This is clearly illustrated by Table 3.4-7, which shows the relative concentrations of gold

colloids prepared from 0.00144 mol/L $KAuBr_4$ solution were all similar (similar A_{350} values), and gold colloids prepared from 0.00721 mol/L had higher A_{350} values.

Table 3.4-7 A_{350} values of the gold colloids prepared in this study as an indirect indicator of relative concentrations of the gold colloids between preparations

Sample	Concentration of $KAuBr_4$ (mol/L)	Concentration of Reducing Agent (mol/L)	A_{350}
010806-1	0.00144	0.007	1.81
010806-2	0.00144	0.014	1.85
010806-3	0.00144	0.029	1.89
040806-1	0.00144	0.007	2.01
040806-2	0.00144	0.014	2.11
040806-3	0.00144	0.029	1.99
070806-1	0.00144	0.007	1.69
070806-2	0.00144	0.014	1.56
070806-3	0.00144	0.029	1.07
130806-1	0.00721	0.036	9.66
130806-2	0.00721	0.072	8.61
160806-1A	0.00144	0.07	1.15
160806-1B	0.00144	0.07	1.16
160806-2A	0.00144	0.014	1.1
160806-2B	0.00144	0.014	1.12

3.4.4 Particle size measurements of gold colloids using TEM

Colloidal dispersions were deposited on TEM copper grids using a Venturi tube (see Figure 3.4-7). The deposition process involved connecting one end of the Venturi tube to a compressed nitrogen gas cylinder. The vertical tube of the apparatus was immersed in a colloidal sample. By turning on the nitrogen gas stream and blocking

(using a finger) the opening at the top of the Venturi tube, a vacuum was created at the inlet on the Venturi so allowing colloid solution to be sucked up and expelled as a fine mist from the outlet. By aiming this fine mist to an immobilised collodion coated copper grid (obtained from the Department of Biological Sciences, University of Auckland), colloid samples were able to uniformly sprayed onto the grid. The copper grid was dried and stored in a desiccator containing activated silica gel until required for analysis.

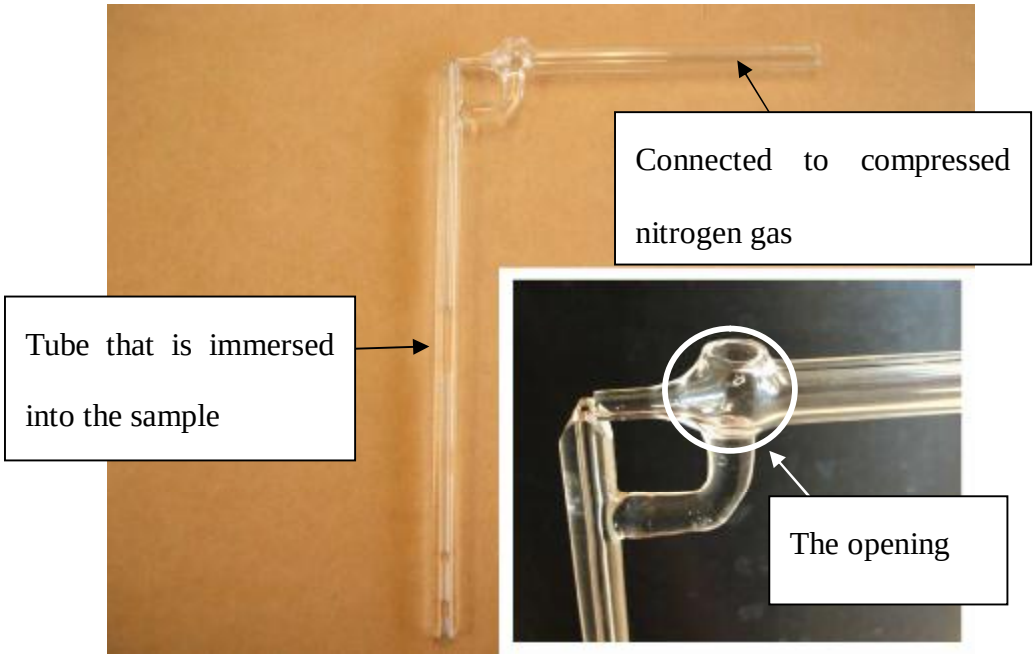

Figure 3.4-7 A Venturi used to transfer the gold colloids onto the TEM grids

The colloidal samples deposited on the copper grids were analysed by a Philips CM12 TEM (at University of Auckland), which has an acceleration voltage range of 80-120 kV so giving 50k to 750 k magnification. All TEM images were captured using a digital camera attached to the microscope. The digital images were analysed using Adobe Photoshop 7.0 which employed screen calipers, to measure the particle diameters in terms of the number of pixels. Over a hundred particle sizes were

selected and measured from each digital image. These values were averaged on a Microsoft Excel worksheet and a mean particle size obtained. The size distributions were represented as bar-graphs of percentage of total population of colloidal particle versus the size range in nanometres.

The TEM images of hydrazine reduced gold colloids are shown in Figure 3.4-8. The particle size distributions of hydrazine reduced gold colloids were not obtained due to coagulation of the colloidal samples. As shown in Figure 3.4-8, individual particles are impossible to be distinguished. The size results of the hydrazine reduced gold colloids obtained from the Zetasizer (see Figure 3.4-15) also suggested that large aggregates were present in the colloidal dispersions generated by hydrazine reduction.

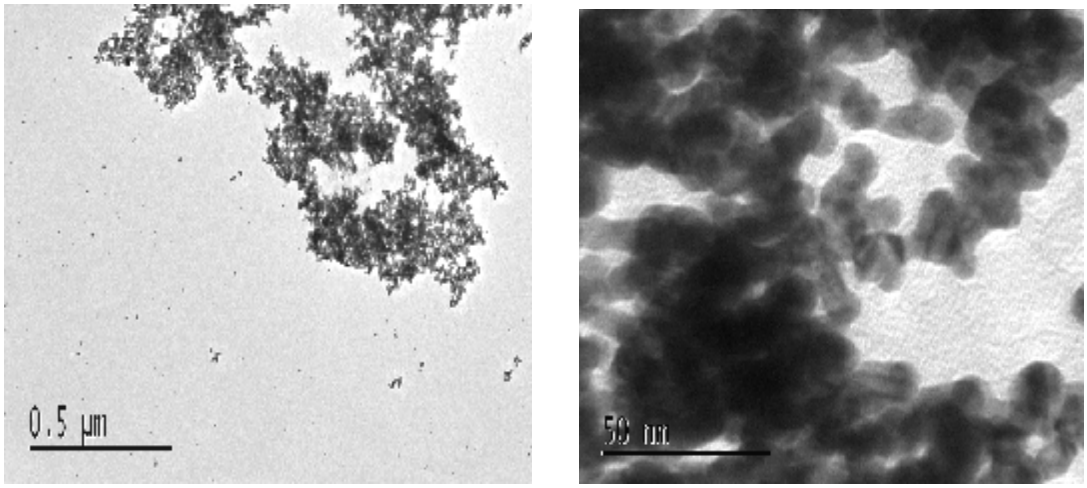

Figure 3.4-8 TEM images of AG-protected hydrazine-reduced gold colloids (using 0.00144 mol/L $KAuBr_4$ solution and 0.007 mol/L hydrazine hydrate). Left image is a low magnification image showing aggregation of the gold particles. Right image is a high magnification image showing more clearly the morphology of the aggregated colloid particles

Colloids from the sodium borohydride reduction were more stable to aggregation. The TEM images showed that the colloidal particles were finely dispersed with very few

aggregates as were apparent in the hydrazine reduced gold colloids. This means that the added 5 g/L arabinogalactan was more effective in preventing the gold colloidal particles from aggregating in borohydride-reduced gold colloid samples than hydrazine-reduced gold colloid samples. The main size-distribution of the gold colloids prepared from higher concentration (0.072 mol/L) of sodium borohydride was similar to the sample with lower concentration (0.036 mol/L) of sodium borohydride. However, the gold colloids prepared from 0.072 mol/L sodium borohydride had larger particles with diameter of 20-30 nm present in the colloidal dispersion.

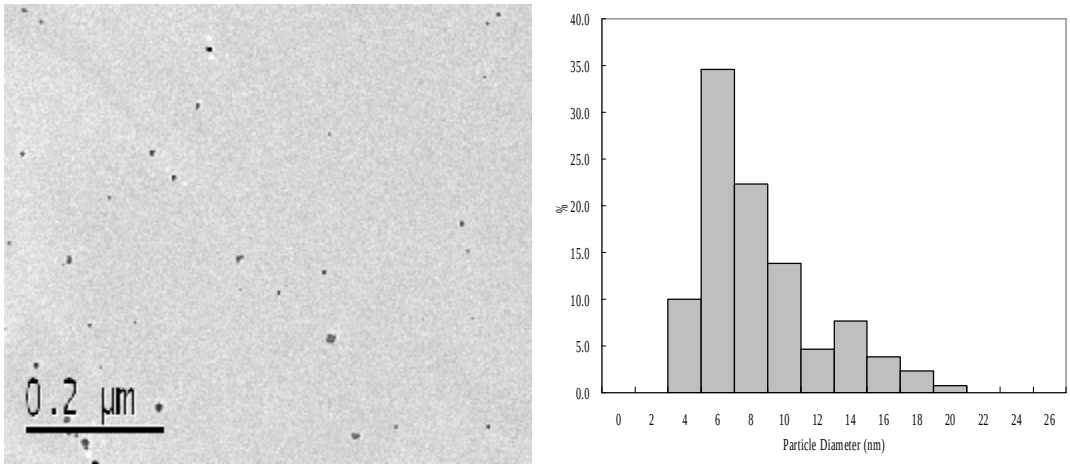

Figure 3.4-9 The TEM image of AG-protected sodium borohydride reduced gold colloids (using 0.00721 mol/L $KAuBr_4$ solution and 0.036 mol/L sodium borohydride) is shown on the left. The bar-graph on the right is the size distribution plot obtained from the TEM image

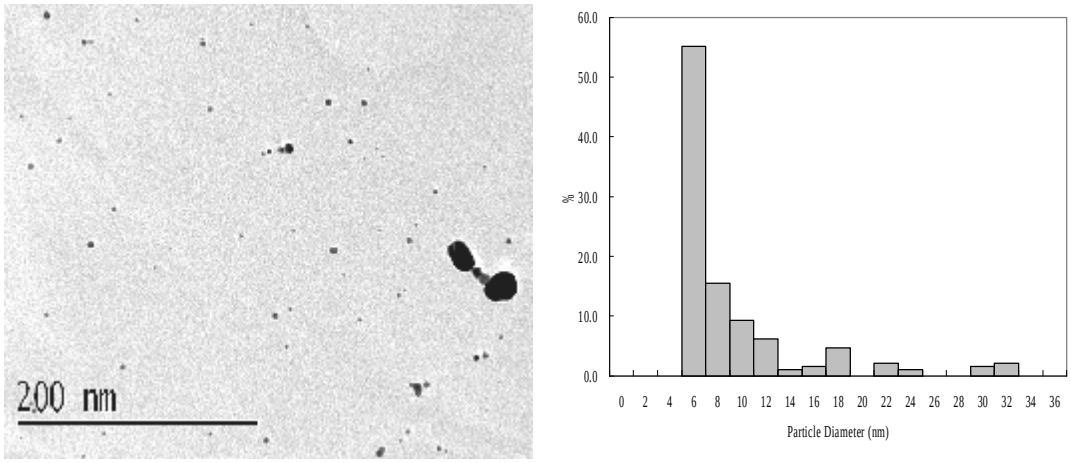

Figure 3.4-10 The TEM image on the left is a AG-protected sodium borohydride reduced gold colloids (using 0.00721 mol/L $KAuBr_4$ solution and 0.072 mol/L sodium borohydride). The size distribution is shown in the graph on the right.

The effectiveness of arabinogalactan as a protecting agent against aggregation was clearly illustrated by the TEM images of protected and unprotected gold colloids prepared by citrate reduction. Flocculation was observed in images of the unprotected samples (see Figure 3.4-13 to Figure 3.4-16). Samples with added arabinogalactan were more dispersed.

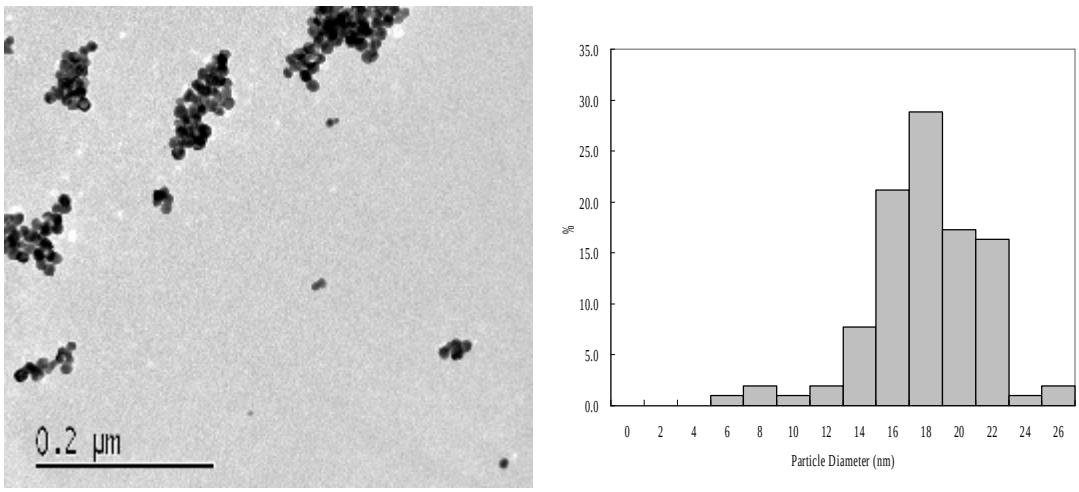

Figure 3.4-11 TEM image of unprotected citrate reduced gold colloids prepared from 0.00144 mol/L $KAuBr_4$ solution and 0.007 mol/L tri-potassium citrate. Flocculation clearly occurs between the

colloidal particles. The size distribution of the sample is shown in the bar-graph on the right.

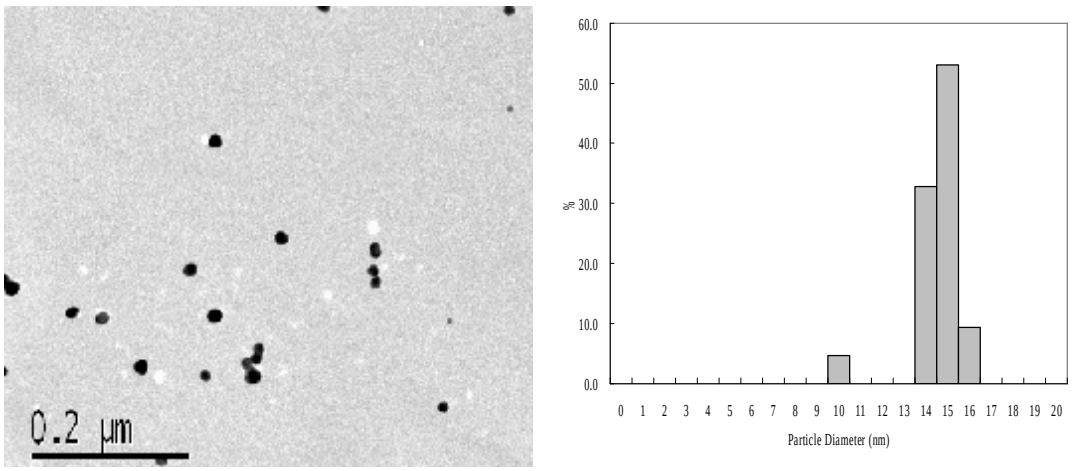

Figure 3.4-12 TEM image (left) and size distribution (right) of arabinogalactan protected gold colloids (prepared from 0.00144 mol/L $KAuBr_4$ solution, 0.007 mol/L tri-potassium citrate, and 5 g/L arabinogalactan).

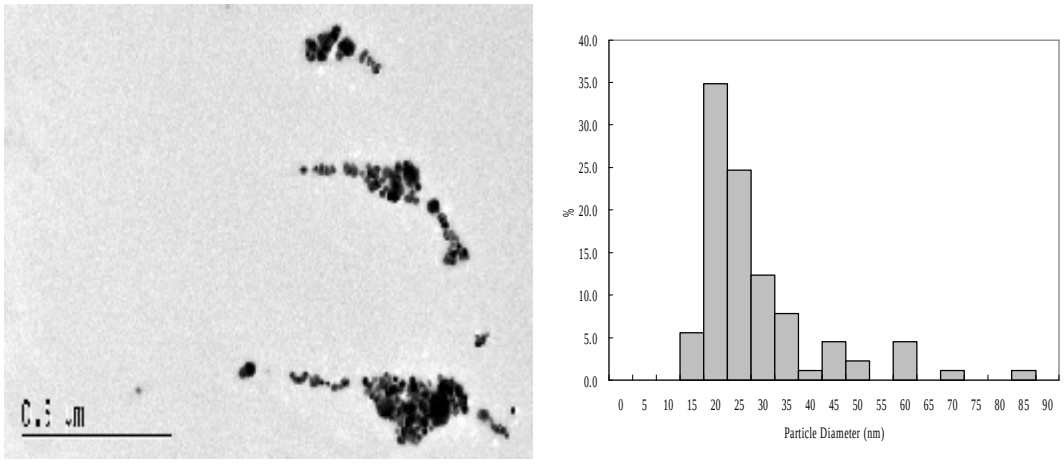

Figure 3.4-13 TEM image (left) and size distribution (right) of unprotected gold colloids prepared from 0.00144 mol/L $KAuBr_4$ solution and 0.014 mol/L tri-potassium citrate. With increased concentration of citrate used, , aggregation and particle coalescence were observed in this TEM image. In contrast, the TEM image of gold colloids generated from a lower concentration (0.007 mol/L) of citrate, featured the colloidal particles that had merely flocculated.

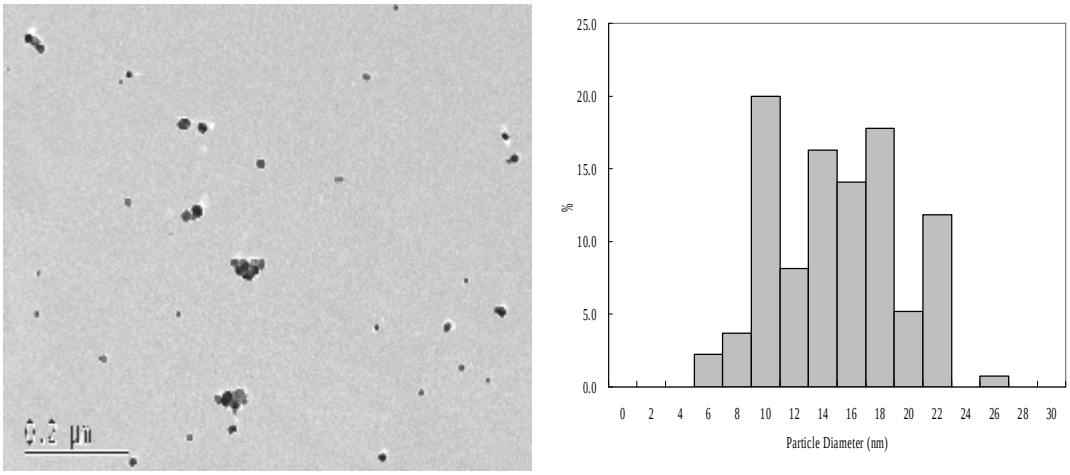

Figure 3.4-14 TEM image (left) and size distribution (right) of arabinogalactan protected gold colloids (prepared from 0.00144 mol/L $KAuBr_4$ solution, 0.014 mol/L tri-potassium citrate, and 5 g/L arabinogalactan). The size distribution shows there were more larger-sized particles in this sample than the arabinogalactan protected gold colloids prepared using 0.007 mol/L citrate.

3.4.5 Zetasizer size determination

The instrument used in this study was a Malven Zetasizer 3000HS, which has a Helium-Neon laser light source. Size measurements were carried out using standard 1 cm plastic fluorescence cuvettes. All measurement settings were set on default and are listed below in Table 3.4-8.

Table 3.4-8 Some instrumental settings used in the Malvern Zetasizer 3000HS

Mode of Analysis	Auto
Temperature of Sample	25°C
Dectection Angle	90°
Refractive Index of Dispersant (Relative to Air)	1.33
Wavelength of Laser	633
Viscosity of Sample	0.89
Attenuation Factor	Auto

As mentioned in Section 2.3 in Chapter 2, Zetasizer has five modes of analysing the raw data. The Auto mode was recommended and used in this study as it uses the averaged calculation of the other four modes.

Sample dilution was required before carrying out the size analysis. 1 mL of sample was diluted with 3 mL of 5 g/L arabinogalactan solution. All samples were measured at 25 °C. Each sample was measured in triplicate and each measurement was composed of ten sub-measurements. The duration of each measurement was set on Auto. Sizes were determined from a combination of scattering intensity generated by the colloidal particles, volume of the colloidal particles (calculated from the raw intensity measurement), and number (number of particles in the measured size) based mean values, where the latter two mean values are calculated (automatically by the instrument) from the intensity-based data. The Z_{ave} value is the mean hydrodynamic diameter of the colloidal particle that is calculated from the raw light scattering intensity data using the mononodal mode of data analysis. The Z_{ave} value is being included in the size result of each sample; however, it does not reflect the size distribution of a colloidal dispersion. There is always a finite particle size distribution in a colloidal dispersion, even with monodisperse colloids, in which the particle size distribution is merely narrower. In this study, the intensity, volume, number based mean values, and Z_{ave} value were used together to interpret the size and size distribution of each colloidal sample. The size results given by the Zetasizer are based on the assumption that all particles in the colloid sample are spherical. The drawback of this assumption is that large aggregates (especially flocs of loosely bound particles) may be treated as large individual particle by the Zetasizer, thus the size results may be overrated.

The Zetasizer size results were compared with the size distribution of each colloidal sample obtained from the TEM size analysis described in the previous chapter. The direct size measurements of colloidal particles using TEM provide an accurate comparison with the indirect colloidal size measurements (using PCS technique) using the Zetasizer.

As shown in Figure 3.4-15, hydrazine reduced gold colloids had wide size distributions. Aggregation occurred for all hydrazine reduced samples even with added arabinogalactan. The sample with 0.029 mol/L of hydrazine hydrate was the most unstable, as sedimentation occurred immediately after preparation. All hydrazine reduced gold colloids were inappropriate for Zetasizer measurement due to the low stability (presence of aggregates) and high polydispersity of the dispersions. The result shown in Figure 3.4-15 represents the gold colloid sample generated using the lowest concentration (0.007mol/L) of hydrazine hydrate. The sample was analysed three times, and size distribution of each measurement was indicated by different colours. The result was, however, not reliable since the count-rate for the measurement was less than 30 kCps (as mentioned earlier in Section 2.3.3 in Chapter 2, the best working count-rate should be at around 100-300 kCps) and the high polydispersity had prompted fail message in the size measurement reports (See Section 2.3.3 in Chapter 2 for details on the fail criteria of size measurement). Despite the failed result, the size distribution plots were still able to signal that large aggregates existed in the colloidal dispersion, which was supported by similar observations in the TEM images of the hydrazine reduced gold colloids shown in Section 3.4.4.

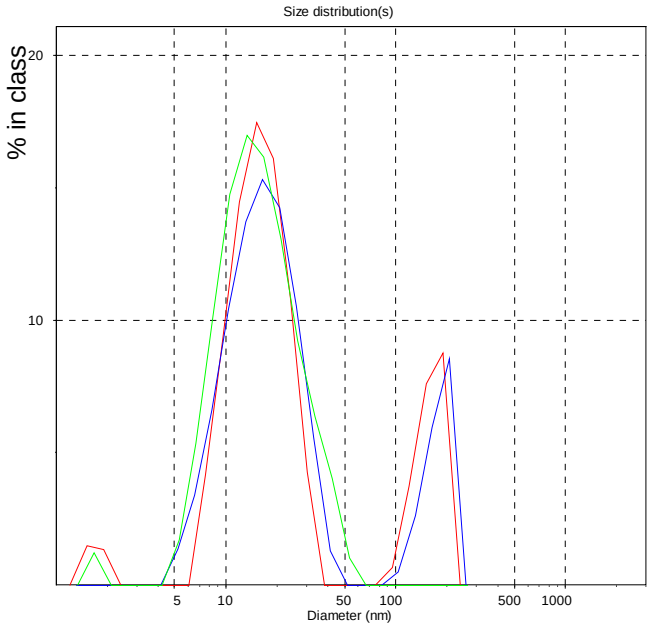

Figure 3.4-15 Size distribution plots based on three intensity based measurements of gold colloids prepared from 0.00144 mol/L $KAuBr_4$ solution and 0.007 mol/L hydrazine hydrate (Sample no. 010806-1).

For certain concentrations of sodium borohydride and $KAuBr_4$ solutions (such as samples 040806-1 to 040806-3 listed in Table 3.3-1), the particle size of borohydride-reduced gold colloids was often difficult to measure using the Zetasizer due to the low particle count-rate (see Section 2.3.3 in Chapter 2 for details on valid measurement). A drawback of borohydride reduction (in terms of particle size measurement by the Zetasizer) is that it produced colloids with small particle size (shown in the TEM images of borohydride-reduced gold colloids in Section 3.4.4). Hence, many samples could not be analysed by the Zetasizer due to the low intensity of scattered light induced by the small particles.

The zetasizer size measurements of the resulting gold colloids prepared from 0.0072 mol/L $KAuBr_4$ solution and 0.072 mol/L sodium borohydride (sample 130806-2) are

shown in Tables 3.4-9 to 3.4-11. Figure 3.4-16 illustrates the size distributions of 130806-2 Au colloids obtained from three repeated measurements. The figure shows that 130806-2 was reasonably monodisperse as the size distribution was narrow. This was also confirmed by the size distribution obtained from TEM shown in Figure 3.4-9.

Table 3.4-9 Intensity based measurements of 130806-2

Spectrum	No. of Distributions	Mean (nm)	Peak Area
Green	1	27.1	100
Blue	1	28.8	100
Red	1	29.6	100

Table 3.4-10 Volume based measurements of 130806-2

Spectrum	No. of Distributions	Mean (nm)	Peak Area
Green	1	26.8	100
Blue	1	28.4	100
Red	1	29.4	100

Table 3.4-11 Number based measurements of 130806-2

Spectrum	No. of Distributions	Mean (nm)	Peak Area
Green	1	26.6	100
Blue	1	27.6	100
Red	1	28.7	100

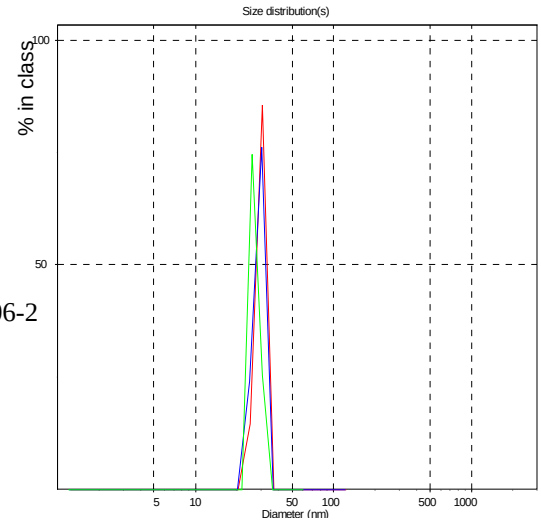

Figure 3.4-16 Size distribution plots of 130806-2 based on intensity measurements

$Z_{ave} = 17.3 \pm 0.2$ nm

The discrepancy between the Z_{ave} value and the intensity, volume, and number based mean particle sizes shown in Tables 3.4-9 to 3.4-11 is due to the fact that Z_{ave} is the average particle size of *all* particle sizes determined and in this case there may be some low intensity small particle sizes that are not showing with much intensity hence lower average size was obtained. The size measurements of 130806-2 obtained from

the Zetasizer (*ca.* 17 nm) were also different from the size distribution observed in the TEM image (*ca.* 10 nm) of the same sample. The discrepancy between the results obtained from the Zetasizer and TEM will be discussed later in this section, where a plot of the mean particle size obtained from the Zetasizer versus the mean particle size obtained from TEM is illustrated.

Citrate reduction is commonly known to produce colloids of near monodisperse character. This was confirmed by the monomodal size-distribution illustrated by the Zetasize results shown in Table 3.4-12 to 3.4-14 and Figure 3.4-17.

Table 3.4-12 Intensity based measurements of 070806-1

Spectrum	No. of Distributions	Mean (nm)	Peak Area
Green	1	32.2	100
Blue	1	32.6	100
Red	1	32.7	100

Table 3.4-13 Volume based measurements of 070806-1

Spectrum	No. of Distributions	Mean (nm)	Peak Area
Green	1	31.7	100
Blue	1	32.3	100
Red	1	32.1	100

Table 3.4-14 Number based measurements of 070806-1

Spectrum	No. of Distributions	Mean (nm)	Peak Area
Green	1	30.8	100
Blue	1	31.4	100
Red	1	31.2	100

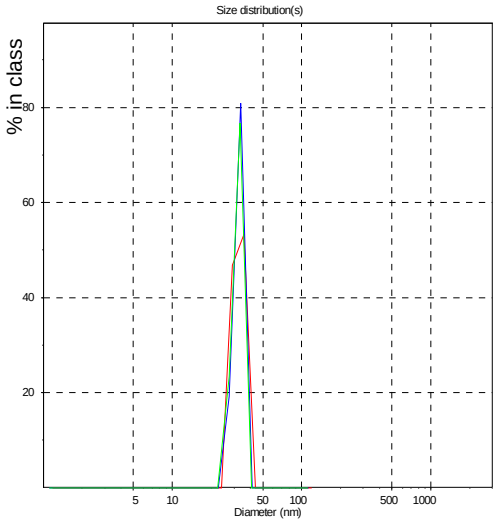

Figure 3.4-17 Size distribution plots of 070806-1 based on intensity measurements

$Z_{AVE} = 16.2 \pm 0.6$ nm

As listed in Table 3.3-1, sample 070806-2 had higher concentration (0.014 mol/L) of

tri-potassium citrate than sample 070806-1, thus the mean particle size of this sample was expected to be higher than 070806-1. The size results of 070806-2 shown in Table 3.4-15 to 3.4-17 have confirmed the hypothesis. Once again there must be a large number of smaller particles which do not "show up on the radar" which are dragging down the Z_{ave}.

Table 3.4-15 Intensity based measurements of 070806-2

Spectrum	No. of Distributions	Mean (nm)	Peak Area
Green	1	31.2	100
Blue	1	32.5	100
Red	1	32.7	100

Table 3.4-16 Volume based measurements of 070806-2

Spectrum	No. of Distributions	Mean (nm)	Peak Area
Green	1	31.3	100
Blue	1	32.4	100
Red	1	32.6	100

Table 3.4-17 Number based measurements of 070806-2

Spectrum	No. of Distributions	Mean (nm)	Peak Area
Green	1	30.8	100
Blue	1	32.2	100
Red	1	32.2	100

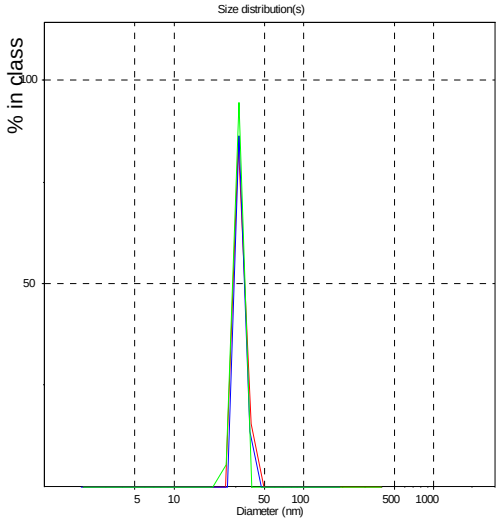

Figure 3.4-18 Size distribution plots of 070806-2 based on intensity measurements

$Z_{AVE} = 27.7 \pm 0.6$ nm

When the concentration of the citrate reducing agent was increased to 0.029 mol/L (Sample 070806-3) aggregation occurred. The plot of the size distribution based on intensity measurement of the sample is shown in Figure 3.4-19. The mean particle size measurements were not reported here as the quality of the measurement was actually failed by the Zetasizer. However, the two size distributions shown in the

Figure 3.4-19 were able to indicate that 070806-3 was not stable (ie it contained aggregated colloidal particles) compared to the citrate-reduced gold colloids prepared using 0.007 and 0.014 mol/L citrate reducing agent (Sample 070806-1 and 070806-2).

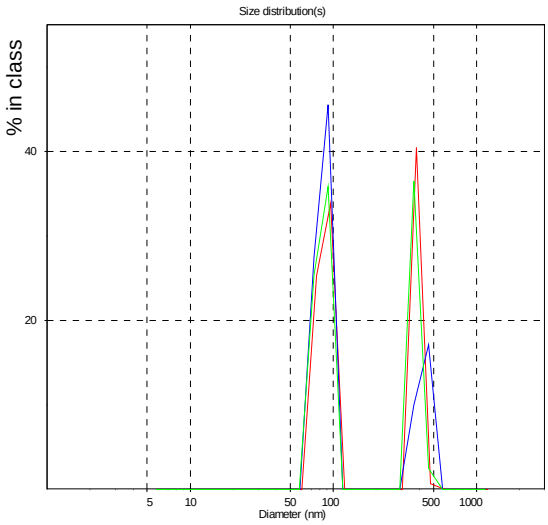

Figure 3.4-19 Size distribution plots of 070806-2 based on intensity measurements. Two size distributions are present (showing aggregation had occurred in the colloidal sample) with the larger more highly scattering particles giving rise to the distribution at higher particle sizes

In this thesis, the general procedure for preparing protected gold colloids using arabinogalactan followed the methodology reported previously by Mucalo et al [50]. This involved the mixing of arabinogalactan with the starting $KAuBr_4$ salt ***before*** the reduction step was carried out. However, as heat was involved in the citrate reduction method, there was concern that the arabinogalactan could degrade to unknown byproducts during the boiling, hence as a precaution, the arabinogalactan was added to the gold colloids ***after*** heating and cooling of the colloid.

Figure 3.4-20 is the intensity-based size distribution plot of the citrate-reduced Au colloids prepared using 0.007 mol/L citrate without added AG (Sample 160806-1A). The intensity, volume, and number based size results are listed in Table 3.4-18 to 3.4-20.

Table 3.4-18 Intensity based me0asurements of 160806-1A

Spectrum	No. of Distributions	Mean (nm)	Peak Area
Blue	2	26.5	84.6
		229	15.4
Red	2	27.3	66.4
		197.3	33.6

Table 3.4-19 Volume based measurements of 160806-1A

Spectrum	No. of Distributions	Mean (nm)	Peak Area
Blue	1	25.9	99.9
Red	1	26.6	99.8

Table 3.4-20 Number based measurements of 160806-1A

Spectrum	No. of Distributions	Mean (nm)	Peak Area
Blue	1	24.9	100
Red	1	25.9	100

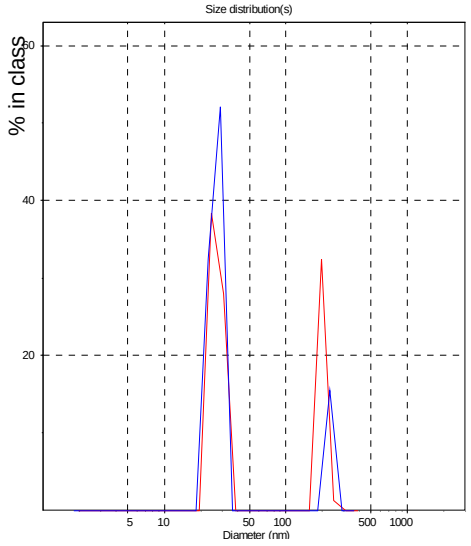

Figure 3.4-20 Size distribution plots of 160806-1A (unprotected) based on intensity measurements

$Z_{AVE} = 25.3 \pm 1.1$ nm

Theses results clearly suggested that aggregation had occurred in the colloidal sample (because two size distributions were detected as illustrated in Figure 3.4-20).

Figure 3.4-21 and Tables 3.4-21 to 3.4-23 are the Zetasizer size results of the AG protected Au colloids generated from use of 0.014 mol/L tri-potassium citrate (Sample 160806-1B). From the intensity, volume, and number based size results of 160806-1A (unprotected) and 160806-1B (AG protected), there was a clear difference in size

between the AG protected and the unprotected colloids. Unprotected colloids clearly had larger particle size (along with two size distributions exhibited) than the protected colloids. This indicated that aggregation must have occurred soon after the colloids were prepared. With protected colloids, arabinogalactan was able to prevent aggregation by adsorbing on to the surface of the colloidal particles and inducing steric repulsion between them.

Table 3.4-21 Intensity based measurements of 160806-1B

Spectrum	No. of Distributions	Mean (nm)	Peak Area
Blue	1	34.2	100
Red	1	32.4	100

Table 3.4-22 Volume based measurements of 160806-1B

Spectrum	No. of Distributions	Mean (nm)	Peak Area
Blue	1	31.6	100
Red	1	33.6	100

Table 3.4-23 Number based measurements of 160806-1B

Spectrum	No. of Distributions	Mean (nm)	Peak Area
Blue	1	30.4	100
Red	1	32.6	100

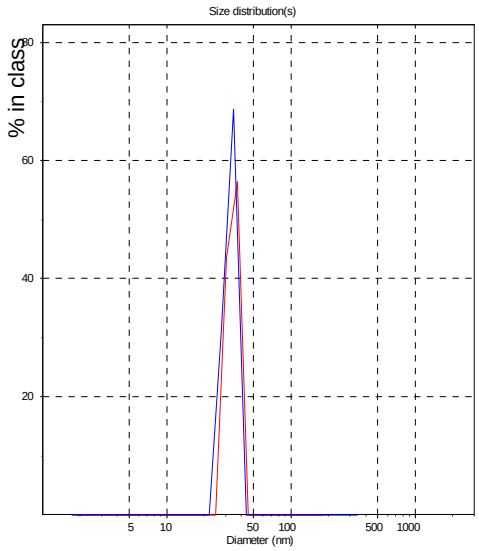

Figure 3.4-21 Size distribution plots of 160806-1B (AG protected) based on intensity measurements

$Z_{AVE} = 26.7 \pm 1.3$ nm

The Zetasizer size results for the citrate-reduced Au colloids generated using 0.014 mol/L citrate (unprotected) (Sample 160806-2A) are reported in Tables 3.4-24 to 3.4-26 and Figure 3.4-22. The results suggest that large coalesced (aggregated) particles were formed in this sample of colloids rather than the formation of large flocs made up of small loosely held together particles as observed for the sample

160806-1A. The TEM image of 160806-2A (see Figure 3.4-13) showed that both coalesced colloidal particles and flocs of loose particles had formed in this sample of citrate-reduced Au colloids.

Table 3.4-24 Intensity based measurements of 160806-2A

Spectrum	No. of Distributions	Mean (nm)	Peak Area
Blue	1	44.1	100
Red	1	45.2	100

Table 3.4-25 Volume based measurements of 160806-2A

Spectrum	No. of Distributions	Mean (nm)	Peak Area
Blue	1	43.7	100
Red	1	45.1	100

Table 3.4-26 Number based measurements of 160806-2A

Spectrum	No. of Distributions	Mean (nm)	Peak Area
Blue	1	42.3	100
Red	1	44.0	100

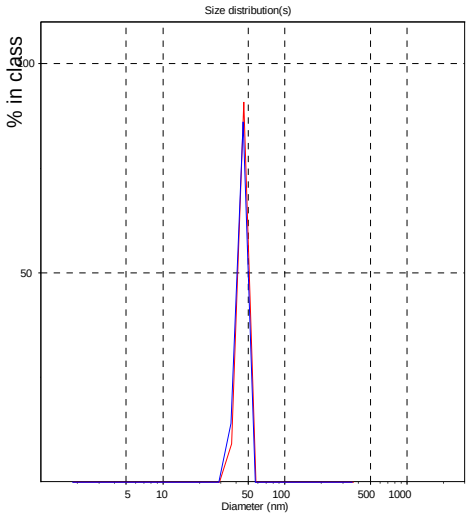

Figure 3.4-22 Size distribution plots of 160806-2A (unprotected) based on intensity measurements

$Z_{AVE} = 25.7 \pm 0.3$ nm

The size measurements of 0.014 mol/L citrate-reduced Au colloids with added AG (Sample 160806-2B) are reported in Table 3.4-27 to 3.4-29 and Figure 3.4-23. The results further illustrated that citrate-reduced Au colloids were stable with AG added after the preparation. The TEM image of 160806-2B (shown in Figure 3.4-14) also confirmed that the stability of these citrate-reduced colloids was better (since little aggregation between colloidal particles was observed in the TEM image of 160806-2B) than the sample without added AG (160806-2A).

Table 3.4-27 Intensity based measurements of 160806-2B

Spectrum	No. of Distributions	Mean (nm)	Peak Area
Blue	1	27.6	100
Red	1	29.1	100

Table 3.4-28 Volume based measurements of 160806-2B

Spectrum	No. of Distributions	Mean (nm)	Peak Area
Blue	1	27.3	100
Red	1	28.7	100

Table 3.4-29 Number based measurements of 160806-2B

Spectrum	No. of Distributions	Mean (nm)	Peak Area
Blue	1	26.9	100
Red	1	28.2	100

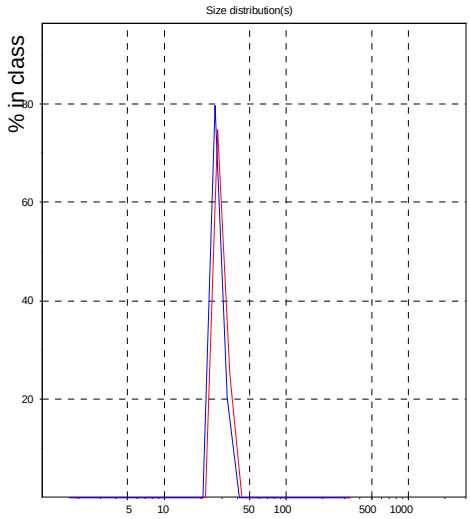

Figure 3.4-23 size distribution plots of 160806-2B (AG protected) based on intensity measurements

$Z_{AVE} = 23.8 \pm 0.7$ nm

The discrepancy between the size distributions obtained from the Zetasizer and the TEM images was noted. A non-linear relation between the particle sizes measured by TEM and Zetasizer is illustrated by Figure 3.4-24. This non-linear relationship between the size results obtained from the two techniques could be explained by the size-detection limit of the Zetasizer. As shown earlier, the particle size from the Zetasizer for the larger particles are not reliable given they could represent aggregates present only in a small quantity, thus the Zetasizer might have overrated the particle size (ie the plot shown in Figure 3.4-24 has flattened at larger particle size).

Despite the size discrepancy, the Zetasizer was still a technique to use to indicate the stability of the colloidal dispersion (as the size distribution plots obtained from the Zetasizer could qualitatively indicate the real size distribution in the samples).

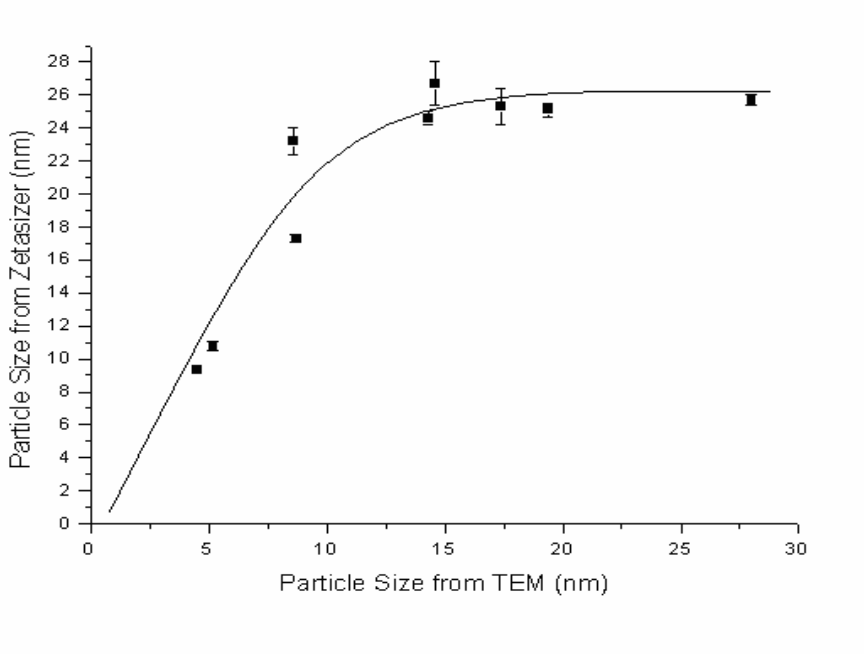

Figure 3.4-24 Correlation plot of particle sizes measured by TEM and Zetasizer

4. BIAcore Sensitivity Enhancement Using the Gold Colloids Generated from this Study

4.1 Introduction

As mentioned earlier in Section 2.4.3 in Chapter 2, SPR technology can study the ligand-analyte interactions by monitoring the changes in mass/refractive index on the surface of a sensor chip, where the SPR phenomenon occurs. However, it suffers from low sensitivity when the technique is used to detect small molecules with masses < 2 kDa. Two ways of overcoming the low sensitivity of SPR for detecting small molecules have been reported by Mitchell et al [14]. The first was to immobilise the small molecule (the analyte) and then to use antibody as the ligand to bind to the surface. Usually, antibody (the ligand) is immobilised on the sensor surface, and the small molecule (the analyte) is passed over this surface for analysis. Since the change in mass on the sensor surface is negligible (due to the small mass of the small molecule), the sensitivity of the SPR technique is insufficient to detect the small mass change. Thus the detection of small molecules using SPR technology is difficult. However, when the small molecule is immobilised on the sensor surface and the antibody (which has a higher overall mass than the small molecule) is flowed over the sensor surface the SPR technique becomes more sensitive (due to the higher overall mass change on the surface). This indirect measurement of progesterone concentration was used in this study. The second means of signal enhancement method as reported

by Mitchell et al was to couple the ligand (the antibody) with a high mass label such as a gold colloidal particle (enhancement species), which would enhance the binding signal intensity by providing a more massive component to cause RI changes by accumulation at the BIAcore gold chip interface. Signal enhancement achieved through accumulation of mass on the surface of the sensor chip can be illustrated by Figure 4.1-1.

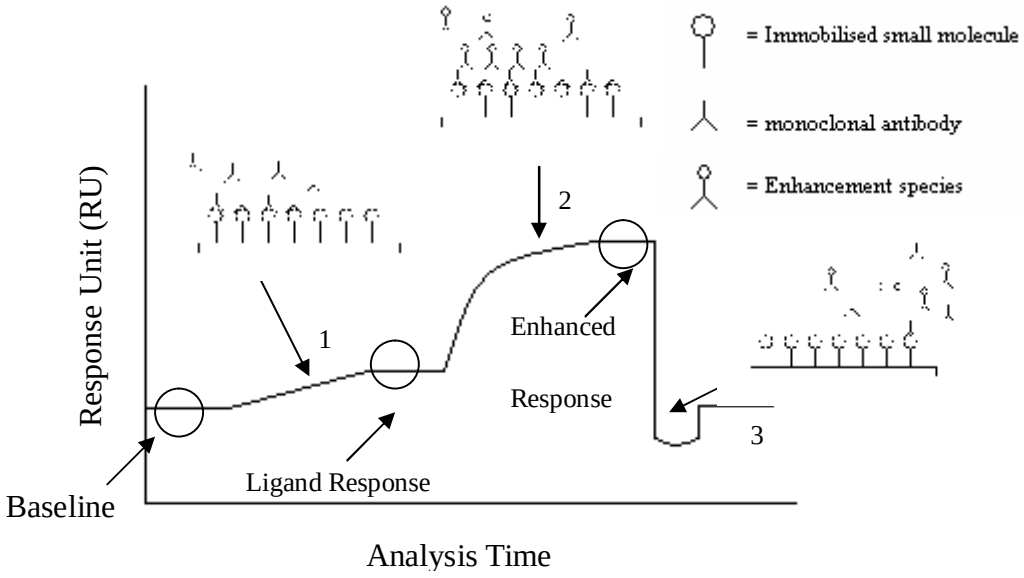

Figure 4.1-1 SPR Sensorgram illustrating how the analyte response is enhanced by accumulation of mass at the chip interface. 1) the binding of the ligand (monoclonal antibody) which gives rise to the "ligand response". 2) the signal enhancement step which involves the binding between the enhancement species with the ligand. The accumulation of mass on the surface of the sensor chip gives rise to a much higher signal response. This is the "enhanced response". 3) the regeneration step washes away the analyte and the enhancement species. The response is reduced back to the baseline so that the sensor surface is fully regenerated and ready for the next analysis.

Three major steps were carried out in developing the assay for indirect measurement of progesterone concentrations. These were: 1) preparation of the sensor chip surface,

which involved immobilisation of progesterone on the coupling layer of the sensor chip (see Section 4.3 in Chapter 4). 2) determination of the optimum concentration of the enhancement species and the level of signal enhancement using the enhancement species (see Section 4.4.3 in Chapter 4). The objective of this experiment was to achieve high (> 13 fold) level of signal enhancement using lowest possible concentration of the enhancement species. 3) determination of the limit of detection (LOD) of the progesterone assay developed from the previous step (see Section 4.6 in Chapter 4).

4.2 Preparation of Buffer Solutions Used for Sensor Chip Preparation

4.2.1 Preparation of pH 4.0, 0.01 mol/L sodium acetate immobilisation buffer

The preparation of pH 4.0, 0.01 mol/L sodium acetate immobilisation buffer was followed the procedure described in the study by Mitchell et al [30]. 0.6866 g of sodium acetate (BDH Chemical Ltd, Poole, England) was dissolved in 5 mL of 18 MΩ Milli Q deionised water to make 1 mol/L sodium acetate solution. 400 µL of the 1 mol/L sodium acetate solution was diluted with 39.6 mL of Milli Q deionised water to make 40 mL of 0.01 mol/L sodium acetate. This buffer solution was then titrated to pH 4.0 with 5mol/L HCl. The buffer was stored in a closed sample tube at ~4 °C in a refrigerator.

4.2.2 Preparation of the pH 2.0, 0.01mol/L glycine regeneration buffer

0.3758 g of 99% glycine (Sigma, St. Louis, MO, USA) was dissolved in 5 mL of 18 MΩ Milli Q deionised water to make 1 mol/L glycine regeneration buffer solution. 400 μL of the 1 mol/L glycine solution was diluted with 39.6 mL of Milli Q deionised water to make 40 mL of 0.01mol/L glycine. This regeneration buffer was then adjusted to pH 2.0 with 5 mol/L HCl. The buffer was stored in a closed sample tube at ~4 °C in a refrigerator.

4.3 Sensor Chip Preparation

4.3.1 Preparation of the CM5 sensor chip

The CM5 sensor chip is a commercially available pre-modified sensor chip containing a carboxymethylated dextran coupling layer covalently bonded to the gold film of the sensor chip (see Figure 4.3-1). The immobilisation of molecules is achieved through covalent coupling of amine, thiol, aldehyde, or carboxyl groups with the dextran layer, which contains carboxylic groups. The dextran layer is approximately 100 nm thick [31].

The CM5 sensor chip was purchased from BIAcore AB in Uppsala, Sweden, which is now part of GE Healthcare.

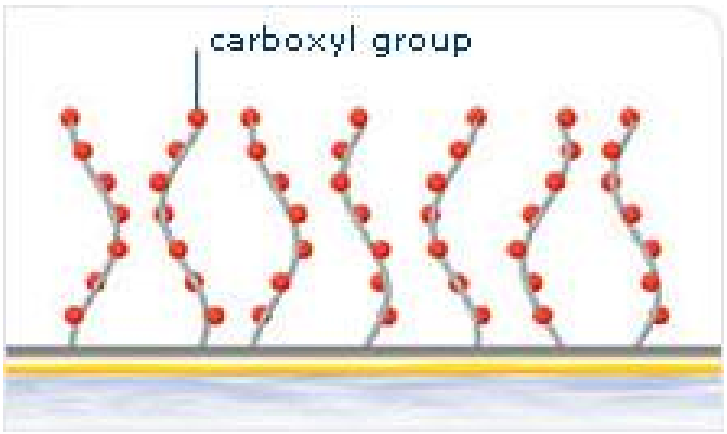

Figure 4.3-1 Dextran layer on the gold sensor surface

For this study, progesterone molecules (from Sigma Chemical Co.) were immobilised on the sensor chip surface through ovalbumin (OVA) with a polyethylene glycol (PEG) linkage. The progesterone-OVA conjugate used in the study was the progesterone-4-OVA (P4-PEG-OVA) analogue previously described by Wu et al [56]. Preparation of the P4-PEG-OVA conjugate was not required in this study as 4.8 mg/mL P4-PEG-OVA conjugates previously prepared by Wu et al. were available for use. These had been stored at -20°C and were defrosted before use.

Two flow-cells were prepared for the analysis of progesterone. A reference flow-cell containing immobilised OVA was prepared along with a sample flow-cell containing immobilised P4-PEG-OVA conjugates. The reason for preparing a reference flow-cell is to monitor and also subtract the non-specific binding that the analytes (the monoclonal antibody and the enhancement species) might exhibit with OVA. The immobilised P4-PEG-OVA flow-cell was used to monitor the progesterone-antibody interactions.

In order to immobilise OVA onto the dextran layer of the sensor chip, surface activation was required before the protein could be coupled with the carboxyl groups

of the dextran layer. Activation was achieved by injecting a mixture of 1:1 3-dimethylaminopropyl carbodiimide hydrochloride (EDC) (BIAcore AB, Uppsala, Sweden) and *N*-hydroxysuccinimide (NHS) (BIAcore AB, Uppsala, Sweden) through the reference flow-cell using 100 μL of the mixture over 20 minutes at 5 μL/minute (this is often expressed as 100 μL/ 20 minutes).

10 mg/mL OVA was prepared by dissolving OVA (Albumin from Chicken egg white, Sigma) in 18 MΩ deionised water. 0.5 mg/mL OVA was then prepared by diluting the 10 mg/mL OVA prepared in pH 4.0, 0.01 mol/L sodium acetate. 150 μL of the 0.5 mg/mL of OVA was injected in the same flow-cell over 30 minutes at a flow-rate of 5 μL/minute. The OVA became attached to the activated dextran layer via amine coupling.

The surface of the reference flow-cell was deactivated to prevent any active sites from coupling with undesired molecules such as the monoclonal antibody, which would be later injected as analytes (see later). 100 μL of ethanolamine hydrochloride (EAH) (BIAcore AB, Sweden) was flowed through the reference flow-cell over 20 minutes at a flow-rate of 5 μL/minute. 10 μL of 0.01 mol/L glycine at pH 2.0 was then flowed through the reference flow-cell over 30 seconds (at a flow-rate of 20 μL /minute) twice to wash off any unbound OVA.

The immobilisation of OVA reference flow-cell and P4-PEG-OVA sample flow-cell can be illustrated in Figure 4.3-2 (in the case of OVA immobilisation, progesterone molecule should be absent from the diagram).

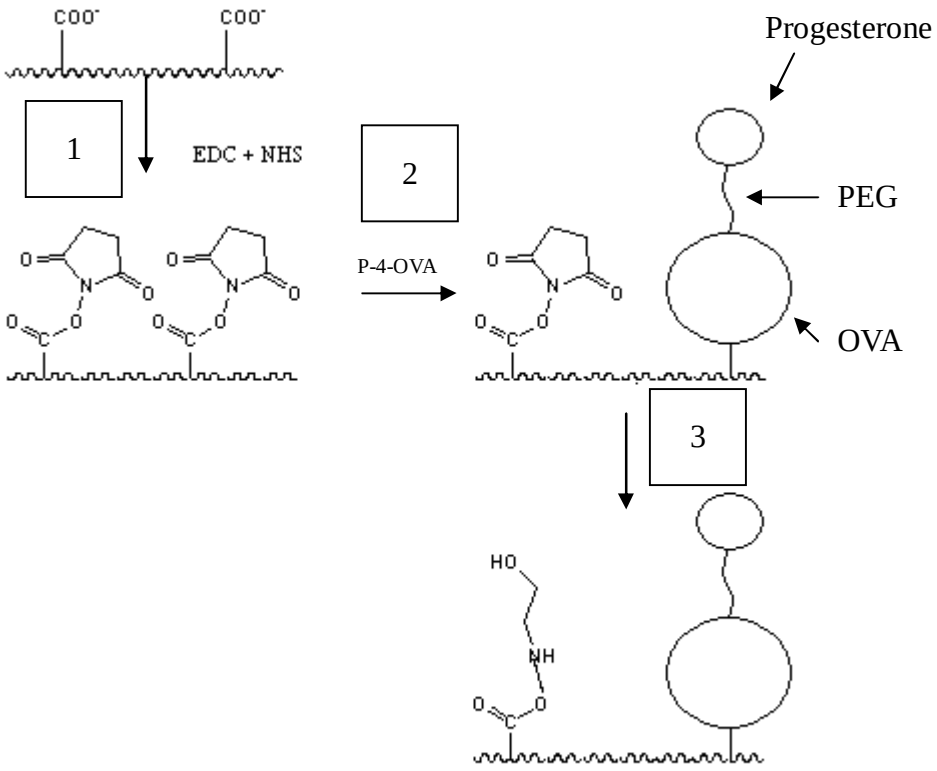

Figure 4.3-2 Schematic diagram illustrating surface immobilisation with P4-PEG-OVA. 1. the carboxyl groups of the dextran layer is activated with EDC/NHS mixture; 2. a P-4-OVA conjugate was immobilised on one of the activated site on the dextran layer; 3. Deactivation of free activated carboxyl sites on the dextran layer.

The sample flow-cell was immobilised with 0.5 mg/mL P4-PEG-OVA. 1:1 EDC/NHS mixture was injected at 100 μL over 20 minutes into the sample flow-cell. 0.5 mg/mL of P4-PEG-OVA was prepared in pH 4.0, 0.01 mol/L sodium acetate. 150 μL of it was then injected into the same sample flow-cell over 30 minutes at a flow-rate of 5 μL/minute. The surface of the sample flow-cell was deactivated with an injection of 100 μL EAH over 20 minutes at a flow rate of 5 μL/minute. The surface was then washed four times with 10 μL pH 2.0, 0.01 mol/L glycine for 30 seconds at a flow-rate of 20 μL/minute. The sensorgram of the P4-PEG-OVA immobilisation on

the CM5 chip is illustrated in Figure 4.3-3. The level of 500 µg/mL OVA binding (in the reference flow-cell) and 500 µg/mL P4-PEG-OVA binding (in the sample flow-cell) on the CM5 chip was *ca.* 9900 and 9200 RU respectively. The surface was assessed with 100 µg/mL mAb for quality of the immobilisation. The 100 µg/mL mAb was flowed over the reference and sample flow-cell surfaces at 60 µL/ 3 minutes (60 µL for 3 minutes at flow-rate of 20 µL/minute). The level of mAb binding was *ca.* 70 RU (see Figure 4.3-4). The levels of 500 µg/mL OVA and 500 µg/mL P4-PEG-OVA binding should be similar to the values defined above for every immobilisation.

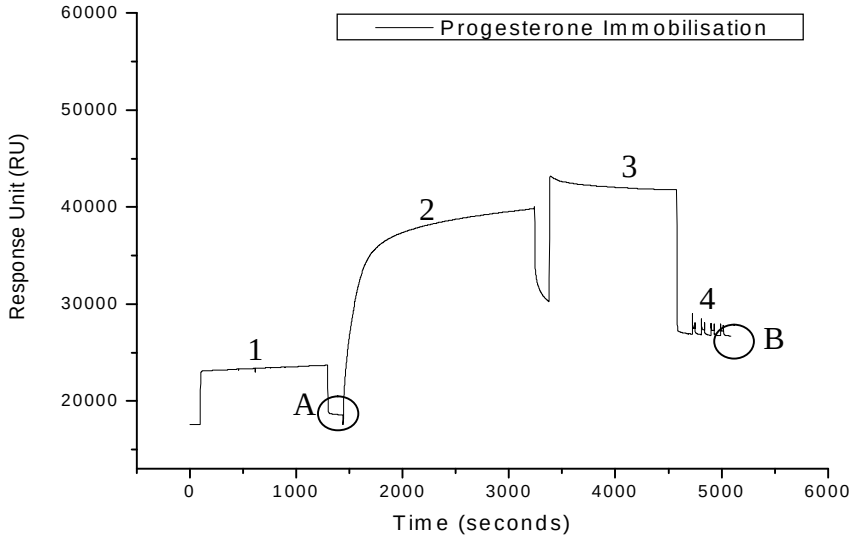

Figure 4.3-3 Sensorgram of P4-PEG-OVA immobilisation on the CM5 chip. 1) Surface activation with EDC/NHS. 2) 500 µg/mL P4-PEG-OVA immobilisation. 3) Surface deactivation with EAH. 4) four surface washes with pH 2.0, 0.01 mol/L glycine. The large increase in responses observed for 1) and 3) were caused by solvent effect (change in refractive index due to solvent) rather than binding on the sensor surface. A) Response (*ca.* 1050 RU) due to surface activation. B) Response (*ca.* 9200 RU) cuased by P4-PEG-OVA binding after the unbound P4-PEG-OVA was washed away.

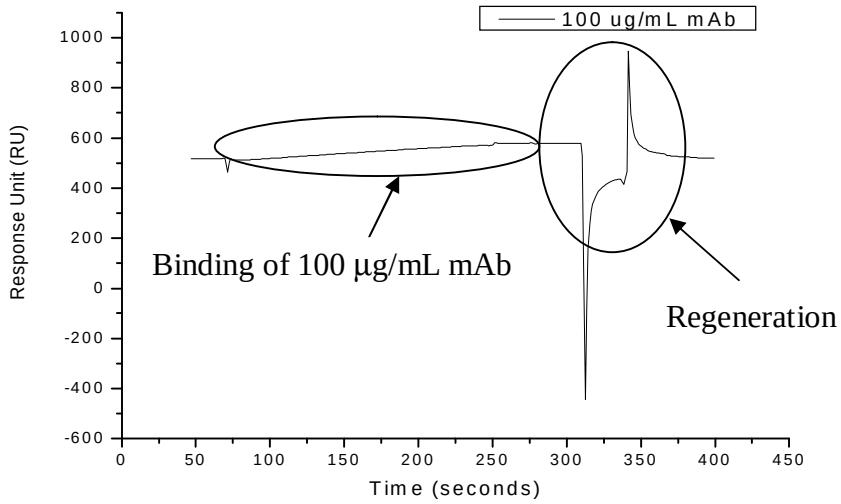

Figure 4.3-4 Sensorgram showing the binding of 100 μg/mL mAb on the immobilised progesterone (CM5 chip) surface. The surface was regenerated with Regen Buffer 1. The spikes shown in the sensorgram were due to the solvent effect (change in refractive index due to Reg Buffer 1) rather than to any actual binding.

4.3.2 Preparation of the Self-assembled Monolayer (SAM) sensor chip

A self-assembled monolayer (SAM) chip is a sensor chip which allows users to customise the gold surface with binding sites according to their own specification. Unlike the commercially available CM5 chip, which is supplied with a pre-bound 100 nm layer of dextran, the SAM chip allows the user to coat a thinner (< 100 nm) coupling layer on top of the gold surface. This thinner coupling layer should result in an increase in SPR sensitivity, as it then brings any interactions under scrutiny closer to the gold surface where the SPR phenomenon (i.e. field created by the evanescent wave) is at its strongest. The disadvantage of using the SAM chip with its thinner

coupling layer is that the surface becomes more susceptible to degradation than the dextran layer on CM5 chips.

Beakers used in preparing the SAM were treated with a solution containing 15 mL of concentrated (51%) sulphuric acid (H_2SO_4) (J.T.Baker, NJ, USA) and 5 mL of 30% hydrogen peroxide (H_2O_2.) (Labserv, New Zealand). The treatment involved allowing the H_2SO_4/H_2O_2 solution to stand in the beakers for 30 minutes, after which the solution was discarded, and the beakers rinsed with 18 MΩ deionised water. A mixture of 25 mL 18 MΩ deionised water and 5 mL of analytical grade ammonia (NH_3) (Biolab, New Zealand) was added into the beakers before the beakers were placed into a sonication bath for 30 minutes. After that time, the beakers were rinsed with 18 MΩ deionised water and dried with compressed nitrogen gas. A gold sensor chip was placed into one of the beakers, which contained a mixture of 15 mL H_2SO_4 and 5 mL H_2O_2. The beaker containing the gold sensor chip immersed in the solution was then covered with tinfoil and incubated at 50°C for 30 minutes. Once, the gold surface had been cleaned with the H_2SO_4/H_2O_2 solution, the gold sensor chip was rinsed with 18 MΩ deionised water and dried with compressed nitrogen gas. The chip was placed into another beaker, which contained a mixture of 9 mL 0.01 mol/L 11-mercepto-1-undecanol (11-MUOH) and 1 mL 16-merceptohexadecanoic acid (16-MUA). The beaker was covered with tin foil and stored in the dark at room temperature for approximately 24 hours. The coated sensor chip was taken out of the solution and was firstly rinsed well with ethanol and secondly by 18 MΩ deionised water before being dried with a stream of nitrogen gas. Finally, the sensor chip was encased into a plastic chip holder by following a guided procedure in the SAM kit manual provided by the BIAcore manufacturers.

The OVA and P4-PEG-OVA immobilisation procedures described in Section 4.3.1 were carried out with the SAM chip. A reference flow-cell was prepared with 0.5 mg/mL OVA; and a sample flow-cell was prepared with 0.5 mg/mL of P4-PEG-OVA. The sensorgram of the immobilisation procedure using the SAM chip is shown in Figure 4.3-5. The P4-PEG-OVA binding response was at *ca.* 2300 RU after the surface was washed with 0.01 mol/L glycine pH 2.0 for three times.

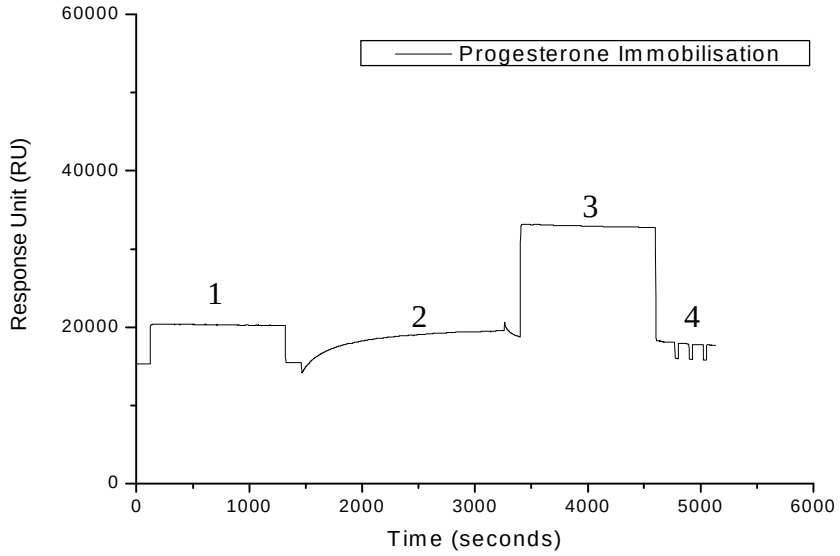

Figure 4.3-5 Sensorgram of the P4-PEG-OVA immobilisation on the SAM chip. 1) Surface activation with EDC/NHS. 2) 500 μg/mL P4-PEG-OVA immobilisation. 3) Surface deactivation with EAH. 4) three surface washes with pH 2.0, 0.01 mol/L glycine. The large increase in responses observed for 1) and 3) were caused by solvent effects (change in refractive index due to solvent) rather than binding on sensor surface.

The newly prepared P4-PEG-OVA surface was checked with 100 μg/mL mAb for quality of the surface prepared. The 100 μg/mL mAb was injected into the reference and sample flow-cells at 60 μL over 3 minutes. The surface was regenerated with 0.05

mol/L sodium hydroxide + 10 mL/ 100 mL acetonitrile regeneration buffer (Reg Buffer 1) at 10 μL over 0.5 minute (see Figure 4.3-6).

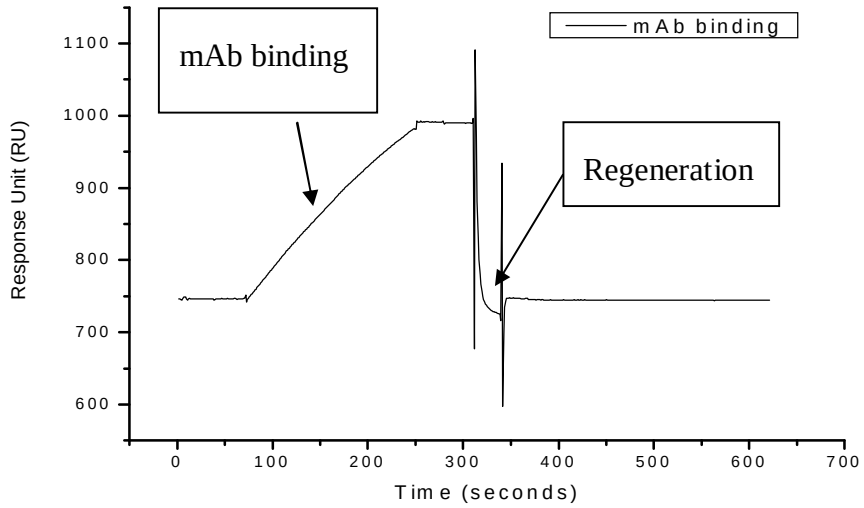

Figure 4.3-6 ensorgram showing the binding of 100 μg/mL mAb on the immobilised progesterone (SAM chip) surface. The surface was regenerated with Regen Buffer 1. The spikes shown in the sensorgram were due to solvent effects (change in refractive index due to Regen Buffer 1) rather than being caused by binding.

4.4 Progesterone-antibody analysis using BIAcore SPR technology

4.4.1 Introduction

As mentioned earlier, progesterone was the small molecular (analyte) being studied, and the monoclonal anti-progesterone antibody raised in rats (Sigma, St. Louis, MO, USA) was the binding ligand. This monoclonal antibody (mAb) binds specifically with the immobilised progesterone and it was able to give reproducible responses from BIAcore within an experimental error of ± 5% [14]. As the concentration of mAb is dropped to around 2 μg/mL, the response from BIAcore became too low and the technique becomes unable to distinguish between samples that are at or below this concentration of 2 μg/mL. The use of enhancement molecules, however, was able to increase the signal responses through mass accumulation on the surface of the sensor chip, thus enabling the instrument to distinguish between samples with < 2 μg/mL mAb concentrations (ie. these enhancement molecules act to lower the limit of detection, LOD).

Enhancement was achieved by a sequential method. The mAb was firstly flowed pass the sensor chip surface with immobilised progesterone, and interaction between mAb and the immobilised progesterone occurred. The enhancement species was then flowed pass the mAb inducing an interaction between the enhancement species with the mAb. Essentially, after doing this there were two layers on top of the immobilised progesterone (see Figure 4.4-1).

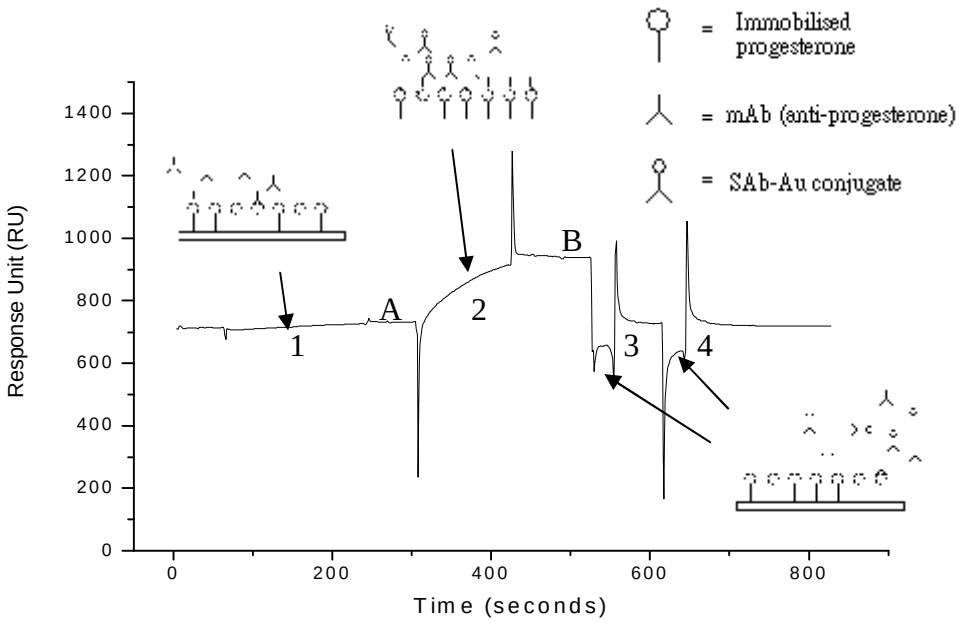

Figure 4.4-1 Sensorgram showing SAb-Au conjugate enhancement of the mAb response signal. 1) The mAb binding response (A). 2) SAb-Au conjugate binding on top of the surface-bound mAb inducing a higher response (B). 3) & 4) Regeneration of the sensor surface.

Binding gold colloids alone to mAb was studied by Mitchell et al, and the study showed that the gold colloids was able to improve the signal response by about 2 fold [57], which meant that the response with gold colloids attached to the mAb was twice as high as the response generated by mAb alone. Signal enhancement using secondary antibody (SAb) and SAb-gold conjugate was also carried out by Mitchell et al. The secondary antibody used in the study by Mitchell et al was anti-rat immunoglobulin G (IgG) raised in rabbits (R5128, Sigma). The enhancement achieved by SAb (IgG) alone was around 8 fold, whilst the SAb-gold conjugate was able to improve the signal response by about 13 fold overall [57].

In this Chapter, the enhancement effect of SAb-gold conjugate was studied using the gold colloids generated earlier in the study. The SAb-gold conjugate was prepared

with more concentrated (compared with the preparation by Mitchell et al) and stabilised gold colloids described in Section 4.4.2.1. The use of Albumin, Bovine (BSA) in the preparation of SAb (IgG) and SAb-Au conjugate was able to reduce the non-specific binding of these enhancement species with the sensor chip surface [31]. A dilution buffer made up of 0.3 mol/L sodium chloride + 1 mL/ 100 mL PEG 400 (Prolab, Fountenay sous bois, France) + HBS buffer were also reported by Jing et al [58] to reduce the level of non-specific binding of the SAb-Au conjugate enhancement species on the BIAcore sensor chip surface. It was shown in the previous study by Jing et al [58] that mixing the SAb-Au conjugate 1:1 with the dilution buffer could reduce the non-specific binding of the SAb (IgG) with the immobilised progesterone on the sensor chip surface. The effectiveness of this dilution buffer to reduce non-specific binding is shown in Section 4.5.1.

The SAb-Au conjugate signal enhancement analysis was carried out with two different sensor chips namely CM5 and SAM sensor chips in this study. The CM5 is the sensor chip that the previous study on progesterone was based on. The CM5 100 nm-thick coupling layer (described previously), however, can limit the signal responses from the instrument as antigen-antibody interactions are happening > 100 nm above the gold surface, where the evanescent electric field induced by the gold surface is not at its strongest. The SAM sensor chip is an alternative sensor surface that allowed a thinner coupling layer to be coated onto the gold surface. As the coupling layer is thinner, the antigen-antibody interactions are occurring closer to the surface and more within the gold evanescent field, thus the signal responses, in theory, should be significantly higher compared to signal responses from the CM5 sensor chip.

4.4.2 Preparation of Materials for Progesterone-antibody analysis

4.4.2.1 Preparation of Au sols

Earlier investigations on the gold colloids showed that arabinogalactan was effective in stabilising Au colloids prepared by the three different reduction methods. However, when preparing SAb-Au conjugates from the three Au colloids only sodium borohydride reduced Au colloids remained stable in the presence of the SAb (IgG). The gold in the hydrazine and citrate reduced colloidal systems aggregated immediately after conjugation with the SAb (IgG). This was suspected to be due to the change in pH of the gold colloids prior to conjugation (though aggregation did not occur immediately after pH adjustment). Since the gold conjugation with SAb (IgG) was carried out at pH 8.5-9.0, pH adjustment was required for all hydrazine (decrease pH) and citrate reduced (increase pH) gold colloids (see Section 3.4.2 in Chapter 3 for pH measurements of the gold colloids). The change in ionic strength in the colloidal dispersion might have affected the overall charge in the colloidal system, and hence causing aggregation.

The procedure for preparation of sodium borohydride reduced Au colloids was similar to the procedure described in Section 3.3.2 in Chapter 3. The only difference was that more diluted gold colloids were prepared than previously. The preparation was carried out using the same starting concentration of $KAuBr_4$ solution defined in Section 3.3.2 in Chapter 3. The resulting colloids were then diluted with 5 g/L arabinogalactan by the various dilution factors defined later in this chapter. The

procedure for preparing the gold colloids is as follows.

0.0072 mol/L of $KAuBr_4$ solution was used for the preparation. *ca.* 0.05 g of arabinogalactan was dissolved in each of two 5 mL aliquots of the $KAuBr_4$ solution. 0.036 mol/L and 0.072 mol/L sodium borohydride samples were prepared in 18 MΩ deionised water. The 5 mL aliquots of 0.0072 mol/L $KAuBr_4$ solution and the two sodium borohydride solutions were then cooled to ~4°C. After cooling, the $KAuBr_4$ solutions were stirred at a medium speed and 5 mL of each concentration of sodium borohydride was added dropwise to the respective 5 mL aliquots of $KAuBr_4$ solutions with stirring. The stirring was continued for a further 30 seconds after the addition of sodium borohydride. The Au colloids were left at room temperature for a few hours to ensure completion of reaction and then stored at ~4°C. The colloids were later diluted for the "optimum Au colloids concentration study" with 5 g/L arabinogalactan by various dilution factors (see later).

4.4.2.2 Preparation of buffer solutions

Regeneration and dilution buffers were prepared freshly on the day of analysis.

Regeneration buffer was used to regenerate the surface of the sensor chip. The characteristic of a good regeneration buffer is its ability to wash away materials coupled to the immobilised molecules without damaging or compromising the sensor chip surface. In this study, 0.05 mol/L sodium hydroxide + 10% v/v acetonitrile (Reg Buffer 1) and 0.05 mol/L sodium hydroxide + 20% v/v acetonitrile (Reg Buffer 2) were the regeneration buffers used. 0.1 mol/L sodium hydroxide was prepared by dissolving sodium hydroxide pellets (Scharlau, Spain) in 18 MΩ deionised water. It

was then diluted in 18 MΩ deionised water to make 0.05 mol/L sodium hydroxide. The 0.05 mol/L sodium hydroxide stock solution was stored at ~4°C. On the day of analysis, 200 µL of neat acetonitrile was added to 1800 µL of 0.05 mol/L sodium hydroxide to make 2 mL of the Reg Buffer 1. 400 µL of neat acetonitrile was added to 1600 µL of 0.05 mol/L sodium hydroxide to make 2 mL of the Reg Buffer 2.

The dilution buffer was made up of 0.3 mol/L sodium chloride + 1 mL/100 mL PEG400 + HBS buffer. It was prepared freshly on the day of analysis by dissolving 17.5 mg sodium chloride in 990 µL HBS buffer, which was then mixed with 10 µL of PEG 400 before it was vortex mixed.

4.4.2.3 Preparation of monoclonal antibody (mAb)

The original concentration of monoclonal anti-progesterone (mAb) raised in rat (P1922, Sigma) was 17 mg/mL. 500 µg/mL mAb was made by adding 5 µL of the 17 mg/mL mAb to 165 µL of HBS-EP buffer (BIAcore AB, Sweden). Different concentrations of mAb were then prepared by diluting the 500 µg/mL mAb in HBS-EP buffer. Samples were vortex mixed after preparation.

4.4.2.4 Preparation of secondary antibody (IgG)

Anti-rat immunoglobulin G (IgG) raised in rabbits was used in this study. The concentration of the stock solution of SAb (IgG) (R5128, Sigma) was 22.5 mg/mL. Lower concentrations of SAb were prepared following a procedure in preparing SAb-Au conjugates, which will be described in the next section of this chapter. Serial dilution was carried out with the original concentration of SAb (IgG); for example,

0.4 mg/mL SAb (IgG) was prepared by firstly diluting 20.4 μL (using Eppendorf micropipettes) of 22.5 mg/mL SAb (IgG) with 79.6 μL of 18 MΩ deionised water to make 100 μL of 4.6 mg/mL SAb (IgG). This 100 μL of 4.6 mg/mL SAb (IgG) was then further diluted with 1000 μL of 18 MΩ deionised water. Finally, 50 μL of 10 g/100 mL Bovine (BSA) prepared by dissolving 10 mg of BSA (Sigma, Albumin, Bovine, A7030 Lot 082K0768) in 100 μL of 18 MΩ deionised water was added to the diluted SAb (IgG) to make 1150 μL of 0.4 mg/mL SAb (IgG).

4.4.2.5 Preparation of SAb-Au conjugate

To prepare 1150 μL of 0.4 mg/mL SAb-Au conjugate, 20.4 μL of 22.5 mg/mL SAb (IgG) was firstly being diluted with 79.6 μL of pH8.5 - 8.9 (18 MΩ deionised) water (which had been adjusted to that pH with 1 mol/L sodium hydroxide) to make 100 μL of 4.6 mg/mL SAb (IgG). 1000 μL of gold colloids (prepared from the procedure described in Section 4.4.2.1), which had also been pH adjusted to pH 8.5 - 8.9 with 1 mol/L hydrochloric acid, was then added to the 100 μL of the 4.6 mg/mL SAb (IgG) while it was vortex mixed. The mixture was agitated on a test-tube shaker at 320 rpm for 5 minutes before incubation at ~4°C for approximately 18.5 hours. After this period, 50 μL of 10 g/ 100 mL BSA was then added to the conjugate during vortex mixing.

During the enhancement study (see Section 4.4.3), different concentrations of the SAb (IgG) and gold colloids were used. However, the preparation procedure remained the same.

4.4.3 Signal Enhancement Study Using SAb (IgG) and SAb-Au Conjugates

4.4.3.1 Introduction

In this chapter, the enhancement effect of secondary antibody and secondary-gold conjugate was studied using the CM5 sensor chip. The particle-size effect (of the Au colloids used) was also studied. The two samples of gold colloids prepared in Section 4.4.2.1 were conjugated with SAb (IgG), and their levels of enhancement were studied with different mAb concentrations.

Preliminary tests such as non-specific binding and optimum concentration determinations were essential in designing a progesterone competition assay (see Section 4.6 for more details on competition assay). Non-specific binding is an important issue for BIAcore. As the instrument is based on monitoring the changes in mass/refractive index that occurs on the sensor chip surface, species other than the ligand, mAb, (ie. SAb (IgG) or SAb-Au conjugate) may also bind to the surface and would be detected as the ligand (mAb). Therefore, it was important in this study to determine the non-specific binding of SAb (IgG) and SAb-Au conjugate and to subtract the level of non-specific binding from the true binding responses (ie the responses caused by the combination of mAb and SAb-Au conjugate rather than the responses from SAb-Au alone).

The optimum concentrations of mAb, SAb (IgG), and Au colloids (with fixed concentrations of arabinogalactan used) for running immunoassays (analysis for

antibody-antigen interactions) were determined by a series of concentration analyses. In some analyses, the concentration of the mAb was fixed in the first of three analyses. Different concentrations of SAb (IgG) were then conjugated with a fixed concentration of gold colloids present. Enhancement tests (described by Figure 4.4-1 in Section 4.4.1) are carried out for each concentration of SAb-Au conjugate. The signal responses obtained for each concentration of SAb-Au were plotted against the concentration of SAb (IgG) used to prepare the SAb-Au conjugates (binding curve), and the lowest concentration at which the SAb-Au signal response is near the maximum in the binding curve determined to be the optimum SAb (IgG) concentration. By fixing the concentration of SAb (IgG) and the Au colloids, the optimum concentration of mAb can then be determined. When all three optimum concentrations of mAb, SAb (IgG) and Au colloids are obtained, an signal enhancement level can be determined. Consequently, an assay for determining the LOD for progesterone can then be carried out.

The schematic process of determining the optimum concentration of mAb, SAb (IgG) and gold colloids for running progesterone immunoassay is illustrated for clarity in Figure 4.4-2.

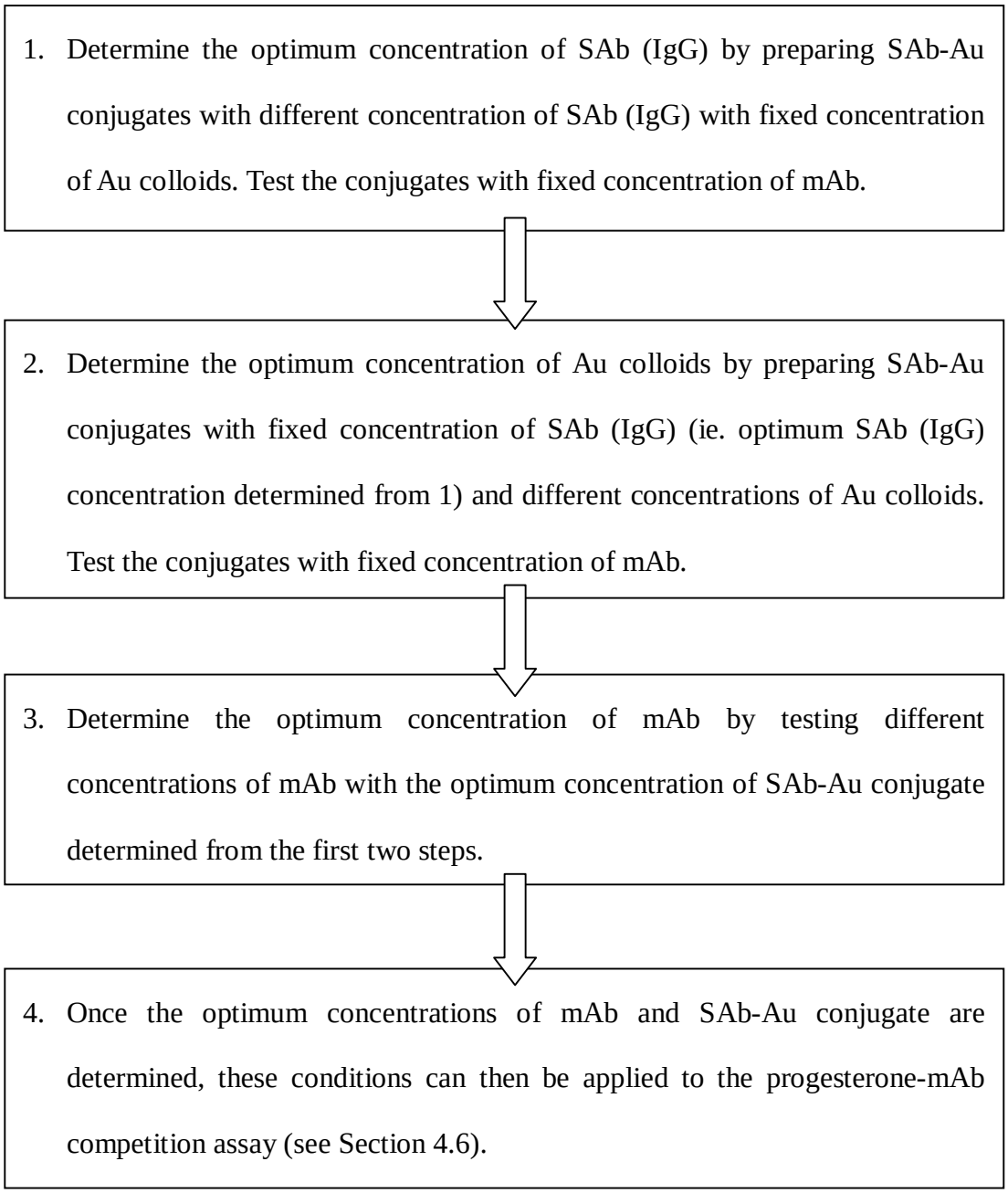

Figure 4.4-2 Four key steps required for the development of the progesterone immunoassay

4.4.3.2 Non-specific binding studies

The enhancement species was made up of three different components, namely SAb (IgG), gold colloids, and arabinogalactan (AG). Each of these might contribute to the non-specific binding on the immobilised progesterone surface. Therefore, each component along with the SAb-Au conjugate were prepared and tested on the CM5

sensor chip with immobilised progesterone.

The gold colloids alone was firstly analysed for non-specific binding using the CM5 chip. The 1:1 diluted colloidal gold was further diluted at 1:1 ratio with the (0.3 mol/L + 1 mL /100 mL PEG400 + HBS) dilution buffer. It was "Quickinjected" into the reference and sample flow-cell at 40 μL over 2 minutes for the non-specific binding test. The surface was then regenerated with the Reg Buffer 1 at 10 μL over 0.5 minute.

The effect of using AG solution versus the HBS solution on the extent of non-specific binding was then studied. In order to determine the role (if any) that AG played in the non-specific binding of SAb-Au conjugate, a mixture of 5 g/L AG and 100 μg/mL SAb (IgG) were tested with and without the 1:1 dilution with the dilution buffer. The concentrations specified were the final concentrations after dilution with either HBS buffer or the dilution buffer at 1:1 ratio. The SAb (IgG) samples were analysed by BIAcore using the same injection procedures described above for gold colloids.

Lastly, SAb-Au conjugates with final concentration of 17.5 and 100 μg/mL were tested for non-specific binding. The samples were diluted with the dilution buffer (0.3 mol/L + 1 mL /100 mL PEG400 + HBS) at 1:1 ratio.

The non-specific binding study using the SAM sensor chip was also carried out. SAb-Au conjugates prepared by adding 1:2 diluted gold colloids with different concentrations of SAb (IgG) were tested for their levels of non-specific binding. Each concentration of SAb-Au conjugate was injected (without the target analyte, mAb) through the reference and sample flow-cells at 40 μL over 4 minutes. Reg Buffer 2

was then used to regenerate the surface by injecting at 10 μL over 0.5 minute to the same reference and sample flow-cells.

4.4.3.3 Signal enhancement using SAb (IgG) vs. signal enhancement using SAb-Au conjugate

Analyses were carried out to confirm experimentally that SAb-Au conjugates have a greater signal response enhancement than SAb (IgG) alone. Gold colloids were prepared by the procedure described in Section 4.4.2.1. The colloids were diluted 1:1 with 5 g/L AG. The diluted samples were then conjugated (by following the procedure for preparing the SAb-Au conjugate described in Section 4.4.2.5) with two different concentrations of SAb (IgG) to make 35 and 200 μg/mL SAb-Au conjugates. 35 and 200 μg/mL SAb (IgG) were also prepared without the gold colloids. The SAb-Au conjugates and the SAb (IgG) were diluted 1:1 with the dilution buffer before they were being analysed. The final concentrations of SAb (IgG) in the gold conjugated and unconjugated samples were 17.5 and 100 μg/mL.

25 and 100 μg/mL of mAb were prepared by the procedure described earlier in Section 4.4.2.3. The level of enhancement using the conjugates and the SAb (IgG) were tested with the two concentrations of mAb. The injection scheme was based on the study by Mitchell et al. The mAb was injected into the reference and sample flow-cell of a modified CM5 chip (using “Quickinjection”) at 60 μL over 3 minutes. This was followed by the enhancement species at 40 μL over 2 minutes. The surface of the sensor chip was regenerated twice with Reg Buffer 1 at 10 μL over 0.5 minute per injection.

4.4.3.4 Effect of Particle Size on Signal Enhancement

The borohydride reduced Au colloids prepared in Section 4.4.2.1 had two different particle size distributions. These are illustrated by the size results of sample 130806-1 and 130806-2 in Section 3.4.5 in Chapter 3. The colloids were used to study the effect of particle size on signal enhancement. The study was carried out on a CM5 sensor chip.

2.3 mg/mL and 400 μg/mL SAb (IgG) were used to make conjugates with Au colloids prepared by the procedure shown in Section 4.4.2.1. The concentrations of SAb (IgG) were only preliminary concentrations (concentrations that were estimated based on previous studies by Mitchell et al and Jing et al). For each size of gold colloids, three conjugates were prepared by the procedure described in Section 4.4.2.5. These included a blank sample containing 1000 μL Au colloids + 100 μL deionised water + 50 μL 10 g/ 100 mL BSA; a sample with 1000 μL Au colloids + 100 μL of 2.3 mg/mL SAb (IgG) + 50 μL 10 g/ 100 mL BSA; and a sample with 1000 μL Au colloids + 100 μL of 400 μg/mL SAb (IgG) + 50 μL 10 g/ 100 mL BSA. The conjugates were diluted in a 1:1 ratio with the dilution buffer before the analysis. After dilution, the final concentrations of SAb (IgG) in SAb-Au conjugates prepared from 2.3 mg/mL and 400 μg/mL SAb (IgG) were 100 and 17.5 μg/mL respectively.

25 μg/mL and 100 μg/mL of monoclonal anti-progesterone were prepared by the procedure described in Section 4.4.2.3. The 25 μg/mL mAb was “Quickinjected” at 60 μL over 3 minutes through the reference and sample cells. This was followed by a “Quickinject” of a sample of the six SAb-Au conjugates at 40 μL over 2 minutes. The surface was regenerated with Reg Buffer 1, which was “Quickinjected” twice at 10

μL over 0.5 minute. This process was repeated until all six SAb-Au conjugates were tested against both concentrations of mAb.

The particle size effect was not tested using the SAM chip. This will be discussed in Section 4.5.

4.4.3.5 Secondary Antibody – Gold Conjugate Binding Curve

SAb-Au conjugate has two factors which can influence its level of enhancement: 1) the concentration of gold colloids used (this was studied by monitoring the effect of varying concentration of Au colloids with fixed concentration of mAb and SAb (IgG)), and 2) the concentration of SAb (IgG) used (the optimum concentration of SAb (IgG) was determined by measuring the level of enhancement of SAb-Au conjugate using various concentrations of SAb (IgG) while holding the concentration of mAb and the gold colloids fixed).

The gold colloids were diluted by dilution factors of 2, 2.5, and 3 with 0.5% w/v AG solution. Samples diluted two-folds were prepared by adding 1 mL of the as-prepared gold colloids to 1 mL 5 g/L AG solution. Colloids diluted 2.5 folds were prepared by adding 1 mL of the as-prepared gold colloids to 1.5 mL of 5 g/L AG solution. Colloids diluted 3 folds were prepared by adding 1 mL of the as-prepared gold colloids to 2 mL of 5 g/L AG solution. The preparations were carried out by using Eppendorf micropipettes.

SAb-Au conjugates with SAb (IgG) concentration of 0.4 and 2.3 mg/mL were prepared with the different concentrations of gold colloids according to the procedure

described above. The conjugates were then diluted 1:1 with the (0.3 mol/L sodium chloride + 1 mL/ 100 mL PEG 400 + HBS) dilution buffer. The 17.5 and 100 μg/mL SAb-Au conjugates were then analysed by BIAcore on the CM5 chip using fixed concentrations (5 μg/mL) of mAb in each. "Quickinjection" was the injection mode used for delivering the samples to the sensor chip surface. The mAb was injected through the reference and sample flow-cells at 60 μL over 3 minutes. It was followed by the SAb-Au conjugate at 40 μL over 2 minutes. Reg Buffer 1 was then injected twice at 10 μL over 0.5 minute. All samples were analysed using this procedure.

Upon identifying the optimum concentration of gold colloids to use, this parameter was kept fixed and the SAb-Au conjugates were prepared by varying the concentration of SAb (IgG) at 0, 50, 100, 200, 400, and 800 μg/mL using the borohydride reduced gold colloids with smaller (*ca.* 10 nm) particle size (130806-1). For gold colloids with bigger (*ca.* 16 nm) particle size (130806-2), the SAb (IgG) concentrations were 0, 10, 17.5, 25, and 50 μg/mL (different concentration scheme was used for the larger colloids due to the different responses that the larger colloids gave in comparison with the smaller colloids (see Section 4.5). The samples were analysed by BIAcore using the same sequential injection scheme: 1) 5 μg/mL mAb was injected through the reference and sample flow-cells at 60 μL over 3 minutes. 2) the SAb-Au conjugate at 40 μL over 2 minutes. 3) Reg Buffer 1 injected twice at 10 μL over 0.5 minute.

When determining the optimum concentrations of Au colloids on the SAM chip, gold colloids with 1:1 and 1:2 dilutions with 5 g/L AG solution were prepared. SAb-Au conjugates with final SAb (IgG) concentration of 100 μg/mL were then prepared with these two different concentrations of gold colloids. The conjugates were tested with

2.5 μg/mL mAb (mAb concentration was determined by "trial and error"), which was injected first at 60 μL over 3 minutes. It was followed by the conjugate at 40 μL over 4 minutes. The surface was regenerated with Reg Buffer 2 twice at 10 μL over 0.5 minute.

When determining the optimum concentration of SAb (IgG) to use in SAb-Au conjugate on the SAM chip 0, 25, 50, 100, and 200 μg/mL SAb-Au conjugates were prepared with 1:2 diluted gold colloids. These were tested again with 2.5 μg/mL mAb using the same injection conditions defined above.

4.4.3.6 Monoclonal Antibody Binding Curve

The monoclonal antibody (mAb) binding curve was determined by fixing the concentration of SAb-Au conjugate and plotting the level of signal responses of the conjugate versus the different concentrations of mAb used.

The concentration of SAb (IgG) in SAb-Au conjugates was fixed at 100 μg/mL for gold colloids with smaller particle size and 17.5 μg/mL for gold colloids with bigger particle size (see Section 4.5.3 in Chapter 4 on how these SAb (IgG) concentrations were obtained). 0, 2, 5, 15, and 25 μg/mL of mAb were prepared in HBS-EP buffer. The enhancement effect of the two SAb-Au conjugates was tested against each concentration of mAb (starting from the lowest concentration). This was carried out by injecting, firstly, the mAb at 60 μL over 3 minutes through the reference and sample flow-cells using "Quickinjection". This was followed by "Quickinjecting" one of conjugates at 40 μL over 2 minutes through the same flow-cells. The surfaces of both flow-cells were regenerated with two injections of Reg Buffer 1 at 10 μL over

0.5 minute. The responses generated from mAb and SAb-Au conjugates were plotted against the concentration of mAb. Level of signal enhancement was calculated from the slopes of the plots.

For the SAM sensor chip, the optimum concentration of mAb was identified by fixing the SAb (IgG) concentration at 100 μg/mL in the SAb-Au conjugate. The conjugate was prepared with 1:2 diluted gold colloids, and it was tested with 0, 0.5, 1, and 2.5 μg/mL mAb. Each sample of mAb was injected into the reference and sample flow-cell at 60 μL over 3 minutes. The conjugate was then injected through the same flow-cells at 40 μL over 4minutes. The surface was regenerated with Reg Buffer 2 twice at 10 μL over 0.5 minute.

4.4.3.7 Binding curves for a fresh CM5 sensor chip

A new progesterone surface was prepared on a new CM5 sensor chip by the procedure described in Section 4.3.1 (The reason for preparing a new CM5 surface is discussed in Section 4.5.4). The optimum mAb, SAb (IgG), and gold concentrations were determined again.

The SAb (IgG) concentration in SAb-Au conjugate was determined by fixing the concentration of gold colloids at 1:1 dilution (prepared by following procedure described in Section 4.4.2.1) and mAb concentration at 2 μg/mL. The non-specific binding of the SAb-Au conjugate at different SAb (IgG) concentrations were also analysed. The injection procedure was exactly the same as before apart from the SAb-Au conjugate, which was injected at 40 μL over 4 minutes instead of 40 μL over 2 minutes.

The Au concentration binding curve was not determined, as the optimum dilution ratio of 1:1 was carried forward from the earlier study. The optimum mAb concentration was determined by fixing the SAb (IgG) concentration of the SAb-Au conjugate and the gold concentration. The concentration of mAb was varied from 0, 2, 2.5, and 3 μg/mL.

4.5 Signal Enhancement Results & Discussions

4.5.1 Non-specific binding study

The non-specific binding of the SAb-Au enhancement species was mainly contributed to by the SAb (IgG). Table 4.5-1 contains the non-specific binding determined from the experiments described in Section 4.4.3.2 of each species in the SAb-Au conjugate. It showed that arabinogalactan and the gold colloids exhibited little (< 10 RU) non-specific binding on the immobilised progesterone surface. The responses listed in Table 4.5-1 were obtained from the sensorgrams obtained from direct injection of each species (listed in Table 4.5-1) without injecting the analyte (mAb) beforehand. An illustration of how the non-specific binding responses were obtained from the sensorgrams is shown in Figure 4.5-1.

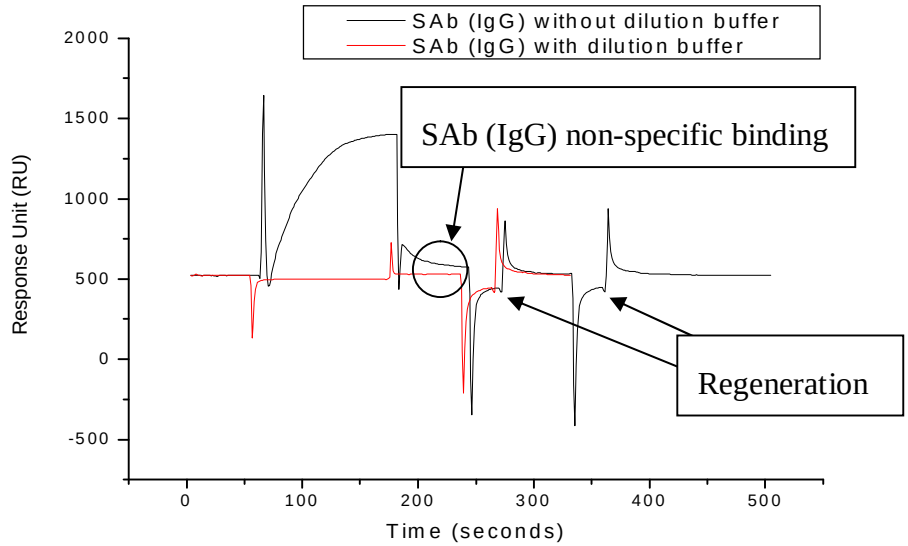

Figure 4.5-1 Sensorgrams of the non-specific binding study of SAb (IgG). The sensorgram shown in black was SAb (IgG) without the (0.3 mol/L NaCl + 1 mL/100 mL PEG + HBS) dilution buffer. The non-specific binding was *ca.*870 RU. SAb (IgG) with added dilution buffer (shown in red) showed significantly lower level (*ca.* 7 RU) of non-specific binding on the progesterone surface (CM5 chip).

The non-specific binding of gold colloids was always analysed after 1:1 dilution with the (0.3 mol/L sodium chloride + 1 mL/ 100 mL PEG400 + HBS) dilution buffer. This is a precautionary procedure to prevent permanent damage to the sensor surface. In the non-specific binding study, the effect of lowering the non-specific binding of SAb (IgG) was tested. The signal response of the sample "SAb (IgG) 100 µg/mL + 0.5% w/v AG without the dilution buffer" (876.9 RU) was similar to the signal response of "SAb (IgG) 100 µg/mL" (885.8 RU). This suggested that AG was ineffective in lowering the non-specific binding of SAb (IgG). The results clearly showed that with the addition of the (0.3 mol/L sodium chloride + 1 mL/ 100 mL PEG400 + HBS) dilution buffer was responsible for the reduction of the SAb (IgG) non-specific binding.

Table 4.5-1 Non-specific bindings of the enhancement species on CM5 sensor chip (average responses from measurement of three replicates of each sample)

Sample	**1:1 Dilution with Dilution Buffer? (Yes/No)**	**Non-specific Binding (RU)**
SAb (IgG) 100 μg/mL	No	885.8 ± 35.5
SAb (IgG) 100 μg/mL	Yes	6.2 ± 0.3
0.5% w/v Arabinogalactan	No	-0.8 ± 0.2
0.5% w/v Arabinogalactan	Yes	2.6 ± 0.6
SAb (IgG) 100 μg/Ml + 0.5% w/v AG	No	876.9 ± 28
SAb (IgG) 100 μg/Ml + 0.5% w/v AG	Yes	8.2 ± 0.3
Au colloids (small size)	Yes	-0.3 ± 0.2
Au colloids (large size)	Yes	2.1 ± 1.8
Au (small size) + 17.5 μg/mL SAb	Yes	1.9 ± 0.4
Au (small size) + 100 μg/mL SAb	Yes	7.3 ± 0.3
Au (large size) + 17.5 μg/mL SAb	Yes	6.1 ± 0.8
Au (large size) + 100 μg/mL SAb	Yes	7.6 ± 0.8

The non-specific bindings of different concentrations of SAb-Au conjugates (prepared from small-sized colloids) on a SAM sensor chip were listed in Table 4.5-2. The non-specific binding of the SAb-Au conjugate had significantly increased on the SAM surface compared to the CM5 surface. The non-specific binding of the 100 μg/mL SAb-Au sample (with small size Au colloids) on the CM5 surface was *ca.* 7.3 RU. Compared to the same concentration of SAb-Au conjugate on the SAM surface (*ca.* 27.8 RU), there was about a 20 RU increase in non-specific binding. This, however, was expected. Since the coupling layer of SAM was thinner than CM5 (as mentioned in Section 4.3.2), the surface-analyte interactions are monitored more within the surface Plasmon region, thus SAM would be more sensitive in detecting any mass changes on the surface of the sensor chip than would the CM5 chip. Hence there would be an enhancement not only of specific binding responses but also non-specific binding responses..

Table 4.5-2 Non-specific binding of SAb-Au conjugates on SAM surface (average responses from measurement of three replicates of each sample)

Concentration of Sab (IgG) (μg/mL)	**Non-specific binding (RU)**
0	1.4 ± 0.4
25	4.9 ± 1.2
50	12.8 ± 0.5
100	27.8 ± 2.8
200	30.9 ± 0.9

4.5.2 Enhancement effect of particle size & SAb-Au

The effect of SAb-Au conjugate containing different particle size of gold colloids in the conjugates is summarised in Table 4.5-3. The enhancement effects of these species were compared with the enhancement level of SAb (IgG) alone. As shown in Section 4.1 and 4.4.1, the enhancement response was the signal response obtained when the SAb-Au conjugate was passed over the mAb (see Figure 4.4-1 in Section 4.4.1), which was bound to the immobilised progesterone. The enhancement ratios shown in Table 4.5-3 were calculated from the SAb-Au enhancement signal response over the mAb signal response. High enhancement ratios were highlighted in the table. The errors in enhancement ratio were calculated from the total percentage error involved in the mAb and enhancement responses.

As the results showed, the enhancement ratio was at the highest (13 fold signal enhancement) when low concentrations of SAb (IgG) (17 μg/mL) were conjugated with Au colloids containing larger particles, or high concentration of SAb (IgG) (100 μg/mL) were conjugated with Au colloids containing smaller particles. This finding might be explained by the packing arrangement of the SAb-Au conjugate on the

sensor surface. When large particles were involved, the large mass of the colloidal particles might be able to induce large changes in the refractive index on the sensor surface; however, steric crowding might have limited the number of the SAb-Au conjugates that could be bound to the sensor surface. Hence, the signal enhancement ratio of the SAb-Au conjugate (with 17 μg/mL SAb (IgG) and large colloids) was similar to the signal enhancement ratio of the SAb-Au conjugate (with 100 μg/mL SAb (IgG) and small colloids), as it did not have steric hindrance issue and more SAb-Au conjugates were able to be packed/bound to the sensor surface.

Table 4.5-3 Comparison of response signals of SAb (IgG), SAb-Au conjugate, and particle effect on CM5 surface (average responses from measurement of three replicates of each sample)

	mAb (25 mg/mL) Response (RU)	**SAb-Au Enhancement (RU)**	**Enhancement Ratio**
SAb (17 mg/mL)	20.3 ± 0.4	45.4 ± 1.7	2.2 ± 6%
SAb-Au 130806-1 (Small)	19.9 ± 0.4	59.0 ± 1.6	3.0 ± 5%
SAb-Au 130806-2 (Large)	**20.1** (0.5	260.2 (18.1	13.0 (9%
SAb (100 mg/mL)	20.5 ± 0.5	101.4 ± 1.4	4.9 ± 4%
SAb-Au 130806-1 (Small)	**21.6** (1.4	281.0 (10.5	13.0 (10%
SAb-Au 130806-2 (Large)	21.7 ± 0.2	210.1 ± 11.4	9.7 ± 6%

	mAb (100 (g/mL) Response (RU)	**SAb-Au Enhancement (RU)**	**Enhancement Ratio**
SAb (17 (g/mL)	69.5 (1.4	137.2 ± 2.2	2.0 ± 4%
SAb-Au 130806-1 (Small)	73.4 ± 1.9	198.3 ± 5.3	2.7 ± 5%
SAb-Au 130806-2 (Large)	**70.7** ± 1.1	**866.4** ± 20.6	**12.3** ± 4%
SAb (100 mg/mL)	73.3 ± 1.5	309.2 ± 7.7	4.2 ± 5%
SAb-Au 130806-1 (Small)	n/a	n/a	n/a
SAb-Au 130806-2 (Large)	n/a	n/a	n/a

SAb-Au conjugates with 100 μg/mL SAb (IgG) were not tested against the 100 μg/mL mAb. Given the level of SAb (IgG) enhancement was already at around 300 RU, the SAb-Au conjugates enhancement might be too high (> 1000 RU), in which case, the regeneration procedure would be difficult and the sensor surface might be damaged irreversibly by the permanently bound species.

4.5.3 Binding curves of the first CM5 sensor chip used

As mentioned in Section 4.4.3.5, the optimum concentration of SAb-Au conjugate is determined by the lowest concentration of SAb (IgG) and Au colloids that can produce the highest possible signal response. In Figure 4.5-2, the response obtained from SAb-Au conjugate made from undiluted Au colloids (with smaller size) was at *ca.* 68 RU. The response of SAb-Au made from 1:1 diluted Au colloids (with smaller size) was *ca.* 64 RU. As the Au colloids dilution increased to 1:2, the response decreased considerably to *ca.* 38 RU. Therefore, the optimum concentration of smaller-sized Au colloids was roughly at 1:1 dilution (or dilution factor of 2) of the Au colloids prepared in Section 4.4.2.1 (which was equivalent to Au colloids prepared from *ca.* 0.0036 mol/L $KAuBr_4$ solution). The optimum concentration of larger-sized gold colloids was also at 1:1 dilution of the Au colloids prepared in Section 4.4.2.1 (see Figure 4.5-3). The Au concentration binding curve of the Au colloids with larger particle sizes has an unusual shape which might be caused by the inconsistent particle size (shown in Section 3.4.4 in Chapter 3) in the sample of gold colloids.

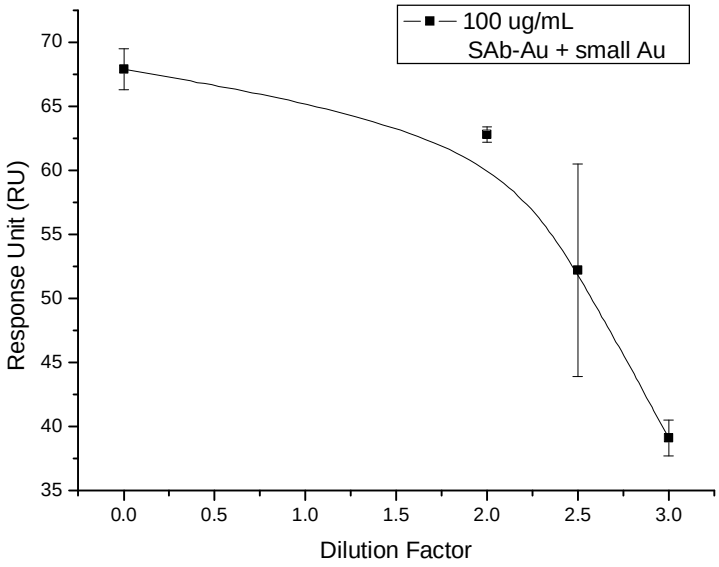

Figure 4.5-2 Response signals of SAb-Au conjugate (100 μg/mL) with different concentration of Au colloids (130806-1) at 5 μg/mL mAb concentration (each data point was averaged from the measurement of three replicates)

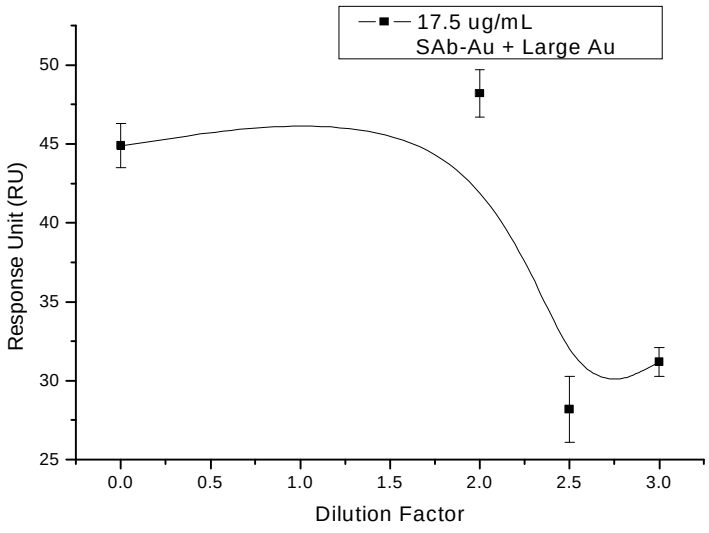

Figure 4.5-3 Response signals of SAb-Au conjugate (17.5 μg/mL) with different concentrations of Au colloids (130806-2) at 5 μg/mL mAb concentration (each data point was averaged from three replicate of measurements)

The SAb-Au conjugate binding curve is shown in Figure 4.5-4 and Figure 4.5-5 for

SAb-Au conjugates prepared from smaller and larger Au colloids respectively. Figure 4.5-4 shows that at SAb (IgG) concentration of 800 μg/mL the SAb-Au (with smaller Au colloids) conjugate had the highest signal response (*ca.* 47 RU). The signal response, however, was only about 8 RU higher than the response from 100 μg/mL SAb (IgG) concentration. Thus 100 μg/mL was chosen as the optimum concentration of SAb (IgG) for preparing SAb-Au conjugate.

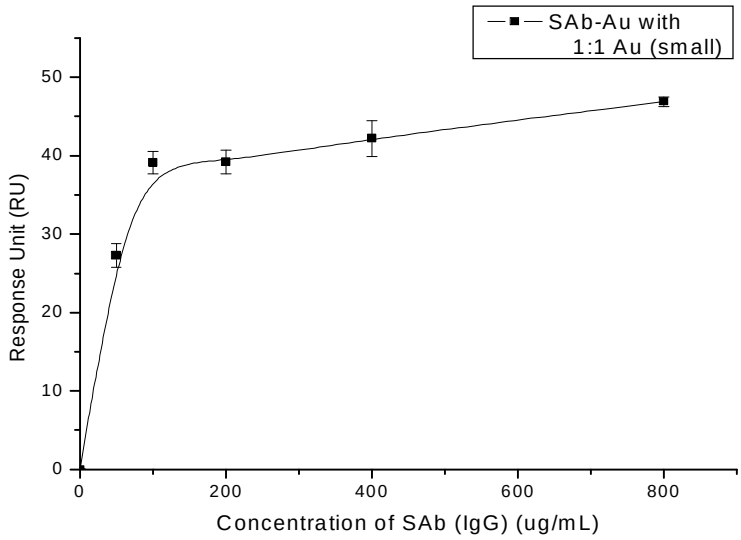

Figure 4.5-4 Binding curve of SAb-Au conjugate using borohydride reduced Au colloids (smaller particle size, *ca.* 10 nm). Signal responses were given rise by SAb-Au conjugate at different concentrations of SAb (IgG) at 5 μg/mL mAb. (each data point was averaged from three replicates of measurement)

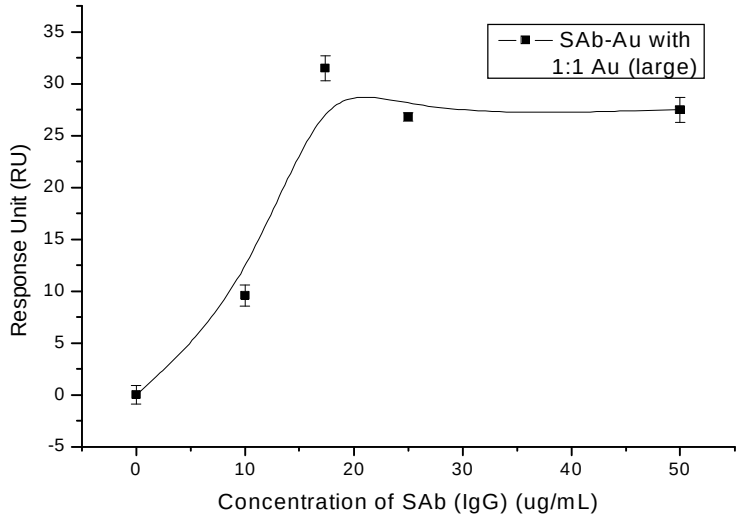

Figure 4.5-5 Binding curve of SAb-Au conjugate using borohydride reduced Au colloids (larger particle size, *ca.* 16 nm). Signal responses are due to the SAb-Au conjugate at different concentrations of SAb (IgG) at 5 μg/mL mAb (each data point was averaged from three replicates of measurement)

For gold colloids with larger particle sizes the optimum concentration of SAb (IgG) was at *ca.* 18 μg/mL. The binding curve in this experiment has demonstrated an unusual shape compare to the binding curve of SAb-Au made from gold colloids with smaller particle size in Figure 4.5-4. There was no clear explanation for why the shape of the curve is as observed. However, one possible reason for the unusual shape could be the inconsistent particle size in the colloidal sample. As shown in Section 3.4.4 in Chapter 3, the particle size distribution of the borohydride reduced Au colloids (130806-2), which contained larger particles, was relatively polydisperse compared those measured for borohydride reduced Au colloids with smaller particles (130806-1). The 130806-2 Au colloids have particles mainly in the 10 nm size range, but it also has particles in the 25-35 nm range. As the 130806-2 Au colloids exhibited a bimodal particle size distribution, the binding of SAb-Au conjugates on the sensor surface could involve some very different sizes of Au colloids (in which case perhaps packing

issues at the surface could be a factor). Thus the shape of the binding curve was less predictable compared to the binding curve obtained from SAb-Au conjugate generated from a more monodisperse Au colloids (130806-1).

Figure 4.5-6 contains two overlaid sensorgrams, which illustrate different levels of 100 µg/mL SAb-Au binding with two different concentrations of mAb.

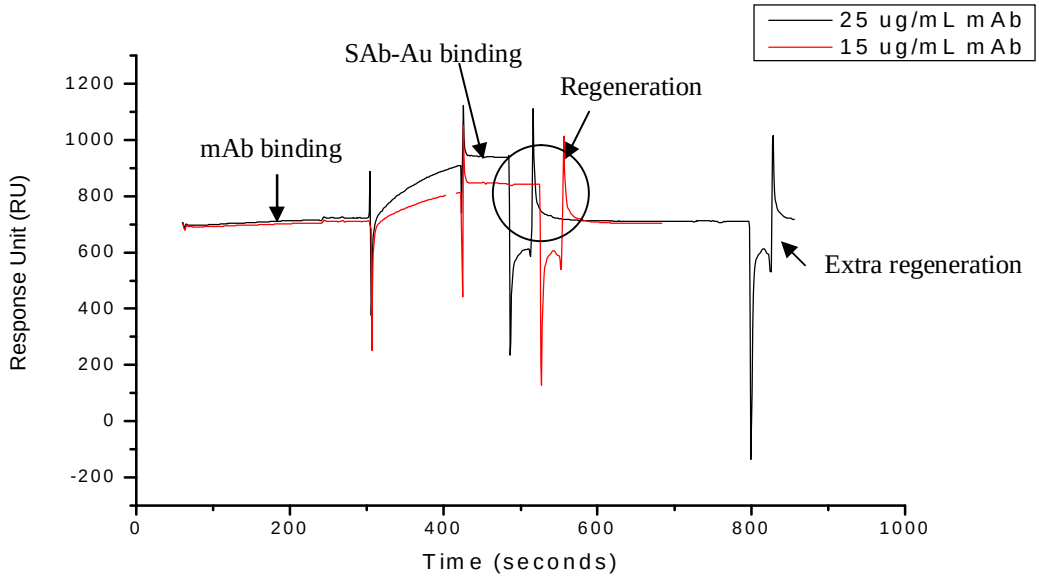

Figure 4.5-6 Sensorgrams of signal enhancement using 100 µg/mL SAb-Au conjugate with 15 and 25 µg/mL mAb

The mAb binding curve with 100 µg/mL SAb-Au conjugate (with smaller colloids) is shown by Figure 4.5-7. The black line is a plot of the responses from the different concentrations of mAb, and the red line indicates the SAb-Au conjugate (with smaller Au colloids) and 100 µg/mL SAb (IgG)) enhancement with different concentrations of mAb. The enhancement effect of SAb-Au conjugate was calculated from the slopes (shown by the equations on the plot) of the two straight lines. The SAb-Au

enhancement ratio was 12.6 fold higher than the signal responses produced by mAb alone. The enhancement ratio was calculated from the ratio between the two slopes. The enhancement level achieved in this study was very similar to the enhancement ratio (*ca.* 13 fold) reported by Mitchell et al. However, the level of enhancement in this study was achieved with the 100 µg/mL SAb-Au conjugate instead of the 800 µg/mL SAb-Au conjugate prepared by Mitchell et al. This means the SAb-Au conjugate developed in this study was more efficient (compared to the SAb-Au conjugate made by Mitchell et al) in achieving the same level of signal enhancement as in the study by Mitchell et al. This represents an advance made in this study over the previous study by Mitchell et al by use of the non-citrate generated Au colloids as signal enhancement species.

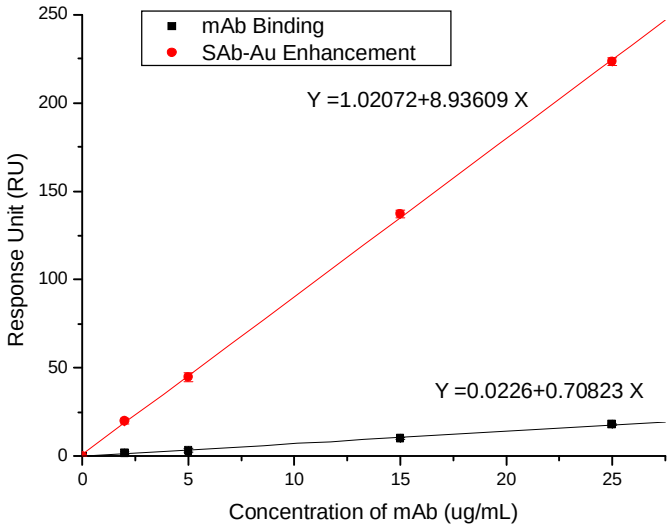

Figure 4.5-7 mAb binding curve with (red) and without (black) SAb-Au enhancement (small colloids). The non-specific binding response of the SAb-Au conjugate has been subtracted from the plot.

MAb binding curve with SAb-Au conjugate with large Au colloids and 100 µg/mL SAb (IgG) is shown by Figure 4.5-8. The enhancement level was 12.3 fold higher

than the level of response from the mAb alone.

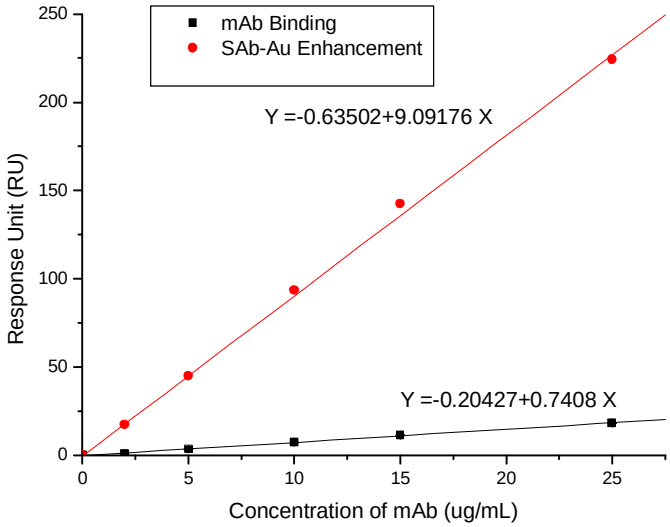

Figure 4.5-8 mAb binding curve with (red) and without (black) SAb-Au enhancement (larger colloids). The non-specific binding response of the SAb-Au conjugate was subtracted off from the plot.

The optimum mAb concentration was determined from the enhanced signal responses. The signal response after SAb-Au enhancement should be no more than 150 RU, as any responses higher than 150 after enhancement would result in problems with regenerating the sensor surface. From Figure 4.5-7 and 4.5-8, the optimum mAb concentration of both systems was at around 10 to 15 μg/mL, since the corresponding enhancement responses were around 100 to 150 RU respectively.

4.5.4 Binding curves of a newly prepared CM5 sensor chip

After the preliminary tests were done, a new progesterone surface was immobilised onto a new CM5 sensor chip, and retested with the optimum conditions determined from the previous CM5 chip. The results showed the responses were slightly different from the previously determined mAb, SAb (IgG), and gold optimum concentrations. Therefore, the optimum mAb, SAb-Au concentrations were re-determined.

One of the differences between the sensorgrams obtained from the previous CM5 surface and sensorgrams from the new CM5 surface is that of the binding of the SAb-Au conjugate. The SAb-Au binding had “high” and “low” points shown on the sensorgram below. This characteristic was not observed in the sensorgrams from the previous CM5 surface (see Figure 4.5-6 in Section 4.5.3). In Figure 4.5-6, the SAb-Au binding did not have the large decrease (from “high” point to “low” point) in response as observed in Figure 4.5-9. Therefore, the binding level (the signal response) of SAb-Au on the previous CM5 surface was easy to determine, as there was only a point on the sensorgram which indicated the response given by the SAb-Au. The SAb-Au signal response on the new CM5 surface, however, had two points which might indicate the level of binding of SAb-Au conjugate on the sensor surface (see Figure 4.5-9). This made the determination of SAb-Au signal response difficult. The study later found that the “high” and “low” points had similar true responses (responses after subtracting the non-specific binding of SAb-Au conjugate from the enhancement responses) (see “True Binding” in Table 4.5-4). Thus only “high” points were used in the determination of mAb binding curve and the progesterone-mAb competition assay in Section 4.6.

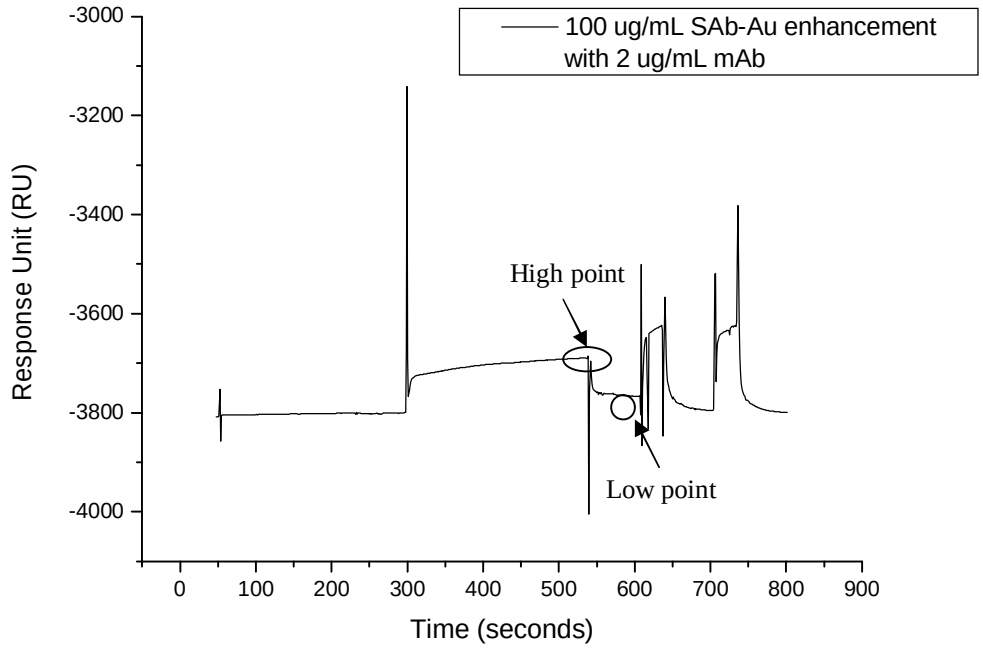

Figure 4.5-9 Sensorgram of SAb-Au enhancement on a new CM5 surface

Table 4.5-4 Non-specific and signal enhancement of SAb-Au conjugate on new CM5 surface

	Non-specific Binding (RU)		**Sab-Au Enhancement (RU)**		**True Binding (RU)**	
SAb-Au Sample (mg/mL)	**High Point**	**Low Point**	**High Point**	**Low Point**	**High Point**	**Low Point**
0	83.2 ± 2.4	9.0 ± 0.4	88.8 ± 0.6	8.2 ± 0.2	5.6 ± 3.0	-0.8 ± 0.6
12.5	82.4 ± 1.2	9.0 ± 0.4	88.9 ± 1.0	12.2 ± 0.4	6.6 ± 2.2	3.2 ± 0.8
25	81.0 ± 1.5	7.7 ± 0.5	87.7 ± 0.9	11.3 ± 0.2	6.7 ± 2.4	3.6 ± 0.7
50	82.0 ± 1.5	8.2 ± 0.4	94.7 ± 1.5	17.3 ± 0.6	12.8 ± 3.0	9.1 ± 1.0
100	82.7 ± 0.8	8.9 ± 0.3	107.8 ± 2.2	33.3 ± 2.3	25.1 ± 3.0	24.3 ± 2.6
200	88.2 ± 0.5	15.2 ± 0.6	141.5 ± 2.0	64.9 ± 1.1	52.4 ± 2.5	49.7 ± 1.7

Three replicates of measurement of each concentration of SAb (IgG) were carried out like previous experiments. The errors in the true binding values were calculated from the total error involved in the non-specific binding and SAb-Au enhancement values.

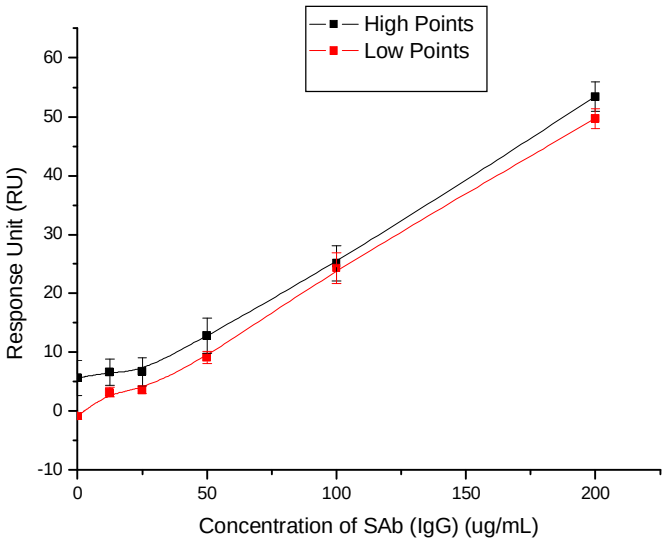

Figure 4.5-9 True SAb-Au enhancement at "High" and "Low" points

200 µg/mL SAb-Au conjugate (with 1:1 diluted gold colloids) was chosen as the optimum concentration for running the competition assay (see Section 4.6) as the 200 µg/mL SAb-Au conjugate had the highest signal response reported in Figure 4.5-9.

The regeneration procedure was also different with the new progesterone surface. The regeneration procedure was normally carried out twice to fully regenerate the surface from > 150 RU (after SAb-Au enhancement). With the new surface, however, it took at least five regenerations to get the baseline from *ca.* 150 RU back down to approximately zero. This meant the concentration of mAb needed to be lowered in order to bring the SAb-Au response down to a certain level at which point surface regeneration could be carried out with only two injections of the regeneration buffer.

The mAb binding curve is shown by Figure 4.5-10. The mAb binding curve should be similar to Figure 4.5-7. However, as Figure 4.5-10 shows, the correlation between the

RU value and mAb concentration was not linear. The optimum mAb concentration (3 µg/mL) was still determined from the plot despite the non-linearity of the results.

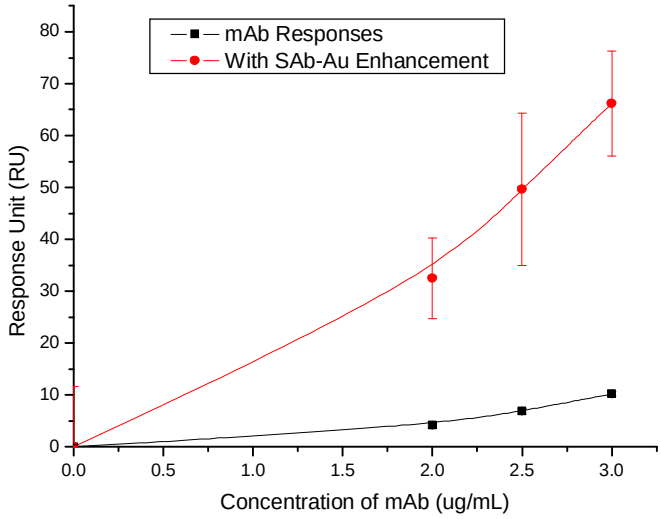

Figure 4.5-10 mAb binding curve with 200 µg/mL SAb-Au conjugate enhancement (with 1:1 diluted gold colloids) on the new CM5 surface

4.5.5 Binding curves for the SAM sensor chip

From the binding curves, it was evident that the reduced thickness of the coupling layer had increased the mAb and SAb-Au responses on the SAM surface. The SAb-Au binding curve is shown in Figure 4.5-11. At 100 µg/mL SAb (IgG), the SAb-Au conjugate had already caused an enhanced response of around 170 RU with 2.5 µg/mL mAb. Compared to the surface on the CM5 chip, this was over 4 times greater than the response given by the 100 µg/mL SAb-Au conjugate, which caused only a *ca.* 40 RU response from use of twice the amount of mAb (5 µg/mL). This shows that the SAM chip is a more sensitive surface for progesterone immunoassays and which could potentially lead to lower LOD value for the mAb binding ligand.

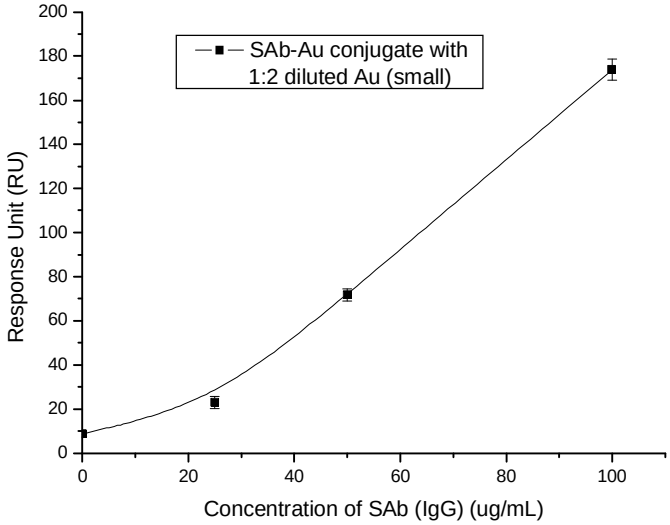

Figure 4.5-11 SAb-Au binding curve (at 2.5 μg/mL mAb concentration) using the SAM surface

The signal enhancement ratio of the SAM surface was calculated from the mAb binding curve shown in Figure 4.5-13. The enhancement ratio was calculated to be *ca.* 29 fold higher than the mAb response alone. This level of signal enhancement ratio through SAb-Au conjugate was more than twice the signal enhancement ratio achieved through the same enhancement species using the CM5 sensor chip (see earlier). The primary disadvantage, however, was the regeneration procedure – for the removal of SAb-Au conjugates from the SAM chip. This proved to be very difficult. Reg Buffer 1, which contained 0.05 mol/L sodium hydroxide + 10 mL /100 mL acetonitrile was used to regenerate the SAM surface initially. However, due to the SAb-Au conjugate developed in this study, complete regeneration was not possible even with a stronger regeneration buffer (0.05 mol/L sodium hydroxide + 20 mL /100 mL acetonitrile, Reg Buffer 2) (see Figure 4.5-12).

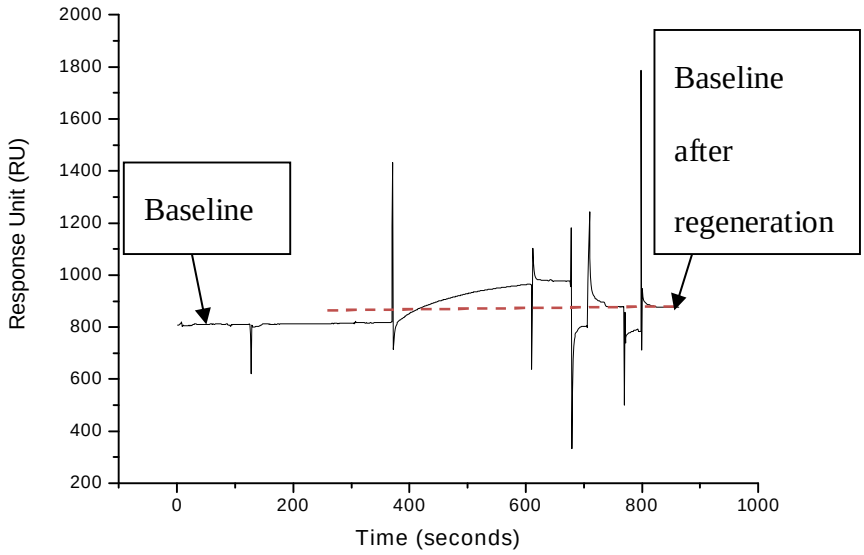

Figure 4.5-12 Sensorgram showing 100 µg/mL SAb-Au conjugate enhancement of response from 2.5 µg/mL mAb. The red dotted line indicates the residue response (*ca.* 60 RU) after 2 regenerations of the progesterone surface on the SAM chip. It was suspected that SAb-Au conjugates were irreversibly deposited on the sensor surface.

Possibly what happened was that the gold exhibited a greater affinity for the gold on the surface (which is more denuded presumably relative to the CM5 chip) so that it was harder to remove. The gold colloids could also be binding to the layers pre-deposited on the gold SAM.

The consequence of this is that the surface could be easily damaged by the materials that were remained on the surface. Thus the number of active sites (number of immobilised progesterone molecule) that are free for mAb binding on the sensor surface can decrease. As a result, the responses generated by the sensor surface also decreases (since less mass can now be bound on the sensor surface). This was thought to be the cause of the non-linearity of the SAb-Au enhancement shown in the mAb

binding curve (see Figure 4.5-13). Indeed, the damaged surface might have induced variability in responses, which were encountered from time to time during the determination of the optimum mAb, SAb-Au concentrations using the SAM chip.

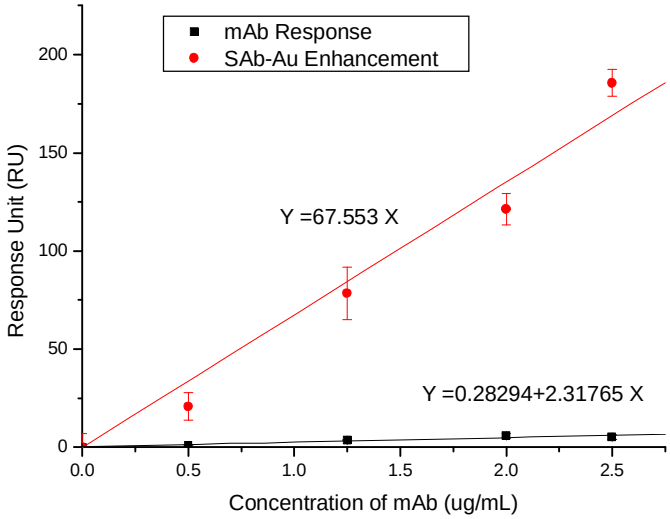

Figure 4.5-13 mAb binding curve with (red) and without (black) 100 µg/mL SAb-Au enhancement using the SAM chip

Despite the problem with surface regeneration, the research using the SAM sensor chip was continued to the next stage, at which a progesterone-mAb competition assay was carried out with 2.5 µg/mL mAb using 100 µg/mL SAb-Au conjugate (with 1:2 diluted Au colloids) as signal enhancement species.

4.6 Progesterone – mAb Competition Assay

4.6.1 Introduction

One of the methods for assaying the concentration of progesterone in "real samples", such as milk or blood serum, is by adding an excess of known concentration of monoclonal anti-progesterone (mAb) to a sample with unknown concentration of progesterone. The mAb would interact with the progesterone in the flowing sample, and cause a reduction in the concentration of free mAb in the mixture. The limited amount of free mAb remaining in the sample can then be detected by complexation with the immobilised progesterone on the sensor chip. This process is called a "competition assay", as immobilised progesterone is competing against free progesterone in the sample for the limited amount of mAb (see Figure 4.6-1).

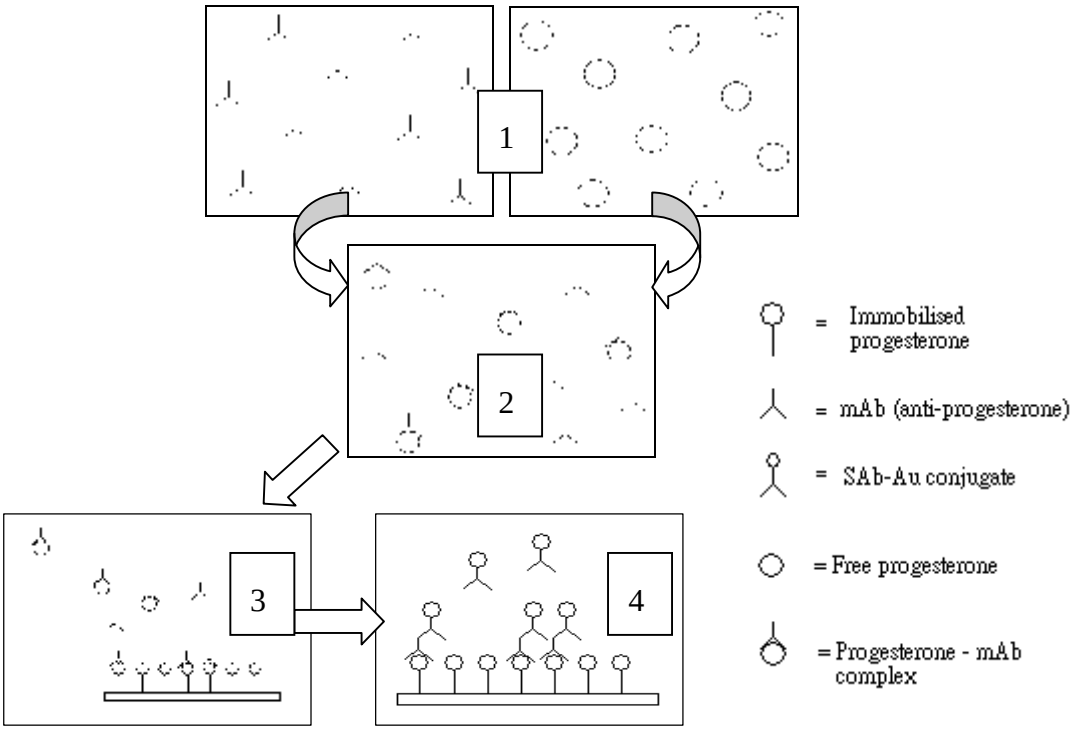

Figure 4.6-1 Schematic diagram showing the principle behind the progesterone-mAb competition assay. 1) The progesterone sample is firstly mixed with a known excess concentration of mAb. 2) Since the

mAb is in excess, after it has been mixed with the progesterone a small amount of free (not bound with progesterone) mAb is still present in the sample. 3) The sample is flowed over the sensor surface with immobilised progesterone. Free mAb will bind to the immobilised progesterone while progesterone-mAb complexes are flowed pass without interacting with the surface. 4) SAb-Au conjugates are then flowed pass over the surface-bound mAb for signal enhancement.

In order to determine the LOD of the assay, it is essential to obtain a competition assay standard binding curve. The concentration of progesterone in a "real sample" can be calculated from the equation [30] that describes the shape of the curve.

$$y = \frac{(a-b)}{1+(x/c)^{d}} + b$$

Where,

y = response

x = concentration

a = maximum response

b = minimum response

c = concentration at 50% response

d = slope of the line at the mid-point

The detection limit of an immunoassay is also calculated using the equation defined above. The response, y, of the LOD is generally defined as the signal response of a blank sample (ie. Sample with the highest concentration of mAb) less two standard deviations (sometimes three standard deviations) of the mean signal response of the blank sample [30]. The LOD concentration can then be calculated providing all the other parameters in the equation are obtained from the competition assay standard binding

curve. The sensitivity can be described by the LOD of the assay, or it can be expressed by the slope (signal per unit concentration change) of the approximated straight line in the middle-region of the binding curve.

The standard binding curve is obtained by running a progesterone-mAb competition assay using mixtures of different concentrations of progesterone standards and a known concentration of mAb. The curve is a plot of Response Unit (RU) (obtained from free mAb) versus the concentrations of progesterone in the progesterone-mAb mixtures. A typical standard binding curve is illustrated in Figure 4.6-1. At near zero concentration of progesterone, the concentration of free mAb is at the highest, thus this region of the curve has high signal responses. When the concentration of progesterone is increased the concentration of free mAb in the sample decreases. This leads to a drop in response to near zero, or to the level of non-specific binding of SAb-Au conjugate if enhancement species are used. A straight line can be approximated at the mid-region of this curve (see Figure 4.6-2).

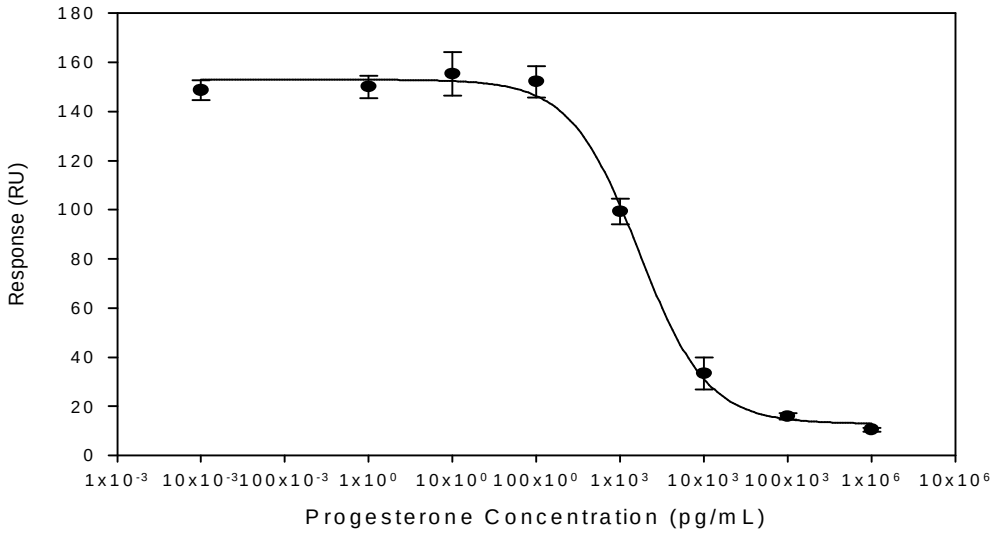

Figure 4.6-2 Assay Standard Curve Using 10nm-Streptavidin / Biotinylated Antibody Pre-Incubation (43.75 µg/mL final mAb concentration) studied by Mitchell et al. The signal responses decreased as the concentration of mAb decreased or the concentration of progesterone in the sample increased.

In this study, progesterone-mAb competition assays were carried out using the stabilised SAb-Au conjugate methodology developed earlier. The assays were carried out using progesterone standards, and the sensitivity was determined from the resulting standard binding curves (similar to the standard binding curve illustrated in Figure 4.6-2).

4.6.2 Sample preparation for progesterone-mAb competition assay

The mAb, SAb-Au conjugate, dilution buffer, and regeneration buffer were all prepared according to the procedures described in Section 4.4. A sample of gold colloids with the same recipe as 130806-1 (0.0072 mol/L of $KAuBr_4$, 0.5% w/v arabinogalactan, and 0.036 mol/L sodium borohydride) was prepared by following the procedure described in Section 4.4.2.1. The colloidal sample was diluted with 5 g/L AG solution in a 1:2 ratio (10 mL of the Au colloids was diluted with 20 mL of 5 g/L AG solution) The sample was stored in a sample tube at ~4°C. 100 μg/mL SAb-Au conjugate was prepared with the gold colloids by following the procedure described in Section 4.4.2.5.

A 10 mg/mL progesterone standard was prepared in a glass vial by dissolving progesterone (Sigma, St. Louis, MO, USA) with 99.8% N, N-dimethylformamide (DMF) (Sigma, St. Louis, MO, USA). 10 μL of the 10 mg/mL progesterone solution was then diluted in 990 μL of HBS-EP buffer to make 1000 μL of 100 μg/mL progesterone. A white precipitate of progesterone was formed when progesterone in DMF was added to HBS-EP buffer (this is because the P4 is relatively hydrophobic and prefers to remain dissolved in the DMF and comes out in aqueous solutions comprising the HBS-EP buffer). To minimise the amount of precipitated progesterone, a hundred-fold dilution was made instead of a ten-fold dilution (as the latter dilution factor resulted in more precipitation than the one hundred-fold dilution). A series of known concentrations of progesterone was prepared by sequential ten-fold dilutions with HBS-EP buffer. 100 μL of the 100 μg/mL progesterone prepared earlier was

diluted in 900 μL of HBS-EP buffer to make 1000 μL of 10 μg/mL progesterone stock solution. This dilution process was repeated for the preparation of 1 μg/mL, 100, 10, 1 ng/mL, 100, 10, 1 pg/mL, 100, 10, and 1 fg/mL progesterone solutions.

5 μg/mL mAb was prepared by the procedure described in Section 4.4.2.3. The 5 μg/mL mAb was then mixed with each of the progesterone standards in a 1:1 dilution ratio. The resulting concentrations of mAb and progesterone were therefore halved (ie after mixing with the progesterone standard, the concentration of mAb in the mixture was 2.5 μg/mL).

4.6.3 Development of the progesterone-mAb competition assay using CM5 sensor chip

The newly prepared CM5 sensor chip described in Section 4.4.3.7 was used for the competition assay. The fresh surface was immobilised with P4-OEG-OVA and a reference flow-cell was immobilised with OVA. The procedure for these immobilisation experiments was described in Section 4.3.1.

Before the competition assay was carried out, the non-specific binding of SAb-Au conjugate was checked again. The 100 μg/mL SAb-Au was injected (using "Quickinjection") into the reference and sample flow-cell at 40 μL over 4 minutes. The non-specific binding of 100 μg/mL SAb-Au on the new CM5 chip was *ca.* 85 RU, which was significantly higher than the non-specific binding of 100 μg/mL SAb-Au on the first CM5 chip (*ca.* 7 RU).

After completion of the check on non specific binding with the SAb-Au conjugate, the competition assay was run using 100, 10, 1 ng/mL, 100, 10 pg/mL progesterone standards. A 6 μg/mL mAb solution was prepared in HBS-EP buffer and 150 μL of the 6 μg/mL mAb was then mixed with 150 μL each of the progesterone standards. Each progesterone/mAb sample was subsequently injected (using "Quickinjection") into the reference and sample flow-cells on the BIAcore at 60 μL over 3 minutes. A 200 μg/mL SAb-Au conjugate with 1:1 diluted gold colloids (10 mL of Au colloids prepared by the procedure described in Section 4.4.2.1 was added to 10 mL of 5 g/L AG) was prepared. It was diluted again (in a 1:1 mixing ration) with the (0.3 mol/L sodium chloride + 1 mL/ 100mL PEG400 + HBS-EP) dilution buffer before it was injected into the reference and sample flow-cells at 40 μL over 4 minutes. This prolonged injection rate allowed more interaction time for the SAb-Au conjugate and surface bound mAb. The surface was regenerated twice with Reg Buffer 2, which consisted of 20 mL/100mL acetonitrile in 0.05 mol/L NaOH solution, at 10 μL over 0.5 minute. The increased concentration of acetonitrile in the regeneration buffer allowed more vigorous removal of the surface-bound SAb-Au conjugates.

Each sample of progesterone/mAb was analysed three times and the standard binding curve (which was a plot of signal responses from each sample versus the concentration (in log scale) of the progesterone standards used in the assay) was obtained.

4.6.4 Development of progesterone-mAb competition assay using SAM sensor chip

The coupling layer of the SAM sensor chip was prepared by the procedure described in Section 4.3.2. The coupling layers on the reference and sample flow-cells of the SAM sensor chip were immobilised with 500 μg/mL of OVA and 500 μg/mL of P4-PEG-OVA respectively. The immobilisation procedure is also described in section 4.3.2.

5 μg/mL mAb along with 10, 1 pg/mL, 100, 10, 1, and 0.1 fg/mL progesterone standards were prepared by the procedure described in Section 4.6.2. The low concentrations of progesterone (compared to the progesterone-mAb competition assay using the CM5 chip) were used in this assay because the SAM chip was proven (as shown in Section 4.5.5) to be very sensitive in the detection of mAb with SAb-Au enhancement. Therefore the LOD of the progesterone-mAb competition assay using the SAM chip was expected to be low compared to the progesterone-mAb carried out on the CM5 chip. 100 μg/mL SAb-Au conjugate with 1:2 diluted gold colloids was prepared according to the previous procedure described in Section 4.4.2.1. 150 μL of the 5 μg/mL mAb was mixed with 150 μL of each of the progesterone standards before each sample was injected (using "Quickinjection") into the reference and sample flow-cells at 60 μL over 3 minutes. The 100 μg/mL SA-Ab conjugate was injected after previous injection of a progesterone-mAb sample. The injection rate for the SAb-Au conjugate was at 40 μL over 4 minutes. Reg Buffer 2 was used to regenerate the sensor surface. It was injected twice, and depending on the effectiveness of regeneration, the injection was varied between 10 μL over 0.5 minute

and 20 μL over 1 minute. Each sample of progesterone/mAb was analysed three times and the standard binding curve (which was a plot of signal responses arising from each sample versus the concentration (in $\log_{10}$ scale) of the progesterone standards used in the assay) was obtained.

4.7 Results & Discussion - Competition Assay

4.7.1 Competition assay using the CM5 sensor chip

Figure 4.7-1 shows the standard binding curve of the progesterone-mAb competition assay carried out on the CM5 chip. This figure shows the plot of the responses arising from the different concentrations of progesterone/mAb samples versus the concentration of progesterone standards (in log scale) used in the experiment. The hyperbolic shape of the binding curve in this experiment was similar to the progesterone-mAb binding curve (shown in Figure 4.6-1 in Section 4.6.1) obtained by Mitchell et al. However, the range between the highest response (response given rise by the blank sample (contained no progesterone)) and the lowest response (response given rise by 100 μg/mL SAb-Au conjugate alone) was only *ca.* 40 RU. This low response range suggested that the progesterone-mAb competition assay developed on the CM5 chip is not practical for analysis of real progesterone samples (ie. milk samples or samples of unknown concentrations of progesterone), since the the 40 RU working range spanned a wide range of progesterone concentrations (from *ca.* 10 pg/mL to *ca.* 10 ng/mL of progesterone) (see the middle part of the binding curve in Figure 4.6-1), so the responses arising from two concentrations of progesterone (say for example 20 pg/mL and 40 pg/mL) are similar, making the distinguishing of the 20 pg/mL from the 40 pg/mL progesterone sample impossible by using this

progesterone-mAb assay developed on the CM5 chip.

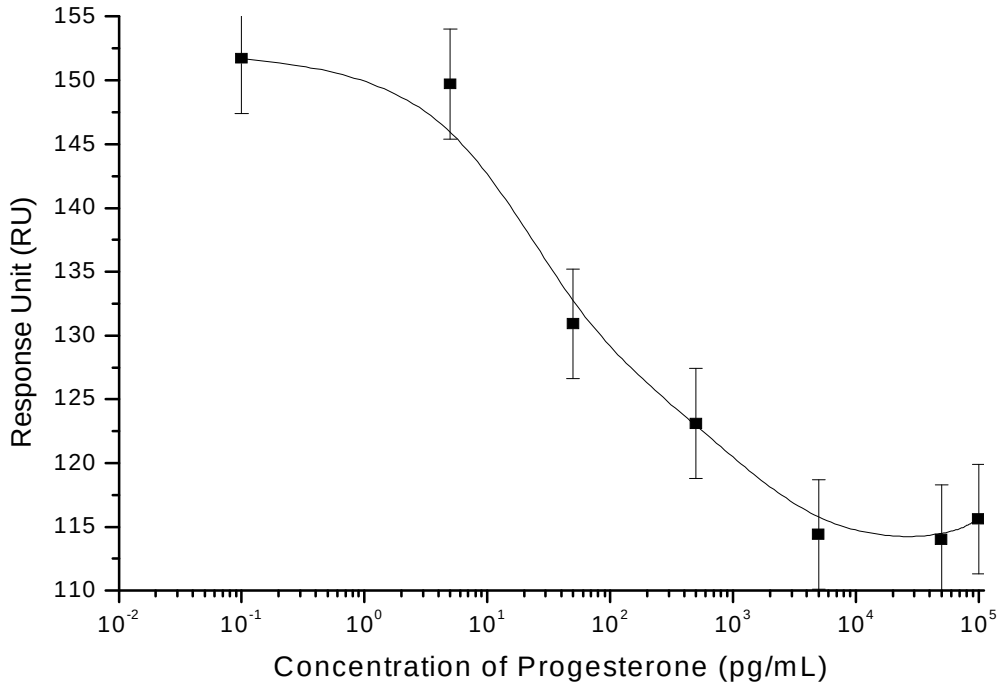

Figure 4.7-1 Progesterone-mAb competition assay binding curve using CM5 surface

The results from the competition assay also suggested that the CM5 surface was inappropriate for carrying out progesterone immunoassay because of the high level of non-specific binding, which after accounting for led to low true responses. The inconsistent responses from the two CM5 sensor chips prepared were also a concern for the viability of this type of surface (ie. the dextran coupling layer) for running the progesterone immunoassay.

Despite the concerns, the progesterone-mAb competition assay was still carried out as a comparison to the competition assay carried out on a SAM chip.

The error bars in the plot were determined by the Student's T test (95% confidence with 2 degrees of freedom). The LOD concentration was not calculated from the equation shown in Section 4.6.1. Due to the narrow range of response across the whole assay, the assay might not be valid and reliable. Hence, the calculated LOD value might be meaningless. Furthermore, to obtain a valid LOD value for the assay, the competition assay was required to be repeated for a number of times, and the error involved in the LOD could then be calculated from the standard deviation between the LOD values. Due to time constraint, this was not carried out in this study. Therefore, the only conclusion that this competition assay binding curve could make is that the LOD value was mostly likely to be in the 5-20 pg/mL range. This work will be discussed in Chapter 5 as one of the tasks to be repeated in future studies.

4.7.2 Competition assay using the SAM sensor chip

Since the SAM was able to improve the signal responses of mAb using the SAb-Au conjugate by *ca.* 29 fold (compared to *ca.* 13 fold mAb signal enhancement using SAb-Au using the first CM5 chip), the progesterone-mAb competition assay was expected to be significantly more sensitive and less problematic than the assay carried out on the CM5 sensor chip. The competition assay binding curve is shown in Figure 4.7-2.

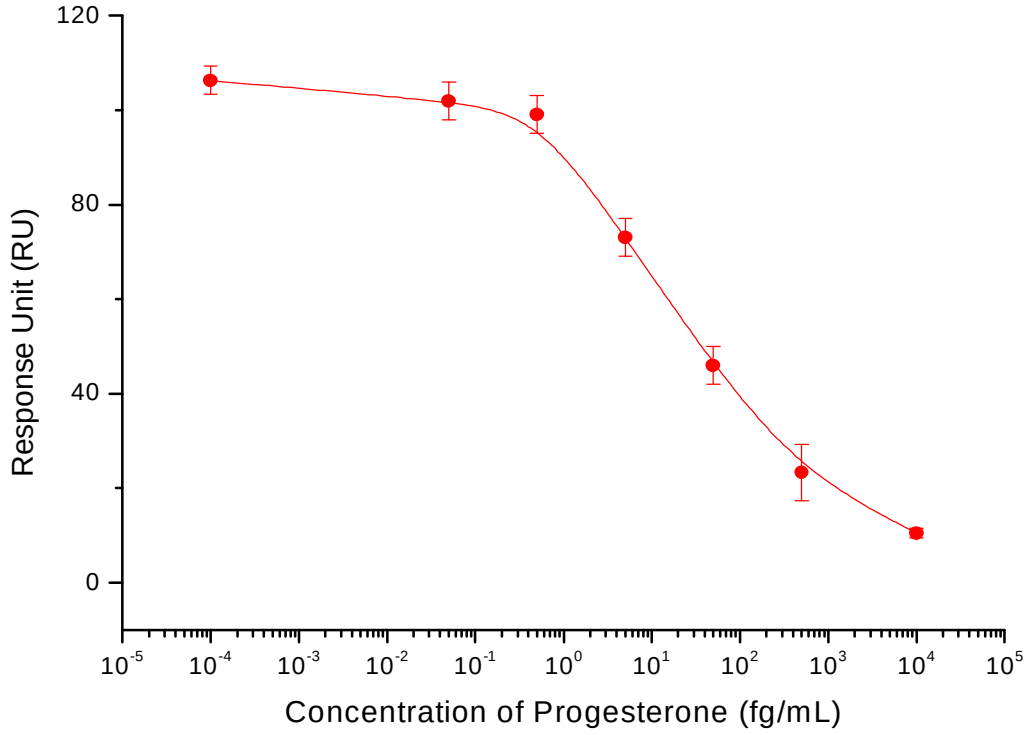

Figure 4.7-2 Progesterone-mAb competition assay binding curve using SAM surface

The binding curve shown above shows that the working range (the difference between the highest response given rise by the blank progesterone/mAb sample and the non-specific binding response of the 100 µg/mL SAb-Au conjugate) was *ca.* 95 RU, which was more than twice the working range of the assay carried out on the CM5 chip (see Section 4.7.1). The higher working range of 95 RU suggests that this assay (developed on the SAM chip) was more applicable in progesterone analysis than the assay developed on the CM5 chip, as the responses arising from two different concentrations of progesterone (say for example 20 fg/mL and 40 fg/mL progesterone samples) were more distinguishable (due to the higher working range).

The LOD value could not be calculated for this competition assay because only one reliable assay (using the SAM) was obtained during the MSc study. To obtain a

meaningful LOD value for this assay, the competition assays should ideally be done in triplicate. The mean LOD value (along with the standard deviations of the mean LOD value) of the three assays could then be calculated. The only conclusion can be gleaned from Figure 4.7-2 is that the LOD of this assay is in the 5-20 fg/mL region, which is about a thousand times more sensitive than the assay developed on the CM5 chip (LOD of *ca.* 5-20 pg/mL).

During the study, attempts to reproduce the progesterone-mAb competition assay using the SAM chip were carried out; however, the sensor chip was damaged due to the irreversibly deposited SAb-Au conjugates on the sensor surface. Thus the mAb binding responses arising from the progesterone/mAb samples with SAb-Au conjugate enhancement became inconsistent. Due to time constraint, the binding curve (Figure 4.7-2) obtained in this study was unable to be replicated. It is suggested in Chapter 5 that this work (obtaining progesterone-mAb competition assay binding curves using the SAM chip) should be repeated in future studies.

5. Conclusions

The first part of the study which was concerned with finding the best gold colloid preparation to use in the BIAcore SPR-based experiments found that arabinogalactan was mostly a good stabilisation or protection agent for the colloids against aggregation, providing that appropriate ratios of reducing agent and arabinogalactan were used. In the case of colloids prepared by reduction with hydrazine hydrate, however, the use of 5 g/L arabinogalactan was insufficient to prevent the colloids from aggregating. For sodium borohydride and tri-potassium citrate, however, 5 g/L arabinogalactan was able to stabilise most of the colloidal gold samples, providing the reducing agent was around ≤10 times the concentration of the gold salt used. Sodium borohydride reduced gold colloids were mostly small in size. The diameter of the colloidal particles was predominantly below 10 nm. However, if the concentrations of the gold salt and the reducing agent were increased, small distributions (< 2%) of particles were found in the 20-35 nm range (using TEM data) in the borohydride-reduced colloidal sample. Citrate reduced gold colloids on the other hand were predominately around 17-20 nm. The citrate-reduced gold colloids prepared in this study were susceptible to aggregation without the addition of 5 g/L arabinogalactan. However, with added 5 g/L arabinogalactan (synergistically with citrate in the colloidal system) the citrate-reduced gold colloids had exhibited prolonged stability (ie. colloidal particles stayed longer in solution without aggregation). This was clearly illustrated in the TEM images of the protected and unprotected gold colloids generated by citrate reduction.

AG-protected sodium borohydride reduced gold colloids were ultimately chosen for

preparing SAb-Au conjugates because of the stability that these colloidal samples possessed. Citrate and hydrazine reduced gold colloids were also subjected to the SAb (IgG) conjugation procedure for BIAcore analysis; however, precipitation occurred during the conjugate preparation. As citrate and hydrazine reduced gold colloids required pH adjustment to pH 8.5-9.0 and addition of electrolyte before SAb (IgG) conjugation, it was reasoned that these steps were responsible for bringing about the destabilisation of the colloids.

The second part of this study investigated the use of the stable SAb-Au conjugate (produced from using the AG-stabilised borohydride-reduced gold colloid) in the progesterone immunoassay developed by Mitchell et al [31]. The study was firstly carried out using a CM5 sensor chip. By determining the optimum SAb-Au concentrations from a series of tests, the SAb-Au conjugate was found to enhance the mAb response signal by approximately 13 fold (which was similar to the enhancement achieved by Mitchell et al); however, in contrast to that earlier study, the signal enhancement achieved in the present study was produced by a much lower concentration of SAb-Au conjugate (100 μg/mL of SAb (IgG)) compared to 800 μg/mL of SAb (IgG) used by Mitchell et al [31].

Two CM5 sensor chips were used during the development of the progesterone immunoassay. The second CM5 chip was found to give inconsistent responses compared to the immobilised progesterone surfaces on the first CM5 chip surface immobilised. The non-specific binding level of the progesterone surface on the second CM5 chip was also far greater than on the first CM5 chip used. This posed a problem when running a progesterone-mAb competition assay as the high level of SAb-Au non-specific binding significantly lowered the true signal responses from the mAb

with SAb-Au enhancement. The CM5 surface was thus deemed unfit for the progesterone immunoassay pending further study. The study then focussed on the use of the SAM sensor chip. When determining the optimum concentrations of mAb and SAb-Au conjugate for running an assay, the study found the SAb-Au conjugate was able to enhance the binding signal of mAb on the immobilised progesterone surface by approximately 29 fold (which was just over twice the SAb-Au signal enhancement ratio achieved using the (first) CM5 chip prepared). The estimated LOD of the progesterone assay developed on the CM5 and SAM chips were 5-20 pg/mL and 5-20 fg/mL respectively. However, these LOD values are only estimates, as valid LOD values require the competition assay to be replicated. Attempts were made to replicate the competition assay using the SAM chip; however, due to sensor surface damage (from permanently bound SAb-Au conjugate on the surface), the result obtained earlier using the SAM chip could not be reproduced.

Even though the true sensitivity of the progesterone immunoassay developed in this study was not determined, the SAb-Au conjugate enhancement species (generated with stabilised borohydride-reduced gold colloids) prepared here had achieved stability and signal enhancement ratio that previous study by Mitchell et al could not achieve. Further work is required to realise the full potential of the SAb-Au enhancement species created in this study.

5.1 Recommendations for further study

It has been shown in this study how regeneration of the SAM sensor chip was challenging with the SAb-Au conjugate. Hence, any future study should be devoted to improving the regeneration procedure. This can be achieved by developing new regeneration buffers which minimise the loss of signal enhancement.

The second objective should be to repeat the progesterone-mAb competition assay using the new optimised regeneration condition.

The gold colloids can also be utilised in other immunoassays studies, as immunoassays for detecting molecules other than progesterone may give different SPR responses from the one given by the SAb-Au conjugates developed in this study.

Lastly, SAb (IgG) conjugation with other metal colloids such as silver, palladium, or platinum could be explored in future investigations. Other systems such as fullerene, nanocomposites (for example, gold colloids with silver shell) could also be considered as a novel (and more massive entity-wise) mass enhancement species.

The studies described above should be carried out on a SAM sensor chip given the better working range of enhancement that is achievable on this chip compared to the CM5 chip.

6. References

1. Goodwin, J. W., *Colloids and Interfaces with Surfactants and Polymers - An Introduction*. 2nd ed.; John Wiley & Sons Ltd.: West Sussex, 2004; p 1,63,65,67.

2. Napper, D. H., *Polymeric Stabilisation of Colloidal Dispersions*. Academic Press Inc.: London, 1983; p 2,8.

3. Everett, D. H., *Basic principles of colloid science*. Royal Society of Chemistry: London, 1988; p xv, 243.

4. Hunter, R. J., *Foundations of colloid science*. 2nd ed.; Oxford University Press: Oxford ; New York, 2001; p xii, 806.

5. Music, S.; Dragcevia, D.; Popovic, S.; Ivanda, M., Precipitation of ZnO particles and their properties. *Materials Letters* **2005,** 59, (19-20), 2388-2393.

6. Choi, S.-H.; Zhang, Y.-P.; Gopalan, A.; Lee, K.-P.; Kang, H.-D., Preparation of catalytically efficient precious metallic colloids by [gamma]-irradiation and characterization. *Colloids and Surfaces A: Physicochemical and Engineering Aspects* **2005,** 256, (2-3), 165-170.

7. Esumi, K.; Wakabayashi, M.; Torigoe, K., Preparation of colloidal silver---palladium alloys by UV-irradiation in mixtures of acetone and 2-propanol. *Colloids and Surfaces A: Physicochemical and Engineering Aspects* **1996,** 109, 55-62.

8. Lee, S. H.; Her, Y. S.; Matijevic, E., Preparation and growth mechanism of uniform colloidal copper oxide by the controlled double-jet precipitation. *Journal of Colloid and Interface Science* **1997,** 186, (1), 193-202.

9. Meyer, W. R.; Pulcinelli, S. H.; Santilli, C. V.; Craievich, A. F., Formation of colloidal particles of hydrous iron oxide by forced hydrolysis. *Journal of Non-Crystalline Solids* **2000,** 273, (1-3), 41-47.

10. Hunter, R. J., *Zeta potential in colloid science : principles and applications*. Academic Press: London, 1981; p xi, 386 p.

11. Birdi, K. S., *Handbook of surface and colloid chemistry*. 2nd ed.; CRC Press: Boca Raton, Fla., 2003; p 765.

12. Finnie, K. S.; Jacques, D. A.; McGann, M. J.; Blackford, M. G.; Barbe, C. J., Encapsulation and controlled release of biomolecules from silica microparticles. *Journal of Materials Chemistry* **2006,** 16, (46), 4494-4498.

13. Veyret, R.; Elaissari, A.; Marianneau, P.; Sall, A. A.; Delair, T., Magnetic colloids for the generic capture of viruses. *Analytical Biochemistry* **2005,** 346, (1), 59-68.

14. Mitchell, J. S. Evaluation of Progesterone – Ovalbumin Conjugates with Different Length Linkers in Enzyme-Linked Immunosorbent Assay and Surface

Plasmon Resonance-Based Immunoassay. Masters Thesis, University of Waikato, Hamilton, 2001.

15. Mosher, B. P.; Wu, C. W.; Sun, T.; Zeng, T. F., Particle-reinforced water-based organic-inorganic nanocomposite coatings for tailored applications. *Journal of Non-Crystalline Solids* **2006,** 352, (30-31), 3295-3301.

16. Hrapovic, S.; Majid, E.; Liu, Y.; Male, K.; Luong, J. H. T., Metallic nanoparticle-carbon nanotube composites for electrochemical determination of explosive nitroaromatic compounds. *Analytical Chemistry* **2006,** 78, (15), 5504-5512.

17. Caruso, F., *Colloids and colloid assemblies : synthesis, modification, organization and utilization of colloid particles*. Wiley-VCH ;: Weinheim
Chichester ; John Wiley distributor ,, 2004; p xviii, 603.

18. Pal, A., Preparation of ultrafine colloidal gold particles using a bioactive molecule. *Journal of Nanoparticle Research* **2004,** 6, (1), 27-34.

19. Miura, K.-i.; Tamamushi, B.-i., The Relation between Colour and Particle Size of Gold Sols. *J Electron Microsc (Tokyo)* **1953,** 1, (1), 36-39.

20. Campion, A.; Kambhampati, P., Surface-enhanced Raman Scattering. *Chemical Society Reviews* **1998,** 27, 241-250.

21. Fontana, E., Thickness optimization of metal films for the development of surface-plasmon-based sensors for nonabsorbing media. *Applied Optics* **2006,** 45, (29), 7632-7642.

22. Mackay, K. M.; Mackay, R. A.; Henderson, W., *Introduction to modern inorganic chemistry*. 5th ed.; Blackie Academic & Professional: London, 1996; p xvi, 468 p.

23. Nath, S.; Ghosh, S. K.; Kundu, S.; Praharaj, S.; Panigrahi, S.; Pal, T., Is gold really softer than silver? HSAB principle revisited. *Journal of Nanoparticle Research* **2006,** 8, (1), 111-116.

24. Lyon, L. A.; Musick, M. D.; Natan, M. J., Colloidal Au-enhanced surface plasmon resonance immunosensing. *Analytical Chemistry* **1998,** 70, (24), 5177-5183.

25. Mullett, W. M.; Lai, E. P. C.; Yeung, J. M., Surface plasmon resonance-based immunoassays. *Methods* **2000,** 22, (1), 77-91.

26. Karlsson, R.; Stahlberg, R., Surface-Plasmon Resonance Detection and Multispot Sensing for Direct Monitoring of Interactions Involving Low-Molecular-Weight Analytes and for Determination of Low Affinities. *Analytical Biochemistry* **1995,** 228, (2), 274-280.

27. Karlsson, R.; Jendeberg, L.; Nilsson, B.; Nilsson, J.; Nygren, P. A., Direct and Competitive Kinetic-Analysis of the Interaction between Human Igg1 and a One Domain Analog of Protein-A. *Journal of Immunological Methods* **1995,** 183, (1), 43-49.

28. Firk, R.; Stamer, E.; Junge, W.; Krieter, J., Automation of oestrus detection in dairy cows: a review. *Livestock Production Science* **2002,** 75, (3), 219-232.

29. Gillis, E. H.; Gosling, J. P.; Sreenan, J. M.; Kane, M., Development and validation of a biosensor-based immunoassay for progesterone in bovine milk. *Journal of Immunological Methods* **2002,** 267, (2), 131-138.

30. Mitchell, J. S. Novel compounds for immunoassay of small biomolecules. University of Waikato, 2005.

31. Flegler, S. L.; Heckman, J. W.; Klomparens, K. L., *Scanning and transmission electron microscopy : an introduction*. W.H. Freeman: New York, 1993; p viii, 225.

32. Nistor, L. C.; Vanlanduyt, J.; Barton, J. D.; Hole, D. E.; Skelland, N. D.; Townsend, P. D., Colloid Size Distributions in Ion-Implanted Glass. *Journal of Non-Crystalline Solids* **1993,** 162, (3), 217-224.

33. Toshima, N.; Wang, Y., Novel Preparation, Characterization and Catalytic Properties of Polymer-Protected Cu/Pd Bimetallic Colloid. *Chemistry Letters* **1993**, (9), 1611-1614.

34. Bradley, J. S.; Hill, E. W.; Klein, C.; Chaudret, B.; Duteil, A., Synthesis of Monodispersed Bimetallic Palladium Copper Nanoscale Colloids. *Chemistry of Materials* **1993,** 5, (3), 254-256.

35. Kaszuba, M.; Connah, M. T., Protein and nanoparticle characterisation using light scattering techniques. *Particle & Particle Systems Characterization* **2006,** 23, (2), 193-196.

36. Zetasizer 1000/2000/3000 Manual - PCS Theory. MAN0152, 1996.

37. Zetasizer 1000HS/3000HS Manual - Size measurements. MAN0149, 2000.

38. Cooper, M. A., Label-free screening of bio-molecular interactions. *Analytical and Bioanalytical Chemistry* **2003,** 377, (5), 834-842.

39. Cambell, C. T., Surface Plasmon Resonance (SPR) Biosensor Development.

40. Catimel, B.; Nerrie, M.; Lee, F. T.; Scott, A. M.; Ritter, G.; Welt, S.; Old, L. J.; Burgess, A. W.; Nice, E. C., Kinetic analysis of the interaction between the monoclonal antibody A33 and its colonic epithelial antigen by the use of an optical biosensor - A comparison of immobilisation strategies. *Journal of Chromatography A* **1997,** 776, (1), 15-30.

41. Daly, S. J.; Keating, G. J.; Dillon, P. P.; Manning, B. M.; O'Kennedy, R.; Lee, H. A.; Morgan, M. R. A., Development of surface plasmon resonance-based immunoassay for aflatoxin B-1. *Journal of Agricultural and Food Chemistry* **2000,** 48, (11), 5097-5104.

42. Cooper, M. A., Optical biosensors in drug discovery. *Nature Reviews Drug Discovery* **2002,** 1, (7), 515-528.

43. Schlecht, U.; Nomura, Y.; Bachmann, T.; Karube, I., Reversible surface thiol

immobilization of carboxyl group containing Haptens to a BIAcore biosensor chip enabling repeated usage of a single sensor surface. *Bioconjugate Chemistry* **2002,** 13, (2), 188-193.

44. Dupont, D.; Rolet-Repecaud, O.; Muller-Renaud, S., Determination of the heat treatment undergone by milk by following the denaturation of alpha-lactalbumin with a biosensor. *Journal of Agricultural and Food Chemistry* **2004,** 52, (4), 677-681.

45. Baird, C. L.; Courtenay, E. S.; Myszka, D. G., Surface plasmon resonance characterization of drug/liposome interactions. *Analytical Biochemistry* **2002,** 310, (1), 93-99.

46. Day, Y. S. N.; Myszka, D. G., Characterizing a drug's primary binding site on albumin. *Journal of Pharmaceutical Sciences* **2003,** 92, (2), 333-343.

47. Karlsson, R., SPR for molecular interaction analysis: a review of emerging application areas. *Journal of Molecular Recognition* **2004,** 17, (3), 151-161.

48. Bokken, G.; Corbee, R. J.; van Knapen, F.; Bergwerff, A. A., Immunochemical detection of Salmonella group B, D and E using an optical surface plasmon resonance biosensor. *Fems Microbiology Letters* **2003,** 222, (1), 75-82.

49. Rasooly, A., Surface plasmon resonance analysis of staphylococcal enterotoxin B in food. *Journal of Food Protection* **2001,** 64, (1), 37-43.

50. Mucalo, M. R.; Bullen, C. R.; Manley-Harris, M.; McIntire, T. M., Arabinogalactan from the Western larch tree: A new, purified and highly water-soluble polysaccharide-based protecting agent for maintaining precious metal nanoparticles in colloidal suspension. *Journal of Materials Science* **2002,** 37, (3), 493-504.

51. Ponder, G. R.; Richards, G. N., Arabinogalactan from Western larch .2. A reversible order-disorder transition. *Journal of Carbohydrate Chemistry* **1997,** 16, (2), 195-211.

52. Christian, T. J.; Manley-Harris, M.; Richards, G. N., A preliminary study of the use of larch arabinogalactan in aqueous two-phase systems. *Carbohydrate Polymers* **1998,** 35, (1-2), 7-12.

53. Duff, D. G.; Baiker, A.; Edwards, P. P., A New Hydrosol of Gold Clusters .1. Formation and Particle-Size Variation. *Langmuir* **1993,** 9, (9), 2301-2309.

54. Andreescu, D.; Sau, T. K.; Goia, D. V., Stabilizer-free nanosized gold sols. *Journal of Colloid and Interface Science* **2006,** 298, (2), 742-751.

55. Verhoeven, J. W., Glossary of Terms Used in Photochemistry. *Pure and Applied Chemistry* **1996,** 68, (12), 2223-2286.

56. Wu, Y.; Mitchell, J.; Cook, C.; Main, L., Evaluation of progesterone-ovalbumin conjugates with different length linkers in enzyme-linked immunosorbant assay and surface plasmon resonance-based immunoassay. *Steroids* **2002,** 67, (7), 565-572.

57. Mitchell, J. S.; Wu, Y. Q.; Cook, C. J.; Main, L., Sensitivity enhancement of

surface plasmon resonance biosensing of small molecules. *Analytical Biochemistry* **2005,** 343, (1), 125-135.

58. Yuan J; Oliver, R. L., J; Aguilar, M; Wu, Y, Nanogold Particles for Sensitivity Enhancement of SPR Assay of Progesterone Based on Mixed Self-Assembled Monolayers. In HortResearch: 2007.

Appendix A

Table A-1 Gold colloids prepared from various concentrations of $KAuBr_4$, AG, and sodium borohydride

Sample	[AuSols] %w/v	[AG] %w/v	Ratio [Au]:[AG]	[NaBH4] %wt	Ratio Au : NaBH4	Ratio AG : NaBH4	Stability (S/U)	Initial Colour	pH	A350
070606-2	0.08%	0.20%	0.4	0.31	0.2	0.6	S	Purple/Brown		3.69
010606-3	0.10%	0.50%	0.2	0.31	0.3	1.6	S	Red/Brown	9.86	4.27
200406-2	0.10%	0.50%	0.2	0.31	0.3	1.6	S	Purple/Red	9.64	
130306-2	0.10%	0.50%	0.2	0.30	0.3	1.7	S	Purple/Blue	9.64	
130306-2	0.10%	0.50%	0.2	0.30	0.3	1.7	S	Purple	11.25	
190706-4	0.10%	0.20%	0.5	0.20	0.5	1.0	S	Purple/Red	10.12	4.50
190706-5	0.10%	0.50%	0.2	0.20	0.5	2.5	S	Purple/Red	10.11	4.57
190706-2	0.20%	0.50%	0.4	0.31	0.6	1.6	S	Purple	10.00	8.39
300506-1	0.20%	5%	0.0	0.31	0.6	16.1	S	Purple/Blue	9.57	7.94
300506-2	0.20%	0.50%	0.4	0.31	0.6	1.6	S	Purple	9.87	8.46
200406-1	0.20%	0.50%	0.4	0.31	0.6	1.6	S	Purple	9.45	
130306-1	0.20%	0.09%	2.2	0.30	0.7	0.3	S	Purple	10.97	8.22
160506-2	0.20%	0.50%	0.4	0.30	0.7	1.7	S	Purple/Red	9.57	8.80
080306-1	0.10%	0.50%	0.2	0.09	1.1	5.6	S	Red/Brown	9.17	5.06
080306-1	0.10%	0.50%	0.2	0.09	1.1	5.6	S	Red/Brown	9.82	4.41
190606-1	0.04%	0.09%	0.4	0.03	1.2	3.1	S	Red/Brown	8.80	1.70
190606-4	0.07%	0.17%	0.4	0.03	2.3	5.6	S	Red/Brown	8.55	3.90
190606-3	0.08%	0.20%	0.4	0.03	2.7	6.7	S	Red/Brown	8.19	4.58
070606-4	0.06%	0.17%	0.4	0.31	0.2	0.5	U	Blue/Black		2.21
070606-3	0.06%	0.17%	0.4	0.31	0.2	0.5	U	Blue/Black		
010606-1	0.10%	0.50%	0.2	0.31	0.3	1.6	U	Blue/Black		
190706-1	0.10%	0.50%	0.2	0.31	0.3	1.6	U	Purple/Blue	10.37	4.32
140606-3	0.15%	0.36%	0.4	0.31	0.5	1.2	U	Blue/Black		
140606-2	0.16%	0.40%	0.4	0.31	0.5	1.3	U	Blue/Black		
300506-3	0.20%	0.05%	4.0	0.31	0.6	0.2	U	Purple	10.04	6.61
140606-1	0.20%	0.50%	0.4	0.31	0.6	1.6	U	Blue/Black	10.01	8.39
130306-1	0.20%	0.09%	2.2	0.30	0.7	0.3	U	Purple/Blue	9.50	8.05
190706-3	0.11%	0.29%	0.4	0.03	3.5	9.3	U	Red	4.36	5.39
190606-2	0.11%	0.29%	0.4	0.03	3.9	9.6	U	Red/Brown	4.21	2.70

Table A-2 Gold colloids prepared from various concentrations of $KAuBr_4$, AG, and hydrazine hydrate

Sample	[AuSols] %w/v	[AG] %w/v	Ratio [Au]:[AG]	[HH] %w/v	Ratio [AG]:[HH]	Ratio [Au]:[HH]	Stability (S/U)	Initial Colour	pH	A350
090206-1 - 10	0.05%	0.50%	10.0%	1%	50.0%	5.0%	S	Dark Purple/Red	11.52-11.78	
170206-1	0.04%	0.05%	80.0%	5%	1.0%	0.8%	S	Clear Dark Purple/Red	12.81	
170206-2	0.05%	0.50%	10.0%	5%	10.0%	1.0%	S	Dark Purple/Red	12.85	
210206-5	0.06%	0.03%	200.0%	10%	0.3%	0.6%	S	Clear Dark Red		
230206-1	0.05%	0.50%	10.0%	5%	10.0%	1.0%	S	Purple	12.89	2.06
170206-3	0.04%	0.05%	80.0%	1%	5.0%	4.0%	S	Brick Red	12.17	
270206-1	0.05%	0.03%	166.7%	5%	0.6%	1.0%	U	Purple	12.65	2.26
280206-1	0.10%	0.50%	20.0%	5%	10.0%	2.0%	U	Dark Purple/Red		
280206-2	0.10%	0.50%	20.0%	10%	5.0%	1.0%	U	Dark Blue/Black		
220206-1	0.06%	0.50%	12.0%	5%	10.0%	1.2%	U	Dark Purple/Red		
220206-2	0.06%	0.05%	120.0%	5%	1.0%	1.2%	U	Dark Purple/Red		
220206-3	0.06%	0.05%	120.0%	10%	0.5%	0.6%	U	Dark Blue/Black		
030306-1	0.05%	0.25%	20.0%	5%	5.0%	1.0%	U	Dark Purple/Red	8.85	2.18
030306-2	0.05%	0.25%	20.0%	5%	5.0%	1.0%	U	Purple	9.53	2.35
070306-1	0.10%	5.00%	2.0%	10%	50.0%	1.0%	U	Dark Blue/Black	13.19	4.03
200206-1	0.20%	0.03%	666.7%	10%	0.3%	2.0%	U	Dark Blue/Black	13.36	
200206-2	0.20%	0.25%	80.0%	10%	2.5%	2.0%	U	Dark Blue/Black	13.30	
200206-3	0.20%	1%	20.0%	10%	10.0%	2.0%	U	Dark Blue/Black		
210206-1	0.10%	0.03%	333.3%	10%	0.3%	1.0%	U	Dark Blue/Black		
210206-2	0.04%	0.03%	133.3%	10%	0.3%	0.4%	U	Purple		
210206-3	0.12%	1%	12.0%	10%	10.0%	1.2%	U	Dark Blue/Black		
210206-4	0.12%	5%	2.4%	10%	50.0%	1.2%	U	Purple		
210206-6	0.09%	0.03%	300.0%	10%	0.3%	0.9%	U	Purple		